Large Scale Integration of Micro-Generation to Low Voltage Grids

Contract No: ENK-CT-2002-00610

WORK PACKAGE A

TASK TA1: MICROSOURCE MODELLING

Version 3.0

10th December 2003

Document Information

Title: DA1
Digital Models for Micro Sources

Date: 2003.06.10 (previous versions: 1.0: 2003-05-09, 2.0: 2003-06-05, 3.0: 2004-02-10)

Task(s): A1 Micro Source Modelling

Coordination:	George **Kariniotakis**[1]	kariniotakis@cenerg.cma.fr
Authors:	Rogério **Almeida**[3]	ralmeida@power.inescn.pt
	Severine **Busquet**[1]	severine.busquet@cenerg.cma.fr
	Cedric **Camez**[1]	cedric.camez@cenerg.cma.fr
	Kostas **Elmasidis**[2]	kelm@germanos.gr
	Nuno **Gil**[3]	
	Nikos **Hatziargyriou**[5]	nh@corfu.power.ece.ntua.gr
	George **Iliadis**[2]	g.iliadis@germanos.gr
	Nilanga **Jayawarna**[6]	T.Jayawarna@postgrad.umist.ac.uk
	Nick **Jenkins**[6]	n.jenkins@umist.ac.uk
	Fotis **Kanellos**[5]	kanellos@power.ece.ntua.gr
	George **Kariniotakis**[1]	kariniotakis@cenerg.cma.fr
	Julien **Labbe**[1]	labbe@cenerg.cma.fr
	Zigor **Larrabe**[4]	zigor@power.inescn.pt, zlarrabe@labein.es
	Xavier **Le Pivert**[1]	xavier.le_pivert@cenerg.cma.fr
	Rudolf **Metkemeyer**[1]	rudolf.metkemeijer@cenerg.cma.fr
	José **Oyarzabal**[4]	joseoyar@labein.es
	Joao A. **Peças Lopes**[3]	plopes@inescporto.pt
	José Sousa **Pinto**[3]	jmpinto@power.inescn.pt
	Aggelos **Tsouchnikas**[5]	aggelos@power.ece.ntua.gr

[1] ARMINES, [2] GERMANOS, [3] INESC, [4] LABEIN, [5] NTUA, [6]UMIST

Access: PUBLIC (for final version)

Status:

_ For Information
_ Draft Version
_ Final Version (internal document)
_ Submission for Approval (deliverable)
x Final Version (deliverable, approved on 10-02-2004)

Contents

Abstract

The purpose of document “DA1. Digital Models for Micro Sources” is to develop models and simulation methods appropriate for studying microgrid system dynamics in the transient stability range and slower. This is essential in order to understand the microgrid operation and its interaction with the interconnected grid, as well as its behaviour in isolated mode.

Models of induction and asynchronous generators, converters, wind energy conversion systems, photovoltaic systems, fuel cells, micro-turbines, battery energy storage systems and supercapacitors are mainly addressed in this document.

1. Introduction[1]

1.1. Objectives of WPA

The main objective of this WP is to develop a simulation platform able to simulate the steady state and dynamic operation of three-phase networks that include micro generation sources.

This involves the development of adequate models for simulating the operation of the different micro sources and storage devices, including the corresponding power electronic interfaces. A generic model is aimed at. The tool will be flexible enough to enable the integration of the control strategies, aggregation of micro source models, and the simulation of disturbances.

Since the MicroGrid may use single-phase circuits and be loaded with single-phase loads, the simulation tool must model the system with its three phases, the neutral conductors, the ground conductors and the connections to ground and to be able to deal with unbalance in the three phase network.

1.2. Tasks of WPA

- **TA1 Micro Source modelling**

Development and selection of micro source and storage models able to describe their steady state and dynamic behaviour.

- **TA2 Three phase system Modelling**

Development of three phase network models, machines (both induction and synchronous) and inverter modelling.

- **TA3 Simulation tool development**

Integration and development of the simulation tool to analyse the steady state and dynamic behaviour of the LV grid.

- **TA4 Aggregation**

Development of algorithms for equivalencing part of the LV network with DGs.

- **TA5 Study Case definition**

Definition of a test network, in order to perform testing evaluation of the developed simulation platform, and also to be exploit as a base case to develop the tasks of WPB, WPC and WPD.

- **TA6 Testing simulation for performance evaluation**

Testing the simulation platform in different operating scenarios, different disturbances and different local control strategies for the defined study case.

[1] Source : Description of Work

2. Modelling of Electrical generators

Models for the three-phase Fixed Speed Induction Generator are represented in a synchronously rotating *dq* reference frame [1]. The Standard 4th Order model and the Reduced 2nd Order model (by neglecting the stator transients) are presented under Dynamic Model followed by the Steady State model.

Models for the Synchronous Generator are represented in a *dqo* reference frame with axes rotating with the rotor [1]. Complete mathematical model that is normally used for analysis of very small systems and three types of reduced models used in stability analysis are given as Dynamic models. Reduced model with stator transients neglected where we lose the dc offset and some high frequency components, Simplified model with amortisseurs neglected which gets rid of the sub-transient contributions and Constant flux linkage model also known as the Classical model are the reduced order models presented. For balanced steady state operation a Steady state model is developed as a voltage source behind a reactance.

A short introduction is given on fixed speed Induction Generators with single-phase supply followed by its steady state model. The dynamic model is developed by modifying the unsymmetrical two-phase induction machine model. A *dq* reference frame fixed to the stator has been selected in order to neglect the time varying coefficients in the machine equations.

2.1. Induction Generators

2.1.1. Three phase fixed speed Induction generator

The following assumptions have been made in developing these models

- Slot effects, saturation, hysteresis and eddy currents neglected
- Purely sinusoidal distribution of flux waves assumed
- Rotor structure considered as symmetrical

All machine equations are in p.u. form denoted with the use of super-bars and are represented in a synchronously rotating *d-q* reference frame. *q*- axis is assumed to be 90° ahead of the *d*- axis in the direction of rotation.

List of symbols common for all models are as follows

ψ = flux linkage

R_s, R_r = Stator and Rotor phase resistance

L_{ss}, L_{rr}	=	Stator and Rotor self inductance
L_s, L_r	=	Stator and Rotor leakage inductance
L_m	=	Magnetizing inductance
ω_s	=	Synchronous angular frequency
s	=	rotor slip
T_e	=	Electromagnetic torque
p	=	differential operator *d/dt*

2.1.1.1. Dynamic model

The full mathematical model to represent dynamic operation of a three-phase induction generator is the standard 4th order model. We can derive the reduced 2nd order 'Voltage behind transient reactance model' by neglecting the stator currents and representing only the fundamental frequency components.

The standard 4th order d-q model

Figure 2.1 shows the circuit applicable to the analysis of an induction generator.

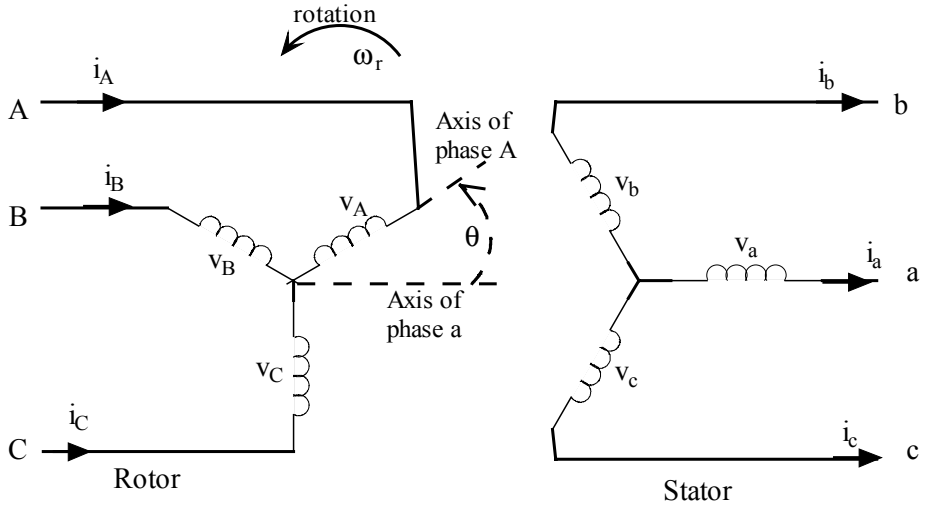

Fig. 2.1 *Stator and rotor circuits in an induction generator*

The stator circuit consists of a, b and c distributed windings while the rotor circuit has A, B and C windings. The angle by which the axis of phase *A* rotor winding leads the axis of phase *a* stator winding in the direction of rotation is defined as θ.

Basic machine equations

Stator voltage equations

$$
\begin{aligned}
v_a &= p\times\psi_a - R_s\times i_a \\
v_b &= p\times\psi_b - R_s\times i_b \\
v_c &= p\times\psi_c - R_s\times i_c
\end{aligned}
\qquad (2.1)
$$

Rotor voltage equations

$$
\begin{aligned}
v_A &= p\times\psi_A + R_r\times i_A \\
v_B &= p\times\psi_B + R_r\times i_B \\
v_C &= p\times\psi_C + R_r\times i_C
\end{aligned}
\qquad (2.2)
$$

The flux linkage in the stator phase *a* winding and the rotor phase *A* winding

$$
\begin{aligned}
\psi_a &= L_{ss}\times i_a + L_{aA}\times\left[i_A\times\cos(\theta) + i_B\times\cos\left(\theta+120^0\right) + i_C\times\cos\left(\theta-120^0\right)\right] \\
\psi_A &= L_{ss}\times i_A + L_{aA}\times\left[i_a\times\cos(\theta) + i_b\times\cos\left(\theta-120^0\right) + i_c\times\cos\left(\theta+120^0\right)\right]
\end{aligned}
\qquad (2.3)
$$

Similar expressions apply to flux linkages in phases *b* and *c* winding of the stator and the rotor.

The d-q transformation

The above machine equations are transformed in to d and q components along axes rotating at synchronous speed as follows:

$$
\begin{aligned}
i_{ds} &= \frac{2}{3}\times\left[i_a\times\cos(\omega_s t) + i_b\times\cos\left(\omega_s t-120^0\right) + i_c\times\cos\left(\omega_s t+120^0\right)\right] \\
i_{qs} &= -\frac{2}{3}\times\left[i_a\times\sin(\omega_s t) + i_b\times\sin\left(\omega_s t-120^0\right) + i_c\times\sin\left(\omega_s t+120^0\right)\right] \\
i_{dr} &= \frac{2}{3}\times\left[i_A\times\cos(\theta_r) + i_B\times\cos\left(\theta_r-120^0\right) + i_C\times\cos\left(\theta_r+120^0\right)\right] \\
i_{qr} &= -\frac{2}{3}\times\left[i_A\times\sin(\theta_r) + i_B\times\sin\left(\theta_r-120^0\right) + i_C\times\sin\left(\theta_r+120^0\right)\right]
\end{aligned}
\qquad (2.4)
$$

Basic machine equations in d-q reference frame

Stator voltages

$$
\begin{cases}
\overline{v}_{ds} = -\overline{R}_s\times\overline{i}_{ds} - \overline{\omega}_s\times\overline{\psi}_{qs} + \overline{p}\,\overline{\psi}_{ds} \\
\overline{v}_{qs} = -\overline{R}_s\times\overline{i}_{qs} + \overline{\omega}_s\times\overline{\psi}_{ds} + \overline{p}\,\overline{\psi}_{qs}
\end{cases}
\qquad (2.5)
$$

Rotor voltages

$$
\begin{cases}
\overline{v}_{dr} = \overline{R}_r\times\overline{i}_{dr} - s\times\overline{\omega}_s\times\overline{\psi}_{qr} + \overline{p}\,\overline{\psi}_{dr} \\
\overline{v}_{qr} = \overline{R}_r\times\overline{i}_{qr} + s\times\overline{\omega}_s\times\overline{\psi}_{dr} + \overline{p}\,\overline{\psi}_{qr}
\end{cases}
\qquad (2.6)
$$

Stator flux linkages

$$\begin{cases} \overline{\psi}_{ds} = -\overline{L}_{ss} \times \bar{i}_{ds} + \overline{L}_m \times \bar{i}_{dr} \\ \overline{\psi}_{qs} = -\overline{L}_{ss} \times \bar{i}_{qs} + \overline{L}_m \times \bar{i}_{qr} \end{cases} \quad (2.7)$$

Rotor flux linkages

$$\begin{cases} \overline{\psi}_{dr} = \overline{L}_{rr} \times \bar{i}_{dr} - \overline{L}_m \times \bar{i}_{ds} \\ \overline{\psi}_{qr} = \overline{L}_{rr} \times \bar{i}_{qr} - \overline{L}_m \times \bar{i}_{qs} \end{cases} \quad (2.8)$$

Electromagnetic torque

$$\overline{T}_e = \overline{\psi}_{qr} \times \bar{i}_{dr} - \overline{\psi}_{dr} \times \bar{i}_{qr} \quad (2.9)$$

Reduced 2nd order model

The reduced 2nd order model is more commonly known as 'voltage behind transient reactance model'. This is derived from the 4th order model as follows.

The terms $p\psi_{ds}$ and $p\psi_{qs}$ representing stator transients in stator voltage relations are neglected. Rotor windings are shorted. Eliminating the rotor currents, the relationship between stator currents and voltage in terms of a voltage behind the transient reactance is deducted. DC component in the stator transient currents is ignored and only the fundamental frequency components are represented

Stator voltages

$$\begin{cases} \bar{v}_{ds} = -\overline{R}_s \times \bar{i}_{ds} + \overline{X}_s{}' \times \bar{i}_{qs} + \bar{v}_d' \\ \bar{v}_{qs} = -\overline{R}_s \times \bar{i}_{qs} - \overline{X}_s{}' \times \bar{i}_{ds} + \bar{v}_q' \end{cases} \quad (2.10)$$

Where

The transient EMF's; $\bar{v}_d' = -\frac{\overline{\omega}_s \overline{L}_m}{\overline{L}_{rr}} \overline{\psi}_{qr}$ and $\bar{v}_q' = \frac{\overline{\omega}_s \overline{L}_m}{\overline{L}_{rr}} \overline{\psi}_{dr}$ (2.11)

Transient reactance; $\overline{X}_s{}' = \overline{\omega}_s \left[\overline{L}_{ss} - \frac{\overline{L}_m^2}{\overline{L}_{rr}} \right]$ (2.12)

$$\tilde{V}_s = -(R_s + jX_s') \times \tilde{I}_s + \tilde{V}' \quad (2.13)$$

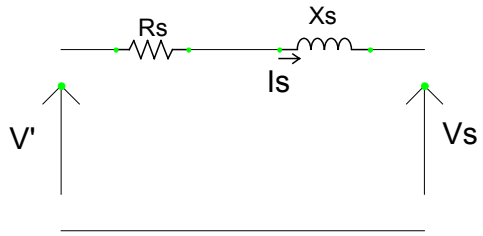

Fig. 2.2 *Induction generator transient equivalent circuit*

Where
Vs = stator terminal voltage

V′ = voltage behind transient impedance

$$\begin{cases} \overline{p}(\overline{v}_d') = -\dfrac{1}{\overline{T}_o'}\left[\overline{v}_d' - \left(\overline{X}_s - \overline{X}_s'\right)\times \bar{i}_{qs}\right] + \bar{s}\times\overline{\omega}_s\times\overline{v}_q' \\ \overline{p}(\overline{v}_q') = -\dfrac{1}{\overline{T}_o'}\left[\overline{v}_q' + \left(\overline{X}_s - \overline{X}_s'\right)\times \bar{i}_{ds}\right] - \bar{s}\times\overline{\omega}_s\times\overline{v}_d' \end{cases} \qquad (2.14)$$

The transient open circuit time constant, $\overline{T}_o' = \dfrac{(\overline{L}_r + \overline{L}_m)}{\overline{R}_r} = \dfrac{\overline{L}_{rr}}{\overline{R}_r}$

$$\overline{X}_s = \overline{\omega}_s(\overline{L}_s + \overline{L}_m) = \overline{\omega}_s\overline{L}_{ss} \qquad (2.15)$$

Electro mechanical torque $$\overline{T}_e = \frac{(\overline{v}_d'\times\bar{i}_{ds} + \overline{v}_q'\times\bar{i}_{qs})}{\overline{\omega}_s} \qquad (2.16)$$

2.1.1.2. Steady state model

Stator currents appear as direct currents in the *d-q* reference frame in balanced steady-state operation.

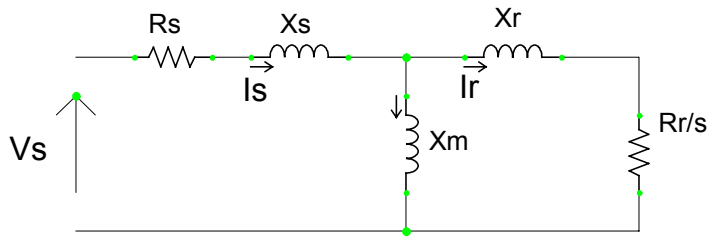

Fig. 2.3 *Equivalent circuit of a three phase Induction machine*

Stator and rotor voltages in phasor form:

$$\begin{aligned} \widetilde{V}_s &= -R_s\times\widetilde{I}_s - jX_s\times\widetilde{I}_s + jX_m(\widetilde{I}_r - \widetilde{I}_s) \\ \widetilde{V}_r &= 0 = \frac{R_r}{s}\times\widetilde{I}_r + jX_r\times\widetilde{I}_r + jX_m(\widetilde{I}_r - \widetilde{I}_s) \end{aligned} \qquad (2.17)$$

Where

$X_s = \omega_s(L_{ss} - L_m)$	=	Stator leakage reactance
$X_r = \omega_s(L_{rr} - L_m)$	=	Rotor leakage reactance
$X_m = \omega_s L_m$	=	Magnetizing reactance
$\widetilde{I}_s, \widetilde{I}_r$	=	Stator and Rotor current in phasor form

2.1.2. Fixed speed induction generator with single phase supply

2.1.2.1. Introduction

Single-phase power supply is universally preferred for fractional horsepower machines for the reasons of simplicity and cost. A single-phase machine resembles a three-phase squirrel cage machine except for the fact that at full speed, only a single winding on the stator is usually excited.

When the stator of a single-phase machine is excited, it produces a pulsating magnetic field in the same direction (no rotating magnetic field as in poly-phase motors). There is no induced voltage due to relative motion in the motor, thus no rotor current flow or induced torque. It is true that a voltage is actually induced in the rotor bars by the transformer action and current flows in short circuited bars. This produces an mmf opposing the stator mmf. But the axis of rotor-mmf wave coincides with the stator-mmf wave and the torque angle is zero. Therefore no net torque is produced at standstill. As there is no inherent torque in single-phase machines, they must be started with special arrangements.

Single-phase Induction generators are proposed for a number of micro-CHP applications. Therefore our aim is to develop steady state and dynamic models for the Single-phase Induction Generator. As such, we do not have to be very much concerned about methods of providing the starting torque (torque would be supplied by the prime mover).

1.1. Starting Methods of Single Phase Induction machines

There are three common techniques to produce the starting torque and all three aim to make one of the two revolving magnetic fields stronger than the other in order to give the motor an initial nudge in one direction or the other.

Normally single-phase induction motors are classified according to its starting method. The major starting techniques in practice are

1.1.1. Split Phase windings

This type of machine has two stator windings (main and auxiliary) set 90 electrical degrees apart along the stator. The ratio of resistance/reactance is higher in the auxiliary winding than the main winding. This type of machine has a moderate starting torque with a fairly low starting current.

1.1.2. Capacitor-type windings

1.1.2.1. Capacitor-start machine

In this machine a capacitor is placed in series with the auxiliary winding. These are more expensive but give a higher starting torque

1.1.2.2. Capacitor-start, capacitor-run machine

There are two capacitors present in this type of machine. A large capacitor (start capacitor) is placed in the auxiliary winding while a smaller capacitor (run-capacitor) is

in the main winding. This machine provides the largest starting torque and the best running conditions.

1.1.2.3. Permanent-split capacitor machine

The starting principle is same as in the capacitor-start machine. But the auxiliary winding is not disconnected after start of the machine.

1.1.3. Shaded pole machine

This has only a main winding. It initiates the required starting torque with shading coils present in its salient poles.

Switching the connection of its auxiliary windings can reverse the direction of rotation of the any type of capacitor-type machine and the split phase machine.

Two theorems are widely used to explain the operation of a single-phase induction motor: **Cross-field theory** and **Double-revolving field theory**. We explain the operating principals of the single-phase motor using the revolving field theory. This states that two counter-rotating fields of equal magnitude can represent a stationary pulsating field. The induction machine responds to each magnetic field separately and the total torque is equal to the algebraic sum of the two torques due to each of the two magnetic fields (figure 11-11 of [3], page 640). But it has to be kept in mind that this is not an accurate description of the torque as it was formed by the super-position of two three-phase characteristics. The fact that both the magnetic fields are present simultaneously in the machine has been ignored.

2.1.2.2. Steady state model

The equivalent circuit for a single-phase induction motor is presented as a series connection of a forward rotating magnetic field and a backward rotating one based on the double revolving theory. This circuit represents only the main winding when the motor is operating alone and the auxiliary winding is absent (note: as mentioned earlier, this is quite acceptable as we are concerned only about the generator model which does not require any starting torque). Core loss is omitted too.

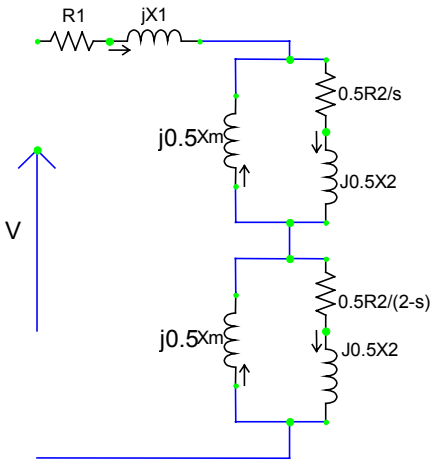

Fig. 2.4 *The equivalengt circuit of a running single-phase motor with its main winding energised*

R_1 = Resistance of the main winding

X_1 = Leakage reactance of the main winding

X_m = Magnetizing reactance

R_2, X_2 = Standstill values of the rotor resistance and the leakage reactance referred to the main stator winding

I_f = Current in the forward rotating field

I_b = Current in the backward rotating field

s = Rotor slip

Rotor slip with respect to forward rotating field, $s_f = s$

Rotor slip with respect to backward rotating field, $s_b = 2 - s$

Total torque, $$T_e = \frac{I_f^2 \times (1-s) \times R_2^{'}}{\omega_m \times s} - \frac{I_b^2 \times (1-s) \times R_2^{'}}{\omega_m \times (2-s)} \quad (2.18)$$

2.1.2.3. Dynamic model

The dynamic model of a Single-phase induction generator is developed with the use of the unsymmetrical 2-phase induction machine. First we will present the model for an unsymmetrical 2-phase induction machine and thereafter modify it to represent a single-phase induction generator.
A reference frame fixed to the stator has been selected (time varying coefficients will appear in the voltage equations in all reference frames except the one fixed to the machine where the asymmetry exists). Please note that these machine equations are not in per unit form like the models presented earlier and Flux linkages are expressed as λ whereas ψ term was used in earlier models.

In the unsymmetrical 2-phase induction machine stator windings are unsymmetrical with unequal resistance and unequal number of turns (m winding and a winding) while the rotor windings are identical. Please refer to figure 1 of [4]

The following assumptions have been made:
- MMF waves are sinusoidal
- The air-gap is uniform
- The magnetic circuit is linear

List of symbols used are as follows

R_{1m}, R_{1a} = Resistance of *m* winding and *a* winding (stator)

N_m, N_a = Effective number of turns of *m* winding and *a* winding

R_{22} = Resistance of the rotor windings

N_2 = Effective number of turns of the rotor windings

λ = Total flux linkage

ω_r = Rotor speed in electrical radians per second

L_m, L_a = Self inductance of *m* winding and *a* winding

L_2 = Self inductance of each rotor winding

M_{m2} = Mutual inductance between *m* winding and identical rotor windings

M_{a2} = Mutual inductance between *a* winding and identical rotor windings

L_{22} = Rotor leakage inductance

L_{1m}, L_{1a} = Leakage inductance of the *m* winding and the *a* winding

P = Number of poles

p = Operator *d/dt*

Stator voltage

$$v_{qs} = R_{1m} \times i_{qs} + p \times \lambda_{qs}$$
$$v_{ds} = R_{1a} \times i_{ds} + p \times \lambda_{ds}$$

Rotor voltage (2.19

$$v_{qr} = R_{22} \times i_{qr} - \omega_r \times \lambda_{dr} + p \times \lambda_{qr}$$
$$v_{dr} = R_{22} \times i_{dr} + \omega_r \times \lambda_{qr} + p \times \lambda_{dr}$$

Flux linkage

$$\begin{aligned} \lambda_{qs} &= L_m \times i_{qs} + M_{m2} \times i_{qr} \\ \lambda_{ds} &= L_a \times i_{ds} + M_{a2} \times i_{dr} \\ \lambda_{qr} &= L_2 \times i_{qr} + M_{m2} \times i_{qs} \\ \lambda_{dr} &= L_2 \times i_{dr} + M_{a2} \times i_{ds} \end{aligned} \quad (2.20)$$

In symmetrical induction machines, all quantities are referred to the stator. For the unsymmetrical 2-phase machine, *q* quantities are referred to the *m* winding and *d* quantities are referred to the *a* winding.

Then

$$\begin{aligned} v'_{qr} &= \frac{N_m}{N_2} \times v_{qr} \\ i'_{qr} &= \frac{N_2}{N_m} \times i_{qr} \end{aligned} \quad (2.21)$$

$$\begin{aligned} v'_{dr} &= \frac{N_a}{N_2} \times v_{dr} \\ i'_{dr} &= \frac{N_2}{N_a} \times i_{dr} \end{aligned} \quad (2.22)$$

$$\begin{aligned} R_{2m} &= \left(\frac{N_m}{N_2}\right)^2 \times R_{22} \\ L_{2m} &= \left(\frac{N_m}{N_2}\right)^2 \times L_{22} \end{aligned} \quad (2.23)$$

$$\begin{aligned} R_{2a} &= \left(\frac{N_a}{N_2}\right)^2 \times R_{22} \\ L_{2a} &= \left(\frac{N_a}{N_2}\right)^2 \times L_{22} \end{aligned} \quad (2.24)$$

Voltage equations

$$\begin{aligned} v_{qs} &= R_{1m} \times i_{qs} + p \times \lambda_{qs} \\ v_{ds} &= R_{1m} \times i_{ds} + p \times \lambda_{ds} \\ v'_{qr} &= R_{2m} \times i'_{qr} - \omega_r \times \frac{N_m}{N_a} \times \lambda'_{dr} + p \times \lambda'_{qr} \\ v'_{dr} &= R_{2a} \times i'_{dr} + \omega_r \times \frac{N_a}{N_m} \times \lambda'_{qr} + p \times \lambda'_{dr} \end{aligned} \quad (2.25)$$

Where

$$\begin{aligned} \lambda_{qs} &= L_{1m} \times i_{qs} + L_{Mm} \times (i_{qs} + i'_{qr}) \\ \lambda_{ds} &= L_{1a} \times i_{ds} + L_{Ma} \times (i_{ds} + i'_{dr}) \\ \lambda'_{qr} &= L_{2m} \times i'_{qr} + L_{Mm} \times (i_{qs} + i'_{qr}) \\ \lambda'_{dr} &= L_{2a} \times i'_{dr} + L_{Ma} \times (i_{ds} + i'_{dr}) \end{aligned} \quad (2.26)$$

In which

$$\begin{aligned} L_{Mm} &= \frac{N_m}{N_2} \times M_{m2} \\ L_{Ma} &= \frac{N_a}{N_2} \times M_{a2} \end{aligned} \quad (2.27)$$

Electromagnetic torque, $$T_e = \frac{P}{2} \times \left(\frac{N_a}{N_m} \times \lambda'_{qr} \times i'_{dr} - \frac{N_m}{N_a} \times \lambda'_{dr} \times i'_{qr}\right) \quad (2.28)$$

The above set of equations form a complete mathematical model of an unsymmetrical 2-phase induction machine. They could represent the different types of the 1-phase induction machine with necessary modifications. But as we are interested only in the single-phase induction generator, it is sufficient to model only the main winding of the stator.

2.1.2.4. A Single Phase Induction Generator with One Stator Winding

This model can be obtained by deleting all the *ds* variables in the above equations and referring all quantities to the *m* winding (denoted by the use of double prime). Convention for generator current was followed.

$$
\begin{aligned}
v_{qs} &= -R_{1m} \times i_{qs} + p \times \lambda_{qs} \\
v'_{qr} &= R_{2m} \times i'_{qr} - \omega_r \times \lambda''_{dr} + p \times \lambda'_{qr} \\
v''_{dr} &= R_{2a} \times i''_{dr} + \omega_r \times \lambda'_{qr} + p \times \lambda''_{dr}
\end{aligned}
\quad (2.29)
$$

Where

$$
\begin{aligned}
\lambda_{qs} &= -L_{1m} \times i_{qs} + L_{Mm} \times (-i_{qs} + i'_{qr}) \\
\lambda'_{qr} &= L_{2m} \times i'_{qr} + L_{Mm} \times (-i_{qs} + i'_{qr}) \\
\lambda''_{dr} &= (L_{2m} + L_{Mm}) \times i''_{dr}
\end{aligned}
\quad (2.30)
$$

and

$$
i''_{dr} = \frac{N_a}{N_m} \times i'_{dr}
$$

Electromagnetic torque, $T_e = \frac{P}{2} \times (\lambda'_{qr} \times i''_{dr} - \lambda''_{dr} \times i'_{qr})$ (2.31) {Equation 72 of [3]}

2.2. Synchronous generator

2.2.1. Modelling of Synchronous Generator

The assumptions made in developing these models (Chapters 3 and 5 of [1]) are as follows:

- Stator windings are sinusoidally distributed along the air-gap as far as the mutual effects with the rotor are concerned
- Stator slots cause no appreciable variation of the rotor inductances with the rotor position
- Magnetic hysterisis and magnetic saturation effects are negligible

All machine equations are in p.u. form denoted with the use of super-bars and are represented in a ***dqo* reference frame**. We have chosen **axes rotating with the rotor** while the induction generator models were presented with axes rotating at synchronous speed.

List of symbols common for all models are as follows

ψ	=	Flux linkage
e_{fd}	=	Field voltage

i_{fd}, i_{kd}, i_{kq}	=	Field and amortisseur (damper winding) circuit currents
R_a	=	Armature resistance per phase
R_{fd}, R_{kd}, R_{kq}	=	Rotor circuit resistances
L_l	=	Leakage inductance
L_{ad}, L_{aq}	=	Mutual inductances
$L_{afd}, L_{akd}, L_{akq}$	=	Mutual inductances between stator and rotor windings
$L_{ffd}, L_{kkd}, L_{kkq}$	=	Self inductances of Rotor circuits
L_{fkd}	=	Mutual inductance between Rotor circuits
X_d, X_q	=	*direct*- and *quadrature*- axis synchronous reactances
X_s	=	Synchronous reactance
ω_r	=	Rotor speed
T_e	=	Electromagnetic torque
p	=	differential operator *d/dt*

2.2.1.1. Dynamic model

(Refer to Figure 3.9 in page 55 of [1])

Complete Mathematical Model (normally used for analysis of very small systems)

- Two *q*- axis amortisseur circuits are considered. Subscripts *1q* and *2q* are used to identify them
- Only one *d*- axis amortisseur circuit is considered and is identified by the subscript *1d.*
- The L_{ad} -base reciprocal per unit system is used. In view of this system

$$\begin{aligned} \overline{L}_{afd} &= \overline{L}_{fda} = \overline{L}_{akd} = \overline{L}_{kda} = \overline{L}_{ad} \\ \overline{L}_{akq} &= \overline{L}_{kqa} = \overline{L}_{aq} \\ \overline{L}_{fkd} &= \overline{L}_{kdf} \end{aligned} \qquad (2.32)$$

Stator voltages

$$\begin{aligned} \overline{v}_d &= -\overline{R}_a \times \overline{i}_d - \overline{\omega}_r \times \overline{\psi}_q + \overline{p}\,\overline{\psi}_d \\ \overline{v}_q &= -\overline{R}_a \times \overline{i}_q + \overline{\omega}_r \times \overline{\psi}_d + \overline{p}\,\overline{\psi}_q \\ \overline{v}_o &= -\overline{R}_a \times \overline{i}_o + \overline{p}\,\overline{\omega}_o \end{aligned} \qquad (2.33)$$

Rotor Voltages

$$\begin{aligned} \overline{e}_{fd} &= \overline{R}_{fd} \times \overline{i}_{fd} + \overline{p}\,\overline{\psi}_{fd} \\ 0 &= \overline{R}_{1d} \times \overline{i}_{1d} + \overline{p}\,\overline{\psi}_{1d} \\ 0 &= \overline{R}_{1q} \times \overline{i}_{1q} + \overline{p}\,\overline{\psi}_{1q} \\ 0 &= R_{2q} \times \overline{i}_{2q} + \overline{p}\,\overline{\psi}_{2q} \end{aligned} \qquad (2.34)$$

Stator flux linkages

$$\begin{aligned}\overline{\psi}_d &= -(\overline{L}_{ad} + \overline{L}_l)\times \bar{i}_d + \overline{L}_{ad}\times \bar{i}_{fd} + \overline{L}_{ad}\times \bar{i}_{1d} \\ \overline{\psi}_q &= -(\overline{L}_{aq} + \overline{L}_l)\times \bar{i}_q + \overline{L}_{aq}\times \bar{i}_{1q} + \overline{L}_{aq}\times \bar{i}_{2q} \\ \overline{\psi}_o &= -\overline{L}_o \times \bar{i}_o\end{aligned} \qquad (2.35)$$

Rotor flux linkages

$$\left.\begin{aligned}\overline{\psi}_{fd} &= \overline{L}_{ffd}\times \bar{i}_{fd} + \overline{L}_{f1d}\times \bar{i}_{1d} - \overline{L}_{ad}\times \bar{i}_d \\ \overline{\psi}_{1d} &= \overline{L}_{f1d}\times \bar{i}_{fd} + \overline{L}_{11d}\times \bar{i}_{1d} - \overline{L}_{ad}\times \bar{i}_d \\ \overline{\psi}_{1q} &= \overline{L}_{11q}\times \bar{i}_{1q} + \overline{L}_{aq}\times \bar{i}_{2q} - \overline{L}_{aq}\times \bar{i}_q \\ \overline{\psi}_{2q} &= \overline{L}_{aq}\times \bar{i}_{1q} + \overline{L}_{22q}\times \bar{i}_{2q} - \overline{L}_{aq}\times \bar{i}_q\end{aligned}\right] Assumption: \overline{L}_{12q} = \overline{L}_{aq} \qquad (2.36)$$

Electromagnetic torque

$$\overline{T}_e = \overline{\psi}_d \times \bar{i}_q - \overline{\psi}_q \bar{i}_d \qquad (2.37)$$

Reduced models for stability analysis

Simplifications essential for large-scale studies (from equations for stator voltages):

1. Neglect transformer voltage terms: $p\psi_d = 0 \;\&\; p\psi_q = 0$
2. Neglect effect of speed variations: $\overline{\omega}_r = 1$

I. **Reduced model with Stator Transients neglected** (lose dc offset + some high frequency components)

Stator voltages

$$\begin{aligned}\bar{v}_d &= -\overline{R}_a \times \bar{i}_d - \overline{\omega}_r \times \overline{\psi}_q \\ \bar{v}_q &= -\overline{R}_a \times \bar{i}_q + \overline{\omega}_r \times \overline{\psi}_d\end{aligned} \qquad (2.38)$$

All the other equations remain the same.

Terminal Electrical Power $\overline{P}_t = \bar{v}_d \times \bar{i}_d + \bar{v}_q \times \bar{i}_q = \overline{T}_e - \overline{R}_a \times \overline{I}_t^2$ (2.39)

Air gap Power $\overline{P}_e = \overline{P}_t + \overline{R}_a \times \overline{I}_t^2 = \overline{T}_e$ (2.40)

II. **Simplified model with amortisseurs (damper windings) neglected** (lose sub-transient contributions)

Stator voltages

$$\begin{aligned}\bar{v}_d &= -\overline{R}_a \times \bar{i}_d - \overline{\psi}_q \\ \bar{v}_q &= -\overline{R}_a \times \bar{i}_q + \overline{\psi}_d\end{aligned} \qquad (2.41)$$

Rotor voltages

$$\bar{v}_{fd} = \overline{R}_{fd} \times \bar{i}_{fd} + \overline{p}\overline{\psi}_{fd} \qquad (2.42)$$

Flux linkages

$$\overline{\psi}_d = -(\overline{L}_{ad} + \overline{L}_l) \times \bar{i}_d + \overline{L}_{ad} \times \bar{i}_{fd}$$
$$\overline{\psi}_q = -(\overline{L}_{aq} + \overline{L}_l) \times \bar{i}_q \qquad (2.43)$$
$$\overline{\psi}_{fd} = -\overline{L}_{ad} \times \bar{i}_d + \overline{L}_{ffd} \times \bar{i}_{fd}$$

$$\overline{T}_e = \overline{\psi}_d \times \bar{i}_q - \overline{\psi}_q \times \bar{i}_d \qquad (2.44)$$

III. **Constant flux linkage model (Classical Model) for transient stability**

Assumptions: Flux linkages are constant

Transient saliency ignored $(X_d^{'} = X_q^{'})$

$$\widetilde{E}_t = \widetilde{E}^{'} - (R_a + jX_d^{'}) \times \widetilde{I}_t$$

where

$$\widetilde{E}^{'} = L_{ad}^{'}\left(-\frac{\psi_{1q}}{L_{1q}} + j\frac{\psi_{fd}}{L_{fd}}\right) \qquad (2.44)$$

$$\overline{T}_e = \overline{\psi}_d \times \bar{i}_q - \overline{\psi}_q \times \bar{i}_d$$

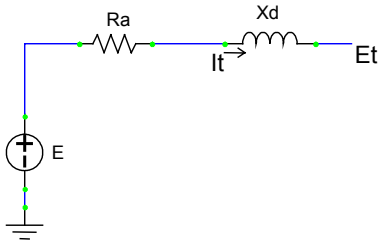

Fig. 2.5 *Simplified Transient model*

2.2.1.2. Steady state model

Per unit machine equations

$$\overline{v}_d = -\overline{R}_a \times \bar{i}_d - \overline{\omega}_r \overline{\psi}_q$$
$$\overline{v}_q = -\overline{R}_a \times \bar{i}_q + \overline{\omega}_r \overline{\psi}_d \qquad (2.45)$$
$$\overline{v}_{fd} = \overline{R}_{fd} \times \bar{i}_{fd}$$

Phasor representation for balanced steady state operation

$$\widetilde{E}_t = \widetilde{E}_q - (R_a + jX_s) \times \widetilde{I}_t \qquad (2.46)$$

where $E_q = X_{ad} \times i_{fd}$

and saliency is neglected, $X_d = X_q = X_s$

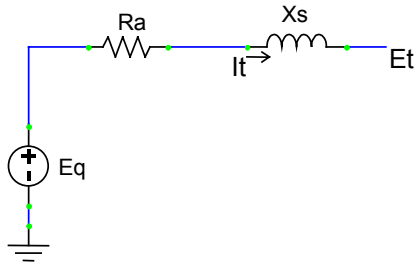

Fig. 2.6 *Steady state equivalent circuit with saliency neglected*

Active Power $\overline{P}_t = \overline{v}_d \times \bar{i}_d + \overline{v}_q \times \bar{i}_q$ (2.47)

Reactive Power $\overline{Q}_t = \overline{v}_q \times \bar{i}_q - \overline{v}_d \times \bar{i}_d$ (2.48)

Steady state torque

$$\overline{T}_e = \overline{\psi}_d \times \bar{i}_q - \overline{\psi}_q \times \bar{i}_d = \overline{P}_t + \overline{R}_a \bar{I}_t^2 \qquad (2.49)$$

2.2.1.3. Permanent Magnet Synchronous Generator

The dc excitation of the field winding can be provided by permanent magnets. Using the equivalent circuit for permanent magnet, the equivalent *dq* circuit is shown as follow:

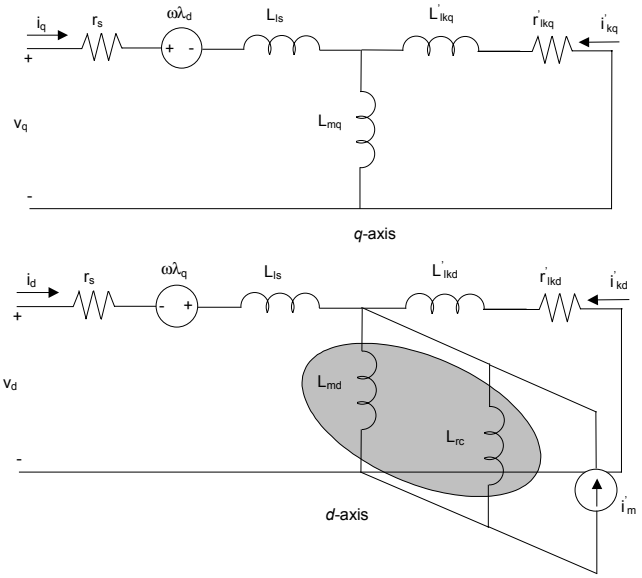

Fig. 2.7 *Equivalent dq circuit for permanent magnet generator*

One obvious change with replacing the electrical excitation with a permanent magnet is the elimination of the copper losses. On the other hand, the magnet characteristic is assumed no change with the time. So, the equations which describe this machine are similar the ones which describe the conventional synchronous machine, as follows:

d-q voltage equations:

$$\begin{cases} v_d = r_s i_d + \dfrac{d\lambda_d}{dt} - \lambda_q \dfrac{d\theta_r}{dt} \\ v_q = r_s i_q + \dfrac{d\lambda_q}{dt} + \lambda_d \dfrac{d\theta_r}{dt} \\ 0 = r'_{kd} i'_{kd} + \dfrac{d\lambda'_{kd}}{dt} \\ 0 = r'_{kq} i'_{kq} + \dfrac{d\lambda'_{kq}}{dt} \end{cases} \quad (2.50)$$

Stator flux equations:

$$\begin{cases} \lambda_d = L_d i_d + L_{md} i'_m \\ \lambda_q = L_q i_q + L_{mq} i'_{kd} \end{cases}$$

Damper winding flux:

$$\begin{cases} \lambda'_{kd} = L_{md} i_d + L'_{kdkd} i'_{kd} + L_{md} i'_m \\ \lambda'_{kq} = L_{mq} i_q + L'_{kqkq} i'_{kq} \end{cases} \quad (2.51)$$

Electromagnetic torque:

$$T_{em} = \frac{3}{2}\frac{P}{2}(\lambda_d i_q - \lambda_q i_d) \quad (2.52)$$

Where:
r_s – armature or stator winding resistance;
r'_{kd}, r'_{kq} – *d*-axis and *q*-axis damper windings referred to the stator, respectively;
$L_d = L_{md} + L_{ls}$, where L_{md} is the *d*-axis stator magnetizing inductance and L_{ls} is the armature or stator winding leakage inductance, respectively;
$L_q = L_{mq} + L_{ls}$, where L_{mq} is the *q*-axis stator magnetizing inductance and L_{ls} is the armature or stator winding leakage inductance, respectively;
$L'_{kdkd} = L_{md} + L_{lkd}$, where L_{lkd} is the *d*-axis damper winding leakage inductance;
$L'_{kqkq} = L_{mq} + L_{lkq}$, where L_{lkq} is the *q*-axis damper winding leakage inductance;
θr – rotor angle.

However it is possible to redefine the equations and represent them by a voltage behind the transient reactance model as conventional synchronous machine equations. From the equations defined previously where the damper windings are considered, the permanent magnet synchronous machine can be represented by a 4th order *d*-*q* model as follow:

$$\frac{dE''_q}{dt} = \frac{1}{T''_{d0}}\left[E'_q - E''_q + I_d\frac{\omega}{\omega_s}(X'_d - X''_d)\right] \quad (2.53)$$

$$\frac{dE''_d}{dt} = \frac{1}{T''_{q0}}\left[-E''_d + I_q\frac{\omega}{\omega_s}(X'_q - X''_q)\right] \quad (2.54)$$

$$\frac{d\omega}{dt} = \frac{1}{2H}(T_m - T_e - D\Delta\omega) \quad (2.55)$$

$$\frac{d\delta}{dt} = \Delta\omega \quad (2.56)$$

- In this model the permanent magnet synchronous generator is represented by the subtransient emfs E''_d and E''_q behind the subtransient reactances X''_d and X''_q
- The differential equations (2.53) and (2.54) include the influence of the damper windings;
- The screening effect of the rotor body eddy-currents in *q*-axis are neglected so that $E'_d = 0$;

The field flux and the field voltage referred to the armature (E_f) are assumed constant, so that $\frac{dE'_q}{dt} = 0$. In this case:

$$E'_q = E_f + I_d\frac{\omega}{\omega_s}(X_d - X'_d) \quad (2.57)$$

In developing the generator model the speed changes are accounted by a factor w/w_s in front of every reactance.

2.3. Converter models

2.3.1. Voltage Source Converters (VSC)

2.3.1.1. Introduction

Power electronics plays a critical role in the microgrids and a majority of the micro sources would be connected through power electronic interfaces. It is quite important to understand about control procedures for such devices. Therefore a model for a VSC with P-Q control is developed and simulated to study its behaviour.

The most common switching technique for switch-mode converters is Pulse Width Modulation (PWM). If the dc quantity of a PWM converter is a constant, there is a linear relationship between the control input and the output (i.e. the converter acts as a power amplifier). But the dc quantity for a VSC, which normally is the voltage across a capacitor, is a variable to be controlled. This introduces non-linearity into the input/ output relationship that makes the control of VSC difficult.

There are several methods proposed in the literature to deal with this problem [11-13]. This section presents the modelling and control of a VSC where a new equation based on the power balance is introduced to replace the original non-linear equation [14].

We have developed two models of the VSC

1. Without considering the capacitor dynamics where dc voltage is assumed to be constant
2. Considering the capacitor dynamics.

2.3.1.2. Model with constant DC voltage

The voltage of the dc source (capacitor) is assumed to be a constant in this model.

The circuit diagram of a VSC is shown in Figure 2.8 and the symbols used are as follows.

$[e] = [e_a \quad e_b \quad e_c]^T$ - AC source (assumed to be ideal)

$[i] = [i_a \quad i_b \quad i_c]^T$ - Source currents (fundamental component)

$[v] = [v_a \quad v_b \quad v_c]^T$ - AC side terminal voltages (fundamental component)

R, L - Resistance and inductance of ac side series R-L circuit

C_{dc} - Smoothing capacitance

v_{dc}, i_{dc} - DC side voltage and current

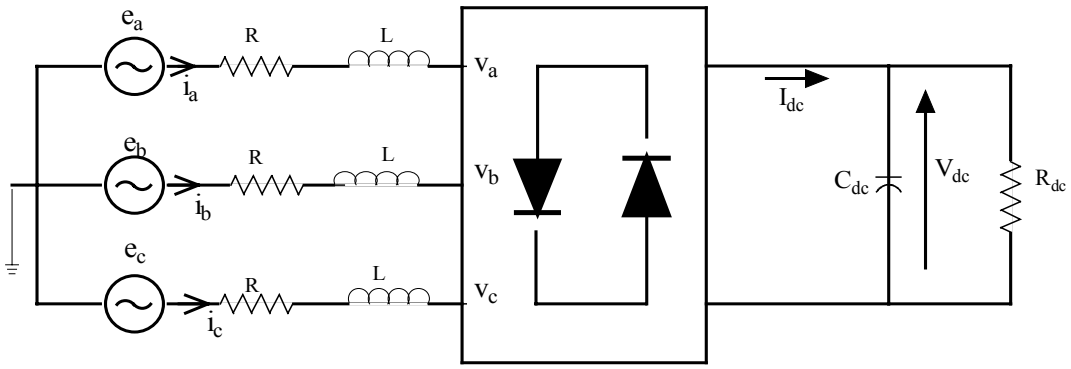

Fig. 2.8*: Circuit diagram of three-phase VSC*

The above model is transformed in to the synchronous orthogonal reference frame rotating at the supply frequency using Park's transformation.

$[E]=\begin{bmatrix}E_d & E_q\end{bmatrix}^T, and [V]=\begin{bmatrix}V_d & V_q\end{bmatrix}^T$ - Voltages in *d-q* reference frame

$[I]=\begin{bmatrix}I_d & I_q\end{bmatrix}^T$ - Currents in *d-q* reference frame

ω - Angular frequency of the ac voltage source

Writing Kirchoff's Voltage equations on the ac side

$$\frac{d}{dt}I_d = -\frac{R}{L}\times I_d + \omega \times I_q - \frac{1}{L}\times V_d + \frac{1}{L}\times E_d \rightarrow (2.58)$$

$$\frac{d}{dt}I_q = -\omega \times I_d - \frac{R}{L}\times I_q - \frac{1}{L}\times V_q + \frac{1}{L}\times E_q \rightarrow (2.59)$$

In order to get the standard linear state space equations, the input variables are defined as

$$U_d = E_d - V_d$$
$$U_q = E_q - V_q$$

Then the equations (2.58) and (2.59) could be re written as

$$\frac{d}{dt}I_d = -\frac{R}{L}\times I_d + \omega \times I_q + \frac{1}{L}\times U_d \rightarrow (2.60)$$

$$\frac{d}{dt}I_q = -\omega \times I_d - \frac{R}{L}\times I_q + \frac{1}{L}\times U_q \rightarrow (2.61)$$

From equations (2.60) & (2.61), the system could be written in a matrix form as follows

$$\frac{d}{dt}\begin{bmatrix}I_d\\I_q\end{bmatrix} = \begin{bmatrix}-R/L & \omega\\ -\omega & -R/L\end{bmatrix}\begin{bmatrix}I_d\\I_q\end{bmatrix} + \begin{bmatrix}1/L & 0\\ 0 & 1/L\end{bmatrix}\begin{bmatrix}U_d\\U_q\end{bmatrix} \rightarrow (2.62)$$

$$y = \begin{bmatrix} 1 & 0 \\ 0 & 1 \end{bmatrix} \begin{bmatrix} I_d \\ I_q \end{bmatrix} \rightarrow (2.63)$$

This is a linear time invariant system (LTI), which could be expressed in the following matrix form

$$\frac{d}{dt}x = Ax + Bu$$

$$y = Cx$$

I_d, I_q - State variables and output variables

U_d, U_q - Input variables

2.3.1.3. Model with capacitor dynamics

As mentioned earlier in this chapter the dc quantity of the VSC is not a constant always. Most often it is the voltage across a capacitor, a variable that introduces non-linearity in to the model equations. A mathematical model for this type of VSC along with its controls is derived below.

The equations (2.62) and (2.63) developed in section 2.3.1.2 for the constant Vdc model still apply for this model too. In addition to them, dynamics of the capacitor have to be taken in to consideration. The instantaneous input power of a VSC is equal to the instantaneous output power. We make use of this power balance equation in developing this model.

The active power absorbed from the ac source

$$P_{ac} = 3/2 \times E_d \times I_d + 3/2 \times E_q \times I_q \rightarrow (2.64)$$

Active power delivered to the converter dc side

$$P_{dc} = V_{dc} \times I_{dc} = C_{dc} \times V_{dc} \times \frac{d}{dt}V_{dc} + \frac{1}{R_{dc}} \times V_{dc}^2 \rightarrow (2.65)$$

Considering Power balance equation,

$$P_{ac} = P_{dc} + P_{loss}$$

We can neglect the converter loss without loss of accuracy. Then

$$C_{dc} \times V_{dc} \frac{d}{dt}V_{dc} + \frac{1}{R_{dc}} \times V_{dc}^2 = \frac{3}{2} \times E_d \times V_d + \frac{3}{2} \times E_q \times I_q \rightarrow (2.66)$$

Which could be arranged as

$$\frac{d}{dt}\left(V_{dc}^2\right) = -\frac{2}{R_{dc} \times C_{dc}} \times \left(V_{dc}^2\right) + \frac{3 \times E_d}{C_{dc}} \times I_d + \frac{3 \times E_q}{C_{dc}} \times I_q$$

This could also be written as

$$\left.\begin{aligned}&\frac{d}{dt}\left(V_{dc}^2\right)=k_d\times I_d+k_q\times I_q+k_c\times\left(V_{dc}^2\right)\\&where,k_d=\frac{3\times E_d}{C_{dc}},k_q=\frac{3\times E_q}{C_{dc}}and,k_c=-\frac{2}{R_{dc}\times C_{dc}}\end{aligned}\right\rangle(2.67)$$

When V_{dc}^2 is taken as the state variable, instead of V_{dc}, this becomes a linear equation.
Thus the state-space model including capacitor dynamics could be represented by the following sets of matrices.

$$\frac{d}{dt}\begin{bmatrix}I_d\\I_q\\\left(V_{dc}^2\right)\end{bmatrix}=\begin{bmatrix}-R/L & \omega & 0\\-\omega & -R/L & 0\\k_d & k_q & k_c\end{bmatrix}\begin{bmatrix}I_d\\I_q\\\left(V_{dc}^2\right)\end{bmatrix}+\begin{bmatrix}1/L & 0 & 0\\0 & 1/L & 0\\0 & 0 & 0\end{bmatrix}\begin{bmatrix}U_d\\U_q\\0\end{bmatrix}\rightarrow(2.68)$$

$$y=\begin{bmatrix}1 & 0 & 0\\0 & 1 & 0\\0 & 0 & 1\end{bmatrix}\begin{bmatrix}I_d\\I_q\\\left(V_{dc}^2\right)\end{bmatrix}\rightarrow(2.69)$$

$I_d, I_q, \left(V_{dc}^2\right)$	-	State variables and output variables
U_d, U_q	-	Input variables

2.3.1.4. Steady state model

For Steady State operation, there are no *p* terms in the equations

AC side circuit equations

$$\begin{aligned}&\frac{\omega_b}{\overline{L}}\times\left(\overline{e}_d-\left|\overline{v}\right|\right)=\frac{\overline{R}_s\times\omega_b}{\overline{L}}\times\bar{i}_d-\omega\times\bar{i}_q\\&\frac{\omega_b}{\overline{L}}\times\overline{e}_q=\frac{\overline{R}_s\times\omega_b}{\overline{L}}\times\bar{i}_q+\omega\times\bar{i}_d\end{aligned}\qquad(2.70)$$

Steady state representation

$$\left(\overline{e}_d+j\overline{e}_q\right)-\left|\overline{v}\right|=\left(\overline{R}_s+j\overline{X}_s\right)\times\left(\bar{i}_d+j\bar{i}_q\right)\qquad(2.71)$$

Where

$$\overline{X}_s=\frac{\omega}{\omega_b}\times\overline{L}$$

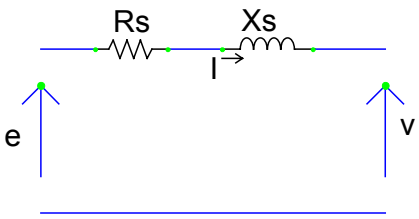

$$I = \bar{i}_d + j\bar{i}_q$$

Fig. 2.9 *Steady State equivalent circuit of a VSC*

2.3.1.5. Single phase VSC

The schematic diagram for a single-phase VSC is as follows (Figure 1(b) of [6]). The symbols used in [6] have been followed for convenience in cross- reference.

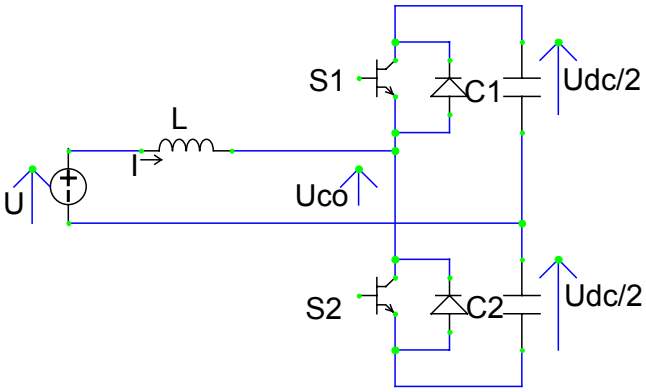

U = Utility Voltage

U_{co} = Fundamental component of converter Voltage

S_1, S_2 = Semiconductor switches

Inductor L acts as the load between U and Uco

Fig. 2.10 *Schematic diagram for a single-phase VSC*

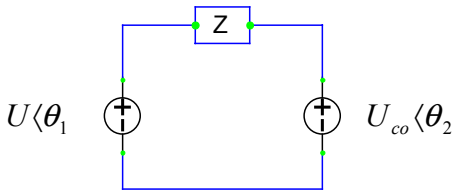

Z = load impedance

Fig. 2.11 *Equivalent circuit of a single-phase VSC*

Direction of the power flow depends on the magnitudes of the voltage sources U and U_{co} and their phase angles, θ_1 and θ_2.

2.3.2. Inverters

Having in mind that the micro sources described in this document are to be connected to three phase LV networks, probably facing unbalanced conditions, the electronic interface should present characteristics to operate under such conditions.
Two inverter models have been developed to interface with the power network in different situations. These models are:

- Current source for balanced operating conditions;
- Voltage source, controlled by current.

When doing that there was also a concern on adopting a modeling capable of representing existing inverter control strategies, like it is the case of the instantaneous power control algorithm [18].

2.3.2.1. Modelling the Inverter system – Current Source

A simple current source model was first developed in this project.
The current source assumes the role of the inverter, by determining the current from the implicit real and reactive power.
The reference voltage used to determine the current is the network nominal voltage (U_n Block). Consequently, the injected current in the network is:

$$I_a = \frac{P}{\sqrt{3}U_n \times \cos\varphi}\sin(wt+\varphi) \qquad (2.72)$$

where:

$$\varphi = \arctan\left(\frac{Q}{P}\right) \qquad (2.73)$$

2.3.2.2. Modelling the Inverter system (Voltage source) using Instantaneous Power Theory

In 1984 Akagi, proposed the instantaneous theory for control of active power filters[18]. Such approach has been used in various schemes to control the PWM-VSI (*Pulse Width Modulation - Voltage Source Inverter*) or PWM-CSI (*Pulse Width Modulation - Current Source Inverter*). Voltages or currents references signals employed to turn on and turn off the switches of the inverter can be obtained from this theory [19], [20]. In this case, the instantaneous voltages and currents in three-phase circuits are adequately expressed as the instantaneous space vectors in *a-b-c* coordinates. The *a*, *b* and *c* axes are fixed on the same plane, apart from each other by $2\pi/3$, as shown in Figure 2.12

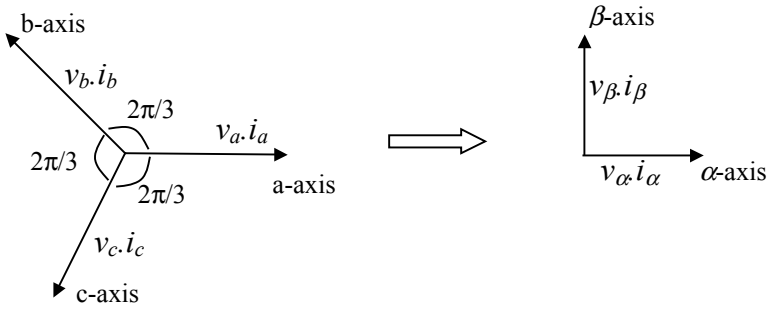

Fig. 2.12 α-β coordinates transformation

According to Figure 2.12, the instantaneous space vectors, $v_a(t)$ and $i_a(t)$ are set on the *a* axis and their amplitude and (+,-) direction vary with the passage of time. Similarly, v_b and i_b are on the *b* axis and v_c and i_c are on the *c* axis. These space vectors are easily transformed into α and β coordinates (*Clark Transformation*) as follows:

$$\begin{bmatrix} v_0(t) \\ v_\alpha(t) \\ v_\beta(t) \end{bmatrix} = \sqrt{\frac{2}{3}} \cdot \begin{bmatrix} 1/\sqrt{2} & 1/\sqrt{2} & 1/\sqrt{2} \\ 1 & -1/2 & -1/2 \\ 0 & \sqrt{3}/2 & -\sqrt{3}/2 \end{bmatrix} \cdot \begin{bmatrix} v_a(t) \\ v_b(t) \\ v_c(t) \end{bmatrix} \quad (2.74)$$

$$\begin{bmatrix} i_0(t) \\ i_\alpha(t) \\ i_\beta(t) \end{bmatrix} = \sqrt{\frac{2}{3}} \cdot \begin{bmatrix} 1/\sqrt{2} & 1/\sqrt{2} & 1/\sqrt{2} \\ 1 & -1/2 & -1/2 \\ 0 & \sqrt{3}/2 & -\sqrt{3}/2 \end{bmatrix} \cdot \begin{bmatrix} i_a(t) \\ i_b(t) \\ i_c(t) \end{bmatrix} \quad (2.75)$$

Where,

$v_a(t)$, $v_b(t)$ and $v_c(t)$ are the instantaneous voltages in *a*-*b*-c coordinates, respectively.
$i_a(t)$, $i_b(t)$ and $i_c(t)$ are the instantaneous currents in *a*-*b*-c coordinates, respectively.
$v_o(t)$, $v_\alpha(t)$ and $v_\beta(t)$ are the instantaneous voltages in *0*-α-β coordinates, respectively.
$i_o(t)$, $i_\alpha(t)$ and $i_\beta(t)$ are the instantaneous voltages in *0*-α-β coordinates, respectively.

In a balanced three-phase system the equations (2.74) and (2.75) are defined as:

$$\begin{bmatrix} v_\alpha(t) \\ v_\beta(t) \end{bmatrix} = \sqrt{\frac{2}{3}} \cdot \begin{bmatrix} 1 & -1/2 & -1/2 \\ 0 & \sqrt{3}/2 & -\sqrt{3}/2 \end{bmatrix} \cdot \begin{bmatrix} v_a(t) \\ v_b(t) \\ v_c(t) \end{bmatrix} \quad (2.76)$$

$$\begin{bmatrix} i_\alpha(t) \\ i_\beta(t) \end{bmatrix} = \sqrt{\frac{2}{3}} \cdot \begin{bmatrix} 1 & -1/2 & -1/2 \\ 0 & \sqrt{3}/2 & -\sqrt{3}/2 \end{bmatrix} \cdot \begin{bmatrix} i_a(t) \\ i_b(t) \\ i_c(t) \end{bmatrix} \quad (2.77)$$

So, the instantaneous real and instantaneous imaginary powers are defined as:

$$\begin{bmatrix} p(t) \\ q(t) \end{bmatrix} = \begin{bmatrix} \bar{p}(t) \\ \bar{q}(t) \end{bmatrix} + \begin{bmatrix} \tilde{p}(t) \\ \tilde{q}(t) \end{bmatrix} = \begin{bmatrix} v_\alpha(t) & v_\beta(t) \\ -v_\beta(t) & v_\alpha(t) \end{bmatrix} \cdot \begin{bmatrix} i_\alpha(t) \\ i_\beta(t) \end{bmatrix} \quad (2.78)$$

where,

p is the instantaneous real power (*W*);
q is the instantaneous imaginary power (VAR).

The symbols ($\bar{}$) and ($\tilde{}$) in equation (2.78) denote the average and oscillatory components, respectively. The oscillatory components may appear if harmonics are present.
In system with sinusoidal balanced voltages and currents, the average value of *q* is equal to conventional reactive power [18]. For unbalanced or balanced systems the instantaneous real power is always equal to the conventional active power.
From equation (2.78) it is possible to obtain the voltages or currents reference signals to control the PWM-VSI. In this work, it is assumed that hysteresis current controller controls the inverter. Neglecting the harmonics and assuming a balanced three-phase system, the currents reference calculation is obtained as:

$$\begin{bmatrix} i^*_{ca}(t) \\ i^*_{cb}(t) \\ i^*_{cc}(t) \end{bmatrix} = \sqrt{\frac{3}{2}} \cdot \begin{bmatrix} 1 & 0 \\ -1/2 & \sqrt{3}/2 \\ -1/2 & -\sqrt{3}/2 \end{bmatrix} \cdot \begin{bmatrix} v_\alpha(t) & v_\beta(t) \\ -v_\beta(t) & v_\alpha(t) \end{bmatrix}^{-1} \cdot \begin{bmatrix} p_c(t) \\ q_c(t) \end{bmatrix} \tag{2.79}$$

A better understanding of the control strategy for the PWM-VSI is shown in figure 2.13

In this case, the references of the compensating currents i^*_{ca}, i^*_{cb} and i^*_{cc} are calculated instantaneously without any time delay by using the instantaneous voltages and currents on the load side. The control circuit consists of several analog multipliers, dividers and operational amplifiers as shown below.

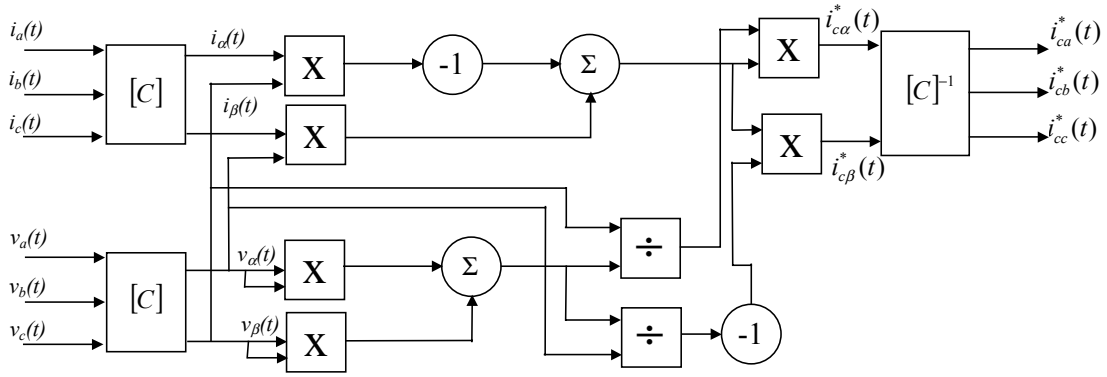

$$[C] = \sqrt{2/3} \cdot \begin{bmatrix} 1 & -1/2 & -1/2 \\ 0 & \sqrt{3}/2 & -\sqrt{3}/2 \end{bmatrix}$$

Fig. 2.13 Control circuit

For unbalanced system, the average value of *q* is distinct to conventional reactive power. In this case, it is possible to extend the instantaneous reactive power theory developed in [18] to the three-phase circuit including zero-phase sequence components. The instantaneous space vectors voltages (v_a, v_b and v_c) and the instantaneous space vectors currents (i_a, i_b and i_c) are transformed as shown in equations (2.74) and (2.75), respectively.
The authors of [18] introduce another instantaneous power p_o, which is defined by the instantaneous space vectors, v_o and i_o on the zero-axis:

$$p_0 = v_0 \cdot i_0 \tag{2.80}$$

In (2.80) p_o has been named “instantaneous zero-phase sequence power”[18]. From (2.74), (2.75) and (2.80), the three independent quantities p_o, p, and q are given by:

$$\begin{bmatrix} p_o \\ p \\ q \end{bmatrix} = \begin{bmatrix} v_o & 0 & 0 \\ 0 & v_\alpha & v_\beta \\ 0 & -v_\beta & v_\alpha \end{bmatrix} \cdot \begin{bmatrix} i_o \\ i_\alpha \\ i_\beta \end{bmatrix} \tag{2.81}$$

Inverse transformation of (2.81) gives:

$$\begin{bmatrix} i_o \\ i_\alpha \\ i_\beta \end{bmatrix} = \begin{bmatrix} v_o & 0 & 0 \\ 0 & v_\alpha & v_\beta \\ 0 & -v_\beta & v_\alpha \end{bmatrix}^{-1} \cdot \begin{bmatrix} p_o \\ 0 \\ 0 \end{bmatrix} + \begin{bmatrix} v_o & 0 & 0 \\ 0 & v_\alpha & v_\beta \\ 0 & -v_\beta & v_\alpha \end{bmatrix}^{-1} \cdot \begin{bmatrix} 0 \\ p \\ 0 \end{bmatrix} + \begin{bmatrix} v_o & 0 & 0 \\ 0 & v_\alpha & v_\beta \\ 0 & -v_\beta & v_\alpha \end{bmatrix}^{-1} \cdot \begin{bmatrix} 0 \\ 0 \\ q \end{bmatrix} \tag{2.82}$$

$$\begin{bmatrix} i_o \\ i_\alpha \\ i_\beta \end{bmatrix} \equiv \begin{bmatrix} i_o \\ 0 \\ 0 \end{bmatrix} + \begin{bmatrix} 0 \\ i_{\alpha p} \\ i_{\beta p} \end{bmatrix} + \begin{bmatrix} 0 \\ i_{\alpha q} \\ i_{\beta q} \end{bmatrix}$$

From(2.82), the instantaneous currents on the a-b-c coordinates are divided in the following three components, respectively, as follow:

$$\begin{bmatrix} i_a \\ i_b \\ i_c \end{bmatrix} = \sqrt{\frac{3}{2}} \cdot \begin{bmatrix} 1/\sqrt{2} & 1 & 0 \\ 1/\sqrt{2} & -1/2 & \sqrt{3}/2 \\ 1/\sqrt{2} & -1/2 & -\sqrt{3}/2 \end{bmatrix} \cdot \begin{bmatrix} i_o \\ 0 \\ 0 \end{bmatrix} + \sqrt{\frac{3}{2}} \cdot \begin{bmatrix} 1/\sqrt{2} & 1 & 0 \\ 1/\sqrt{2} & -1/2 & \sqrt{3}/2 \\ 1/\sqrt{2} & -1/2 & -\sqrt{3}/2 \end{bmatrix} \cdot \begin{bmatrix} 0 \\ i_{\alpha p} \\ i_{\beta p} \end{bmatrix}$$
$$+ \sqrt{\frac{3}{2}} \cdot \begin{bmatrix} 1/\sqrt{2} & 1 & 0 \\ 1/\sqrt{2} & -1/2 & \sqrt{3}/2 \\ 1/\sqrt{2} & -1/2 & -\sqrt{3}/2 \end{bmatrix} \cdot \begin{bmatrix} 0 \\ i_{\alpha q} \\ i_{\beta q} \end{bmatrix} \tag{2.83}$$

$$\begin{bmatrix} i_a \\ i_b \\ i_c \end{bmatrix} \equiv \underbrace{\begin{bmatrix} i_{ao} \\ i_{bo} \\ i_{co} \end{bmatrix}}_{\substack{\text{insatantaneous} \\ \text{zero-phase} \\ \text{sequence-current}}} + \underbrace{\begin{bmatrix} i_{ap} \\ i_{bp} \\ i_{cp} \end{bmatrix}}_{\substack{\text{instantaneous} \\ \text{active-current}}} + \underbrace{\begin{bmatrix} i_{aq} \\ i_{bq} \\ i_{cq} \end{bmatrix}}_{\substack{\text{instantaneous} \\ \text{reacative-current}}}$$

where,

$$i_{ao} = i_{bo} = i_{co} = i_o \Big/ \sqrt{3} \tag{2.84}$$

Let the a-, b- and c-phase instantaneous powers be pa, pb and pc, respectively. By applying (2.83), the following is obtained:

$$\begin{bmatrix} p_a \\ p_b \\ p_c \end{bmatrix} = \begin{bmatrix} v_a.i_{ao} \\ v_b.i_{bo} \\ v_c.i_{co} \end{bmatrix} + \begin{bmatrix} v_a.i_{ap} \\ v_b.i_{bp} \\ v_c.i_{cp} \end{bmatrix} + \begin{bmatrix} v_a.i_{aq} \\ v_b.i_{bq} \\ v_c.i_{cq} \end{bmatrix} \equiv \underbrace{\begin{bmatrix} p_{ao} \\ p_{bo} \\ p_{co} \end{bmatrix}}_{\substack{\text{instantaneous} \\ \text{zero-phase} \\ \text{sequence-power}}} + \underbrace{\begin{bmatrix} p_{ap} \\ p_{bp} \\ p_{cp} \end{bmatrix}}_{\substack{\text{instantaneous} \\ \text{active-power}}} + \underbrace{\begin{bmatrix} p_{aq} \\ p_{bq} \\ p_{cq} \end{bmatrix}}_{\substack{\text{instantaneous} \\ \text{reactive-power}}} \tag{2.85}$$

The instantaneous reactive powers in each phase p_{aq}, p_{bq} and p_{cq} make no contribution to the instantaneous power flow in the three-phase circuit which is represented by the sum of p_a and p, because the sum of the instantaneous reactive powers is always zero, that is:

$$p_{aq} + p_{bq} + p_{cq} = 0 \tag{2.86}$$

Extra work is still needed in order to account for fully unbalanced operation of the inverter, namely when dealing with the simulation of the presence of single phase short-circuits.

2.3.3. Modulation Techniques

2.3.3.1. Sinusoidal Pulse Width Modulation (SPWM)

This method employs individual carrier modulators in each of the three phases. The reference signals of the phase voltages are sinusoidal and are obtained from the reference voltage vector, which is split into its three phase components. Three comparators and a triangular carrier signal, which is common to all three-phase signals, generate the logic signals that control the semi-conductors. How the method operates is shown in figure 2.14. (Synchronized carrier and reference signals)

The aforementioned method operates at constant carrier frequency, while the fundamental frequency can vary. The switching frequency is then nonperiodic in principle and the corresponding Fourier spectra are continuous containing frequencies lower than the lowest carrier sideboard. These harmonics are undesired and produce low-frequency torque harmonics that may stimulate resonances in the mechanical transmission train of the drive system. Synchronization between the carrier frequency and the controlling fundamental avoids this drawback. Adding zero-sequence waveforms to the sinusoidal reference signals can perform a reduction of the harmonic distortion.

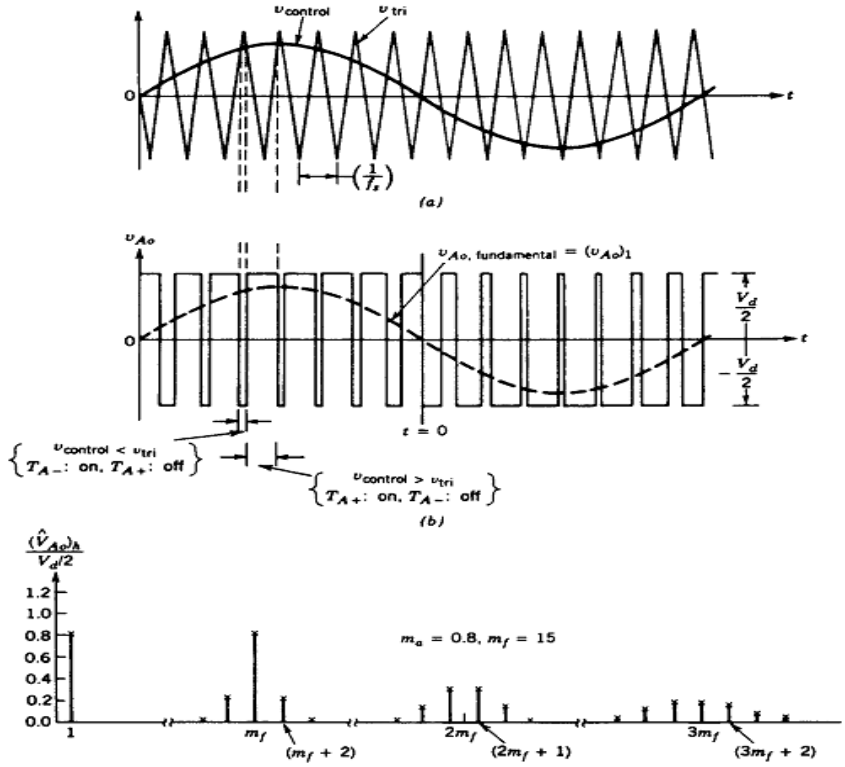

Fig. 2.14 *SPWM method*

2.3.3.2. Space Vector Modulation

In case of space vector modulation technique the complex reference voltage vector is processed as a whole. The switching vectors, the voltage reference and the boundaries between the controllable range, the six-step operation and overmodulation are shown in figure 2.15.

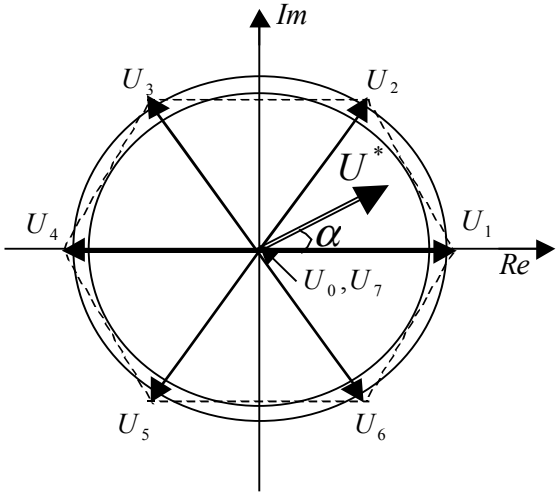

Fig. 2.15 *Voltage reference and switching-state vectors*

This technique averages the three switching-state vectors over a sub-cycle interval t_o = $1/2f_s$ to equal the reference vector $\mathbf{U^*(t_s)}$ as sampled at the beginning of the sub-cycle. The sampled value $\mathbf{U^*(t_s)}$ is used to solve the equations:

$$2f_s \cdot (t_a U_a + t_b U_b) = U^*(t_s)$$
$$t_0 = \frac{1}{2f_s} - t_a - t_b \qquad (2.87)$$

Where $\mathbf{U_a}$ and $\mathbf{U_b}$ are the two switching-state vectors adjacent in space to the reference vector $\mathbf{U^*}$. The solutions of (2.87) are the respective on-durations t_a, t_b, and t_o of the switching-state vectors $\mathbf{U_a}$, $\mathbf{U_b}$, $\mathbf{U_o}$:

$$t_a = \frac{3}{2\pi f_s} U^*(t_s)(\cos\ \alpha - \frac{1}{\sqrt{3}} \sin\ \alpha)$$
$$t_b = \frac{2\sqrt{3}}{2\pi f_s} U^*(t_s) \sin\ \alpha$$
$$t_0 = \frac{1}{2f_s} - t_a - t_b \qquad (2.88)$$

The angle α in these equations is the phase angle between the reference vector and $\mathbf{U_a}$. The zero vector is redundant. It can be either formed as $\mathbf{U_o}$(---) or $\mathbf{U_7}$(+++). Uo is preferred when the previous switching vector is $\mathbf{U_1}$, $\mathbf{U_3}$ or $\mathbf{U_5}$ while $\mathbf{U_7}$ will be chosen following $\mathbf{U_2}$, $\mathbf{U_4}$, $\mathbf{U_6}$. This ensures that only one half-bridge needs to commutate at a transition between an active switching-state vector and the zero vector.

2.3.3.3. Hysteresis Current Control

The behavior of this current controller can be explained in terms of the complex plane switching diagram in figure 2.16. The switching lines are located at a distance h, equal to the hysteresis band, from the tip of the current reference vector. The entire diagram moves with the current reference vector with its center remaining fixed at the tip of the vector.

The controller should confine operation into the hexagonal region. Whenever the actual current vector touches one of the switching lines, the respective inverter leg is switched driving the current error in the opposite direction. The current error can be carried to one of the switching lines by shifting of the current vector $\mathbf{I_{qds}}$ or the current reference vector $\mathbf{I_{qds}^*}$. In case a switching line is encountered because of the reference vector shift and the next applied switching vector is one of U_0, U_7 the system is short-circuited. During this period the motor is out of control. This problem can be overcome by incorporating a second threshold that senses when the boundary is being reached with the inverter in a state that would produce a short-circuited condition.

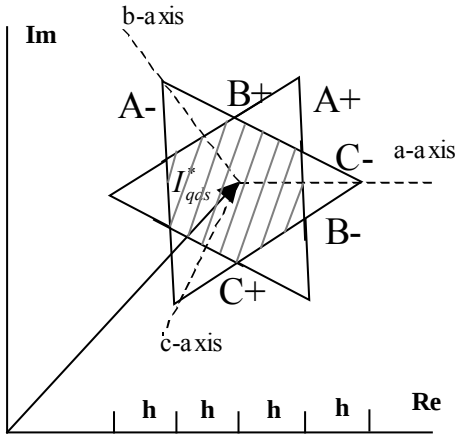

Fig. 2.16 *Switching diagram*

Hysteresis current control tends to lock into limit cycles of high switching frequency. This could be avoided by clocking and controlling the switching frequency. The modulation process generates subharmonics increasing the mechanical stresses and the possibility of undesirable mechanical resonances. Also, it does not adequately ensure the maintenance of the current inside the hysteresis band as a maximum error of twice the hysteresis band occurs on a random basis.

2.3.4. Power Converters Control

2.3.4.1. Grid side controller

The control of the active and reactive power flow to the grid is performed by the DC/AC converter. The general concept for the grid side converter control is shown in figure 2.17 The phasor diagram is also shown in the same figure. R_f, X_f are the resistance and reactance of the used filter, respectively. Because $R_f << X_f$ and δ is quite small for typical cases, active power injected to the grid is proportional to angle δ and reactive

power is proportional to the difference of the voltage amplitudes, $|V_{grid}-V_{conv}|$. In the case of a voltage source inverter, the controlled variables are the frequency ω_{conv} and the magnitude V_{conv} of the fundamental component of its AC voltage, which is synthesized by properly switching on and off its semiconductive elements. The relatively decoupled regulation of P and Q permits the implementation of the control principle schematically illustrated in figure 2.17. The active and reactive power regulation loops are independent but not fully decoupled. The first loop controls the active power injected to the grid, in order to maintain the dc voltage at its set value, $V_{dc,ref}$. In this case the control variable is the angular frequency of the grid-side converter, ω_{conv}. If the converter active output power exceeds the instantaneous supply of the energy source, the DC capacitor is discharged, and vice versa. The second control loop concerns the regulation of the reactive power exchanged with the network. An additional control loop for the network voltage amplitude regulation can be optionally included.

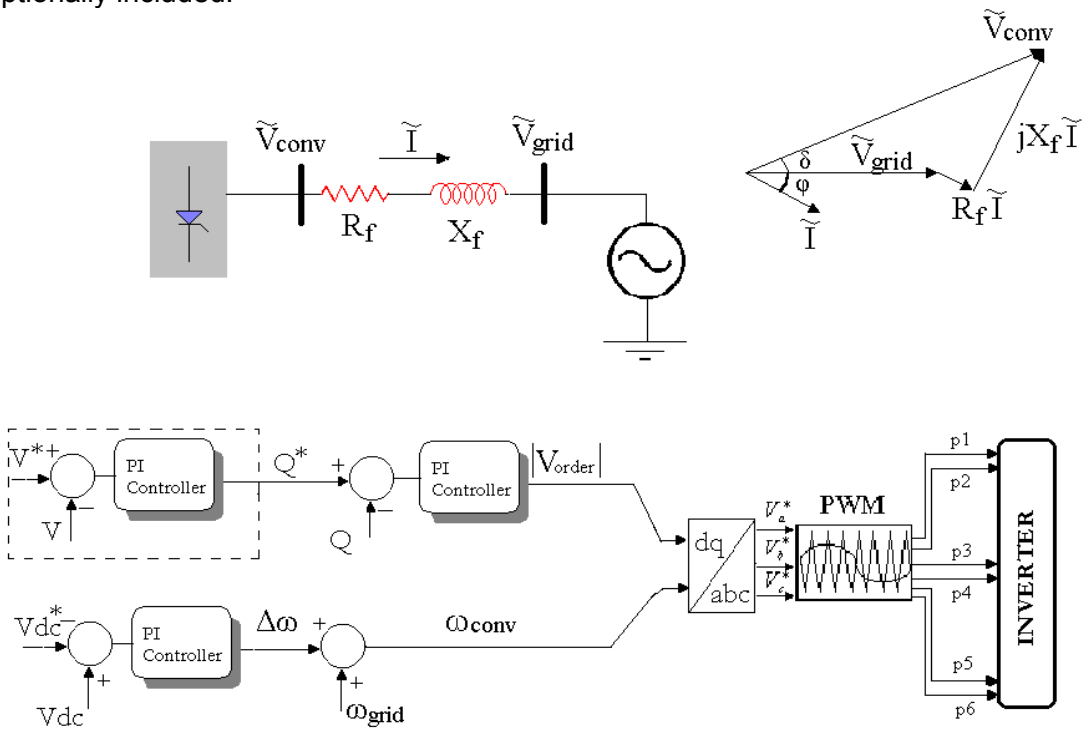

Fig. 2.17 *Grid-side converter controllers*

P* and Q* are the setpoints for the output active and reactive powers, P and Q, whereas the actual P and Q, along with the power angle δ, are calculated from measurements of the phase voltages and currents. The determination of the P* and Q* reference values depends on the specific application and installation considered. A usual practice is to utilize the Q* input in order to maintain constant output power factor (often unity, hence Q*=0). Alternatively, Q* may be varied in order to regulate -or simply support- the bus voltage at (or near to) the output of the converter, provided that the current rating of the converter permits it.

If the DC/AC converter is current controlled (which requires a relatively high switching frequency and is still not common at high power levels), then the full decoupling of the active and reactive power regulation loops can be easily achieved, employing the vector control principle, as shown in Figure 2.18

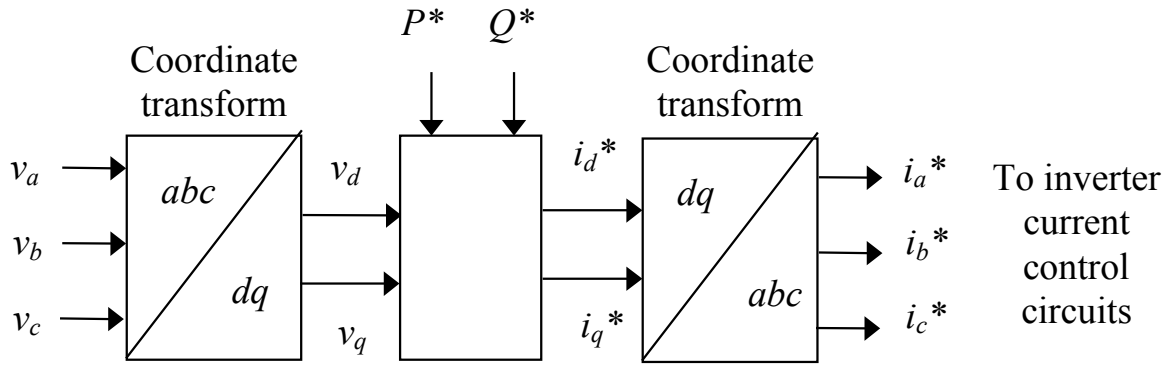

Fig. 2.18 *Active and reactive power regulation with a current controlled converter.*

For the fundamental frequency modeling of the converter system, the differential equations of the DC capacitor and the output inductances are used, along with the power balance equation of the DC/AC converter (input power = output power, if a lossless converter is assumed). In the case of a current controlled converter, the differential equations of the R-L filters are not required.

2.3.4.2. Induction Generator Controller

a) Vector Control

The vector control principle, which is increasingly used in practical applications, is schematically illustrated in Figure 2.19, where a current controlled converter has been assummed, although this is not necessarily the case. Using the coordinate transformation to the rotating flux reference frame, the decoupled control of the machine torque and flux levels can be achieved. Several variations of the vector control principle are encountered in the literature and in practice, requiring different modelling approaches.

In figure 2.20, another approach applied to a WT, is depicted. The control system comprises two control loops one for the blades rotating speed and the other for the rotor flux linkage. Indirect field-oriented voltage control is applied to the generator of the WT. Together with the current controller induction generator model is used for the determination of the current reference. The wind speed is measured and fed to the wind speed – blades optimal rotating speed characteristic, to produce the optimal rotating speed. The reference speed is produced by filtering the optimal rotating speed. Then the speed reference is input to the torque controller, as shown in figure 2.20. For low wind speed, maximum energy efficiency is achieved by tracking the reference rotating speed. At high wind speeds the control scheme imposes a constant rotating speed, taking advantage of the blades stall property for the limitation of the torque and the produced power below the design values. As mentioned before, the desired electromagnetic torque is achieved by the application of a field-orientation control scheme.

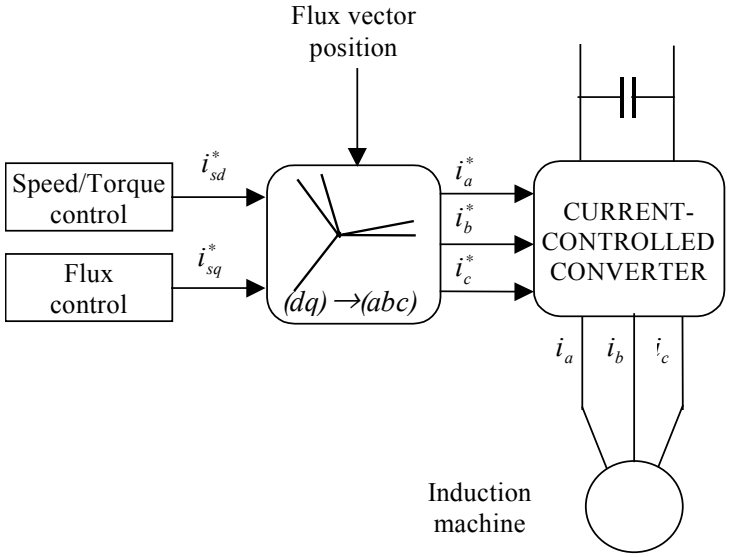

Fig. 2.19 *Vector control principle with a current controlled converter.*

The mathematical processing of vector control method is given next. Knowing the value of the desired electromagnetic torque, the q-axis current component in the field-oriented frame is given by the equation,

$$I_{qs}^{e*} = \frac{4 L_r^{'} T_{em}^*}{3 P L_m \lambda_{dr}^{'e*}} \tag{2.89}$$

It is also known that, when properly oriented, the slip speed and the dq-axis current components in the field oriented frame are related as,

$$\omega^* = \omega_e - \omega_r = \frac{r_r^{'}}{L_r^{'}} \frac{I_{qs}^{e*}}{I_{ds}^{e*}} \tag{2.90}$$

Rotor flux can be controlled by regulating I_{ds}^e. Given some desired level of the rotor flux, the desired value of the d-axis current component can be obtained from,

$$I_{ds}^{e*} = \frac{r_r^{'} + L_r^{'} p}{r_r^{'} L_m} \lambda_{dr}^{'e} \tag{2.91}$$

For the simulation of the whole system, the wind turbine drive train is modelled by a suitable mechanical equivalent (a single inertia if it is stiff, or a multi-inertia equivalent if elasticities are present and have to be taken into account). The rotor aerodynamic torque is usually calculated by its static aerodynamic power coefficient curves, although more elaborate models can be used if required. In the case of pitch controlled wind turbines, the pitch controller must be included in the simulation, since it affects significantly the dynamics of the system, particularly in the high wind region.

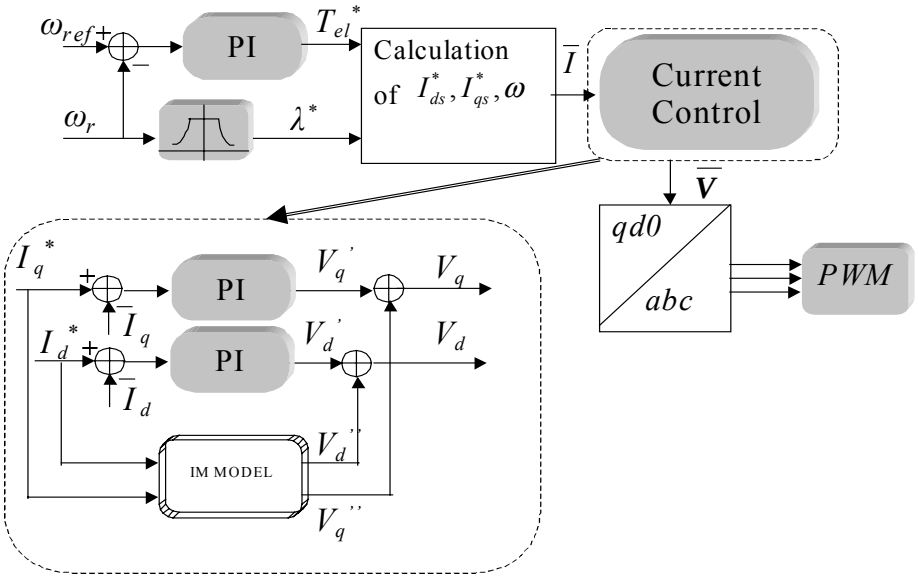

Fig. 2.20 *Indirect field-oriented voltage controllers*

Another option is to calculate the desired dq-axis voltages in the field-oriented frame using only the fourth order model of the induction machine. The major drawback of this control scheme is that it requires accurate knowledge of the machine parameters. It is commonly used with on-line parameter adaptive techniques for tuning the value of the parameters used in the indirect field controller, ensuring in this way successful operation. A modification of the method leads to the use of two PI controllers for the accurate tracking of the optimal dq-axis current and is depicted in figure 2.20. In case of stationary frame PI regulators a cross-coupling term is very useful. In the present study synchronous frame PI regulators are used, as shown in figure 2.20. In case of indirect field-oriented current controlled IM using hysteresis current control, the PI current controllers do not apply. The exact tracking of the reference value of the stator currents is ensured by the application of a hysteresis current control technique.

b) Scalar Control

In Figure 2.21 the simplified block-diagram of a typical scalar control system is shown. V_s and ω_e are the stator voltage and frequency, that is the magnitude and frequency of the inverter AC voltage. The frequency control subsystem basically consists of the PI speed controller. The rotor speed reference, ω_r^*, is externally determined by the optimal control characteristic of the turbine rotor. Output of the speed controller is the slip frequency, ω_{sl}, which is added to the rotor speed, to determine the stator frequency ω_e. For regulating the generator voltage, the constant V/f control principle is employed. It must be noted that practical control systems of this type may comprise several additional blocks (stabilizers, limiters etc.), which have to be included in the dynamic model of the system. For the simulation of the induction generator, the standard 4th order dq model is used.

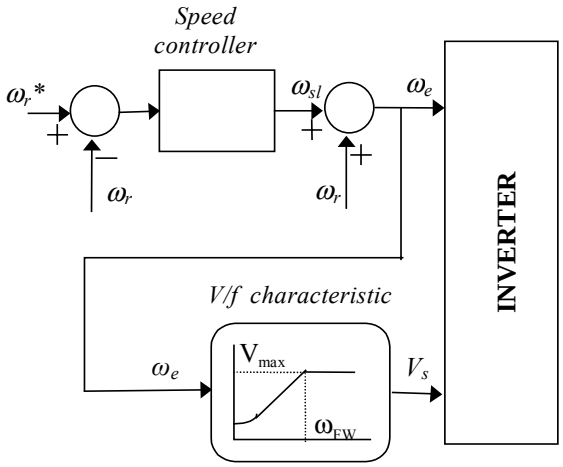

Fig. 2.21 *Scalar control system of the generator-side converter.*

3. Modelling the Energy sources

3.1. Wind Turbine

WTs comprise several subsystems that are modelled independently. These subsystems are the aerodynamic, the generator, the mechanical and the power converters in case of Variable Speed Wind Turbines (*VSWTs).* The models of each subsystem are described next.

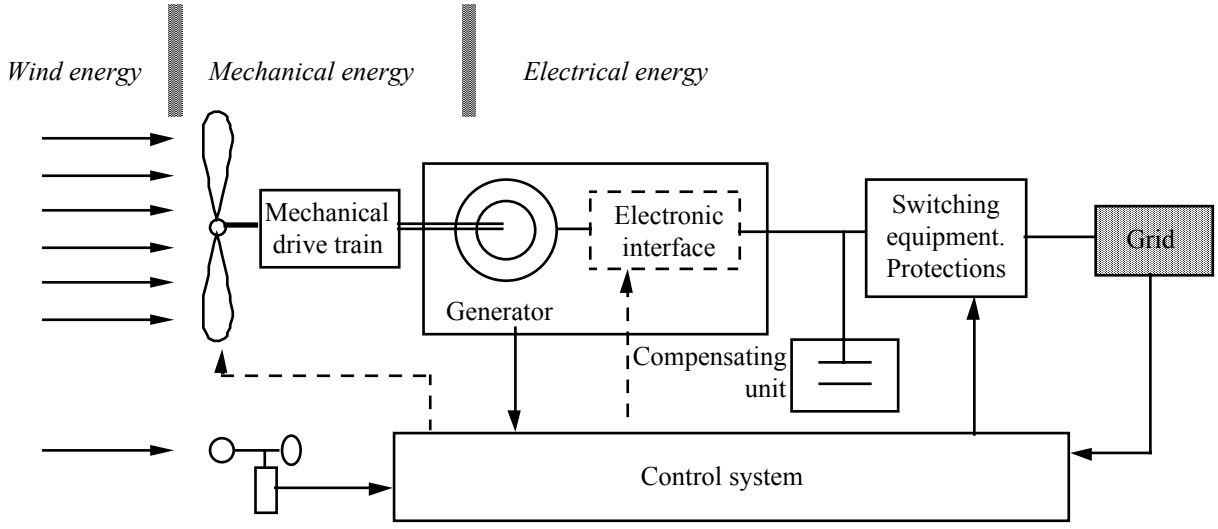

Fig. 3.1 *Wind Turbine Descrption*

3.1.1. Aerodynamic subsystem

The aerodynamic coefficient curves are used for the study of the blades dynamics:

$$P_{aer} = \omega_r \cdot T_w = \frac{1}{2}\rho \cdot A \cdot C_p(\lambda, \beta) \cdot V_w^{\ 3} \tag{3.1}$$

Where $C_p(\lambda,\beta)$ is the dimensionless performance coefficient, $A=\pi R^2$ the rotor area, λ the tip speed ratio, V_w wind speed, ω_r the blade rotating speed and T_w the aerodynamic torque.
The rotor mechanical torque can be calculated from P_{aer} by

$$T_w = \frac{P_w}{\omega_R} \tag{3.2}$$

where ω_R is the rotor angular velocity, in rad/sec.

The rotor aerodynamic power coefficient, C_p, is the percentage of the kinetic energy of the incident air mass that is converted to mechanical energy by the rotor, and it is expressed as a function

$$C_p = C_p(\lambda, \beta) \tag{3.3}$$

where β is the blade pitch angle and
λ is the tip speed ratio of the blade, defined as

$$\lambda = \frac{R\omega_R}{V_w} \tag{3.4}$$

Using the above relations and the rotor $C_p(\lambda)$ characteristic, the rotor aerodynamic torque and power curves can be calculated. These curves are shown in figure 3.2 for a stall regulated 140 kW WT. At low wind speeds, where the rotor torque and power do not exceed the rated values, the rotor speed is varied for optimal wind energy capture, i.e. for operation on the peak of the power curves (curve AB in figure 3.2). At higher winds, the speed is limited to its maximum value (52 rpm in figure 3.2) and the stall properties of the blades are used for limiting the torque and power below the design values (curve BC). Hence, the rotor speed control characteristic ABC is derived. Alternative speed control are also feasible from a static point of view. In practice, however, operation beyond the vertical line BC will result in significant over-torque and over-power situations in case of wind gusts, because the large inertia of the rotor does not permit the fast reduction of its speed, towards point C. In case of pitch controlled WTs, the above restriction may not be valid, because the pitch regulation may be used for limiting the rotor torque above the rated wind speed.

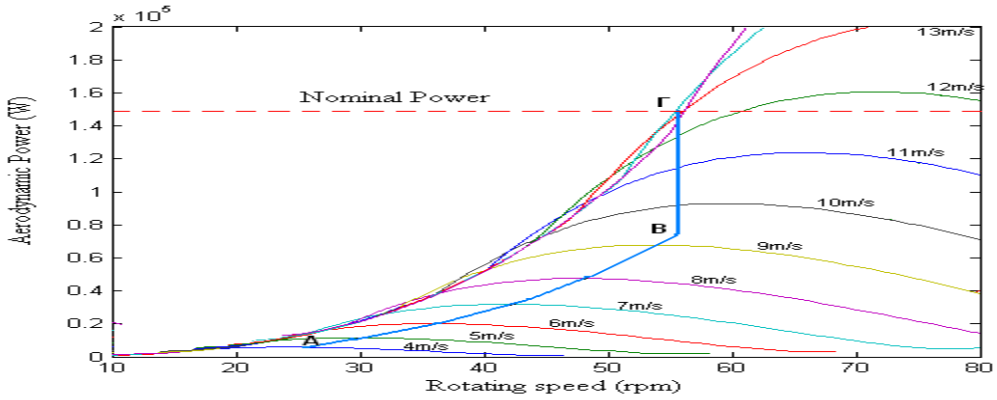

Fig. 3.2 *Rotor aerodynamic power vs. rotor speed curves, with the wind speed as a parameter.*

In order to reproduce the rotor aerodynamic torque harmonics (at frequencies nP, where P the rotor speed and n integer), due to the tower shadow and wind shear effects, each blade must be modelled independently. In this case, the above relations are applied for each individual blade, using the respective aerodynamic power coefficient C_p. For an n-blade rotor, the C_p of each blade can be taken equal to the 1/n of the rotor C_p. The tower shadow is approximated as shown in figure 3.3, by considering a near sinusoidal reduction of the equivalent blade wind speed, as each blade passes in front of the tower. ΔV_{sh} is the maximum wind speed reduction and 2θ the shadow angle.

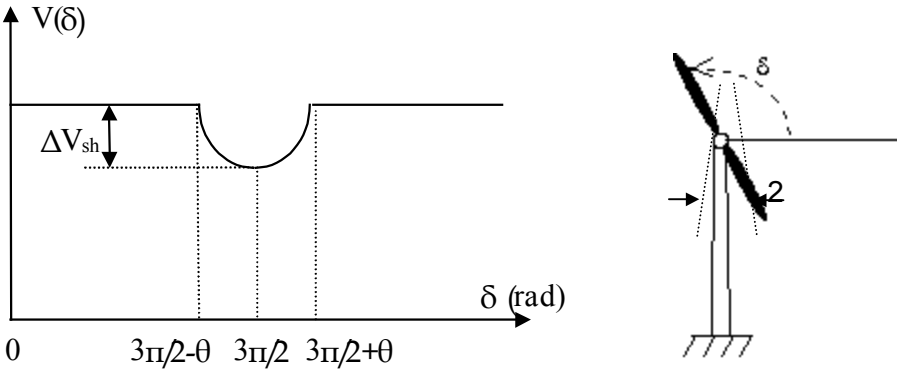

Fig. 3.3 *Tower shadow effect approximation.*

The wind shear effect is represented by the well known exponential law

$$\frac{V_w}{V_{wh}} = \left(\frac{z}{z_h}\right)^{\alpha} \tag{3.5}$$

where V_w is the wind speed at height z, V_{wh} the wind speed at the hub height z_h and α the shear exponent.

3.1.2. Mechanical subsystem

The equivalents of three or six elastically connected masses, shown in figure 3.4, can be optionally used for simulating the mechanical system of the *WT*. The use of at least

two masses is necessary for the representation of the low-speed shaft torsional mode. In case of the three connected masses the state space equations of the mechanical system are the following:

$$\frac{d}{dt}\begin{bmatrix}\theta\\ \omega\end{bmatrix}=\begin{bmatrix}[0]_{3\times3} & [I]_{3\times3}\\ -\frac{1}{2}[H]^{-1}[C] & -\frac{1}{2}[H]^{-1}[D]\end{bmatrix}\begin{bmatrix}\theta\\ \omega\end{bmatrix}+\begin{bmatrix}[0]_{3\times3}\\ \frac{1}{2}[H]^{-1}\end{bmatrix}T \tag{3.6}$$

In case of the three elastically connected masses $\theta^T=[\theta_{\mathrm{R}},\theta_{\mathrm{GB}},\theta_{\mathrm{G}}]$ is the angular position vector, $\omega^T=[\omega_{\mathrm{R}},\omega_{\mathrm{GB}},\omega_{\mathrm{G}}]$ is the angular speed vector and $T^T=[T_W,0,T_G]$ is the external torque vector comprising the aerodynamic and the electromagnetic torque, T_w and T_G, acting on the turbine and generator rotor, respectively.

$[0]_{3x3}$ and $[I]_{3x3}$ are the zero and identity 3x3 matrices, respectively

$[H]=diag(H_R,H_{GB},H_G)$ is the diagonal 3x3 inertia matrix

$$[C]=\begin{bmatrix}C_{HGB} & -C_{HBG} & 0\\ -C_{HBG} & C_{HBG}+C_{GBG} & -C_{GBG}\\ 0 & -C_{GBG} & C_{GBG}\end{bmatrix}$$

C is the the 3x3 stiffness matrix and D is the damping matrix. C matrix represents the low and high-speed shaft elasticities

$$[D]=\begin{bmatrix}D_R+d_{HGB} & -d_{HGB} & 0\\ -d_{HGB} & D_{GB}+d_{HGB}+d_{GBG} & -d_{GBG}\\ 0 & -d_{GBG} & D_G+d_{GBG}\end{bmatrix}$$

D is the 3x3 damping matrix and represents the internal friction and the torque losses.

while subscripts *{gb}, {g}* denote gear-box and generator, respectively.

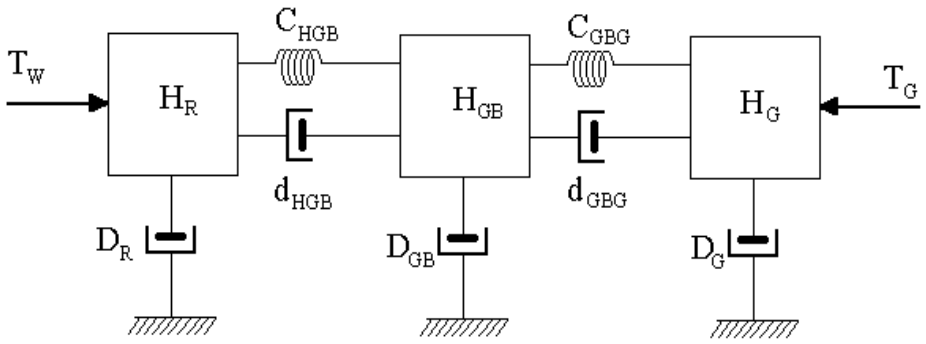

(a)

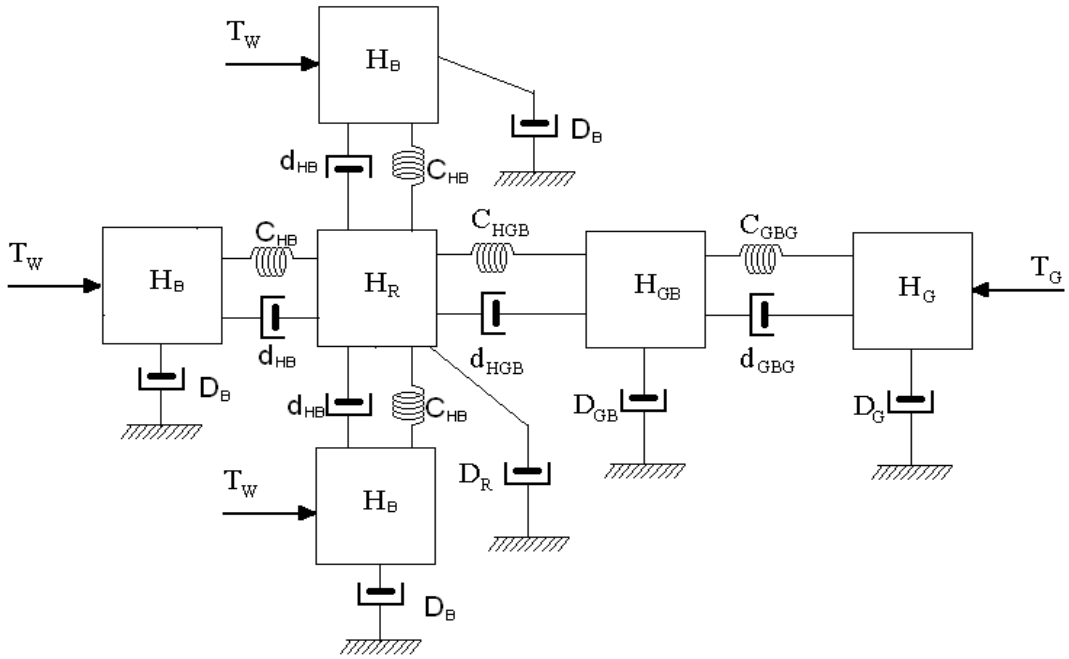

(b)

Fig. 3.4 *(a) 3-mass (b) 6-mass drive train mechanical equivalents (for a 3-blade rotor)*

The state equations of the 6-mass mechanical equivalent of figure 4(b) are the following:

$$\frac{d}{dt}\begin{bmatrix}\underline{\theta}\\ \underline{\omega}\end{bmatrix}=\left[\begin{array}{c|c}[0]_{6x6} & [I]_{6x6}\\ \hline -[2H]^{-1}[C] & -[2H]^{-1}[D]\end{array}\right]\begin{bmatrix}\underline{\theta}\\ \underline{\omega}\end{bmatrix}+\begin{bmatrix}[0]_{6x6}\\ [2H]^{-1}\end{bmatrix}\underline{T} \tag{3.7}$$

where

$\underline{\theta}^{\mathrm{T}}=[\theta_{B1},\theta_{B2},\theta_{B3},\theta_H,\theta_{GB},\theta_G]$ is the vector of the angular positions of the blades, hub, gearbox and generator

$\underline{\omega}^{\mathrm{T}}=[\omega_{B1},\omega_{B2},\omega_{B3},\omega_H,\omega_{GB},\omega_G]$ is the vector of the angular velocities of the blades, hub, gearbox and generator

$\underline{T}^{T}=[T_{W1},T_{W2},T_{W3},0,0,T_G]$ is the vector of the external torques, acting on the turbine blades (aerodynamic torques $T_{W,i}$, i=1,2,3) and on the generator rotor (electromagnetic torque T_G), conventionally accelerating

$[0]_{6x6}$ and $[I]_{6x6}$ is the zero and identity 6x6 matrices, respectively

$[H]=diag(H_B,H_B,H_B,H_H,H_{GB},H_G)$ is the diagonal 6x6 inertia matrix

$$[C]=\begin{bmatrix} C_{HB} & 0 & 0 & -C_{HB} & 0 & 0 \\ 0 & C_{HB} & 0 & -C_{HB} & 0 & 0 \\ 0 & 0 & C_{HB} & -C_{HB} & 0 & 0 \\ -C_{HB} & -C_{HB} & -C_{HB} & C_{HGB}+3C_{HB} & -C_{HBG} & 0 \\ 0 & 0 & 0 & -C_{HGB} & C_{HGB}+C_{GBG} & -C_{GBG} \\ 0 & 0 & 0 & 0 & -C_{GBG} & C_{GBG} \end{bmatrix}$$

is the 6x6 stiffness matrix, where C_{HB}, C_{HGB} and C_{GBG} respectively are the blade to hub, hub to gearbox and gearbox to generator stiffness coefficients

$$[D]=\begin{bmatrix} D_B+d_{HB} & 0 & 0 & -d_{HB} & 0 & 0 \\ 0 & D_B+d_{HB} & 0 & -d_{HB} & 0 & 0 \\ 0 & 0 & D_B+d_{HB} & -d_{HB} & 0 & 0 \\ -d_{HB} & -d_{HB} & -d_{HB} & D_H+d_{HGB}+3d_{HB} & -d_{HBG} & 0 \\ 0 & 0 & 0 & -d_{HGB} & D_{GB}+d_{HGB}+d_{GBG} & -d_{GBG} \\ 0 & 0 & 0 & 0 & -d_{GBG} & D_G+d_{GBG} \end{bmatrix}$$

is the 6x6 damping matrix, where d_{HB}, d_{HGB} and d_{GBG} are the relative dampings of the elastic couplings and D_B, D_H, D_{GB}, D_G the external damping coeffients

3.2. The Photovoltaic Plants

3.2.1. Solar cell characterisation

I-V Characteristic

Fig 3.5 shows the I-V characteristic of the solar cell for a certain ambient irradiation G_a and a certain fixed cell temperature T_c.

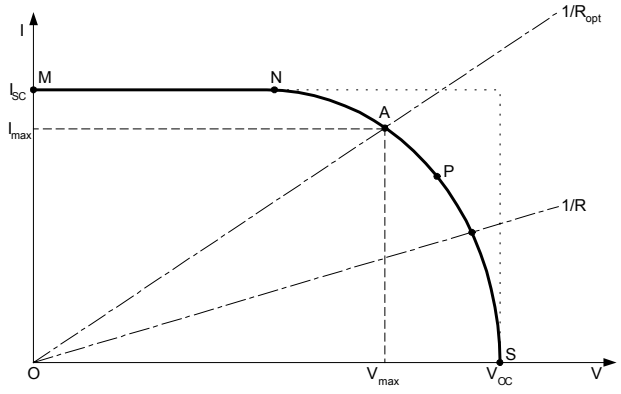

Fig. 3.5 *A typical current-voltage I-V curve for a solar cell*

In the representation of I-V characteristic, a sign convention is used, which takes as positive the current generated by the cell when the sun is shining and a positive voltage is applied on the cell's terminals.

If the cell's terminals are connected to a variable resistance R, the operating point is determined by the intersection of the I-V characteristic of the solar cell with the load I-V characteristic. For a resistive load, the load characteristic is a straight line with a slope I/V=1/R. It should be pointed out that the power delivered to the load depends on the value of the resistance only. However, if the load R is small, the cell operates in the region MN of the curve, where the cell behaves a constant current source, almost equal to the short circuit current. On the other hand, if the load R is large, the cell operates on the region PS of the curve, where the cell behaves more as a constant voltage-source, almost equal to the open-circuit voltage.

Fundamental parameters

A solar cell can be characterised by the following fundamental parameters, which are also sketched in ***Fig*** 3.5:

(a) Short circuit current: $I_{SC}=I_{ph}$. It is the greatest value of the current generated by a cell. It is produced under short circuit conditions: V=0.

(b) Open circuit voltage: corresponds to the voltage drop across the diode (p-n junction), when it is traversed by the photocurrent I_{ph} (namely $I_D=I_{ph}$), namely when the generated current is I=0. It reflects the voltage of the cell in the night and it can be mathematically expressed as:

(c)

$$V_{OC} = m \cdot \frac{k \cdot T_c}{e} \cdot \ln\left(\frac{I_{ph}}{I_0}\right) = V_t \cdot \ln\left(\frac{I_{ph}}{I_0}\right) \tag{3.8}$$

where $V_t = m \cdot \frac{k \cdot T_c}{e}$ is known as thermal voltage and T_c is the absolute cell temperature.

(d) Maximum power point: is the operating point A (V_{max}, I_{max}) in Figure 3.5, at which the power dissipated in the resistive load is maximum:

$$P_{max} = I_{max} \cdot V_{max} \tag{3.9}$$

(e) Maximum efficiency: is the ratio between the maximum power and the incident light power:

$$\eta = \frac{P_{max}}{P_{in}} = \frac{I_{max} \cdot V_{max}}{A \cdot G_a} \tag{3.10}$$

where G_a is the ambient irradiation and A is the cell area

Fill factor: is the ratio of the maximum power that can be delivered to the load and the product of ISC and VOC:

$$FF = \frac{P_{max}}{V_{OC} \cdot I_{SC}} = \frac{V_{max} \cdot I_{max}}{V_{OC} \cdot I_{SC}} \tag{3.11}$$

The fill factor is a measure of the real I-V characteristic. Its value is higher than 0.7 for good cells. The fill factor diminishes as the cell temperature is increased.

Influence of ambient irradiation and cell temperature in the I-V Characteristic

In Fig 3.6 and Fig 3.7, an I-V characteristic of a solar cell for only a certain ambient irradiation G_a and only a certain cell temperature T_c is illustrated.

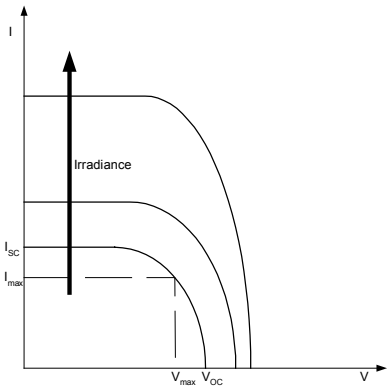

Fig. 3.6 *Influence of the ambient irradiation on the cell characteristics*

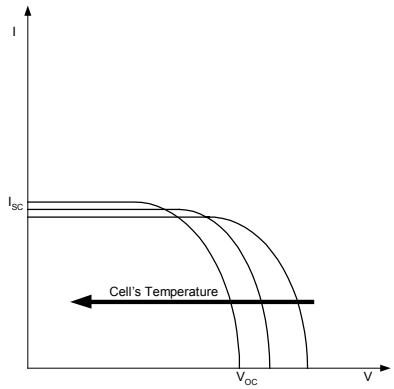

Fig. 3.7 *Influence of the ambient irradiation on the cell characteristics*

The influence of the ambient irradiation G_a and the cell temperature T_c on the cell characteristics is also shown in Fig and Fig. The arrow shows in which sense the irradiation and the cell temperature, respectively, increase.

The influence of the ambient irradiation on the I-V characteristics is illustrated in Fig 3.6. It shows that the open circuit voltage increases logarithmically with the ambient irradiation, while the short circuit current is a linear function of the ambient irradiation.

The influence of the cell temperature on the I-V characteristics is illustrated in Fig 3.7. The dominant effect with increasing cell's temperature is the linear decrease of the open circuit voltage, the cell being thus less efficient. The short circuit current slightly increases with cell temperature.

3.2.2. Solar cells grouping

Series and parallel grouping

The power output from single PV cells is relatively small (approximately 0,5 Watts). To produce the required voltage and power, PV cells are connected in series and parallel.

Fig 3.8 and Fig. 3.9 represent how the I-V curve is modified in the case when two identical cells are connected in series and in parallel.

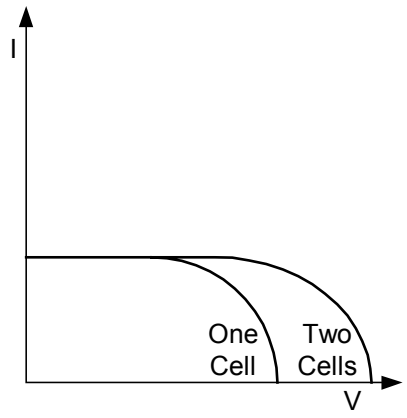

Fig. 3.8 *Series connection of identical cells.*

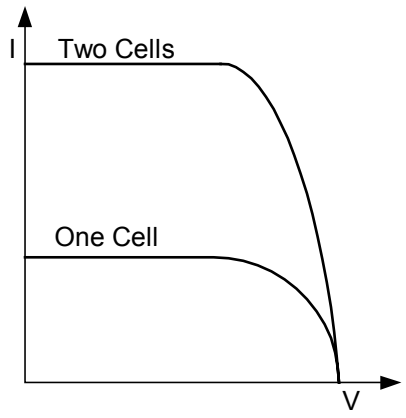

Fig. 3.9 *Parallel connection of identical cells.*

It is seen that I-V characteristics of series interconnected cells can be found by adding, for each current, the different voltages of the individual cells. On the other hand, for parallel cells the currents of the individual cells must be added at each voltage in order to find the overall I-V curve.

So, connecting cells in series will increase the voltage output, and the connecting cells in parallel will increase the current output.

PV Modules

PV cells are groped into modules, which are encapsulated with various materials to protect the cells and the electrical connectors from the environment the smallest unit available from manufacturers.

The manufacturers supply PV cells in modules, consisting of N_{PM} parallel branches, each with N_{SM} solar cells in series, as shown in
Fig 3.10.

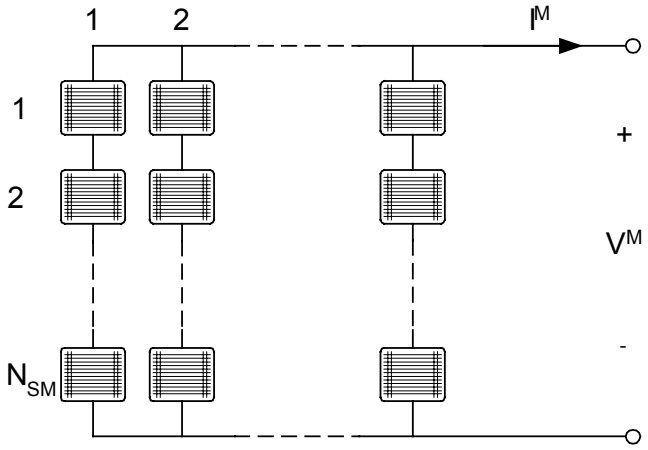

Fig. 3.10 *The PV module consists of N_{PM} parallel branches, each of N_{SM} solar cells in series.*

The module characteristics supplied by the manufacturer are determined under nominal or standard conditions, see
Table 3.1.

Nominal Conditions		Standard Conditions	
Irradiation	$G_{a,ref}$ = 800 W/m^2	Irradiation	$G_{a,0}$ = 1000 W/m^2
Ambient temperature	$T_{a,ref}$ = 20 ºC	Cell temperature:	T_0^C = 25 ºC
Wind speed	WS = 1 m/s		

Table 3.1: *Nominal and standard conditions*

In order to have a clear specification of which element (cell or module) the parameters are regarding, the following notation is used from now on: the parameters with superscript "M" are referring to the PV module, while the parameters with superscript "C" are referring to the solar cell. Thus, the applied voltage at the module's terminals is denoted by V^M, while the total generated current by the module is denoted by I^M.

Under standard conditions (irradiation $G_{a,0}$ and cell temperature T_0^C), at least the following parameters are measured:

-the short circuit current for the module $I_{SC,0}^M$

-the open circuit voltage for the module $V_{OC,0}^M$

-the maximum power for the module $P_{max,0}^M$

Under nominal (reference) conditions the following parameters are delivered:

-the ambient irradiation $G_{a,ref}$

-the ambient temperature $T_{a,ref}$

-the temperature of the cell T_{ref}^C

PV Arrays

As manufacturers supply only a limited range of PV modules, when designing a PV project, modules are combined into panels and those panels are connected together to build up the entire PV array to generate the desired I-V characteristic.

Fig 3.11 illustrates the case of an array with M_P parallel branches each with M_S modules in series.

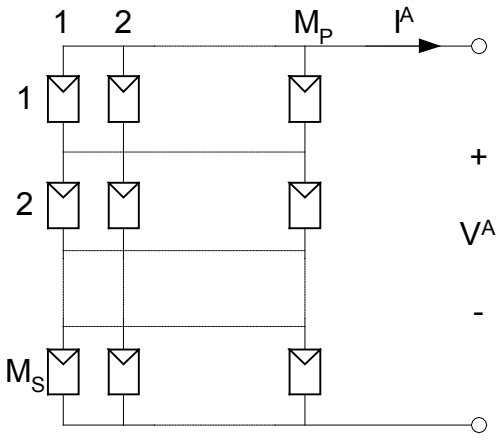

Fig. 3.11 *Solar cell array consists of M_P parallel branches, each with M_S modules in series.*

The applied voltage at the array's terminals is denoted by V^A, while the total current of the array is denoted by $I_A = \sum_{i=1}^{M_P} I_i$. If it is assumed that the modules are identical and the ambient irradiation is the same on all the modules, then the array's current is: $I_A = M_P \cdot I^M$

It is not possible to produce identical modules. In reality there will always be a difference between the overall value and the values of the parameters for each module. For production tolerances of +-5-10% however, the mismatch losses are not significant and the assumption of identical models is considered valid.

3.2.3. PV Array models

3.2.3.1. State of the Art

Many models of varying complexity describing the behaviour of a PV cell/module/array exist. To choose an appropriate model for simulation, several factors need to be considered.

The most important one is the accuracy, which can be obtained. There is always a trade-off between accuracy and simplicity. To minimise the computational effort which is involved in simulating microgrids the model should be kept as simple as possible without sacrificing the required accuracy.

In contrast to the utility grid, a PV cell/module/array is not a fixed voltage source. Simulation requires the model to be able to predict current and voltage over the entire operating voltage range. Some simplified models provide current-voltage behaviour just at maximum power, open voltage and short circuit current points.

Another factor is whether the data needed to drive the model is available, i.e. if data can be obtained in the relevant literature and/or manufacturers publications. Sophisticated models often require data which is generally not available.

Models available in the literature can be classified in the following two groups:

● **Analytical models.** They are based in the use of lumped circuits. There are two main lumped circuit models in use:

> **Single-diode models**: based on the modified Shockley diode equation adding a diode quality factor to account for the effect of recombination in the space-charge region.
>
> Particularly inaccurate in describing cell behaviour at low illuminations.

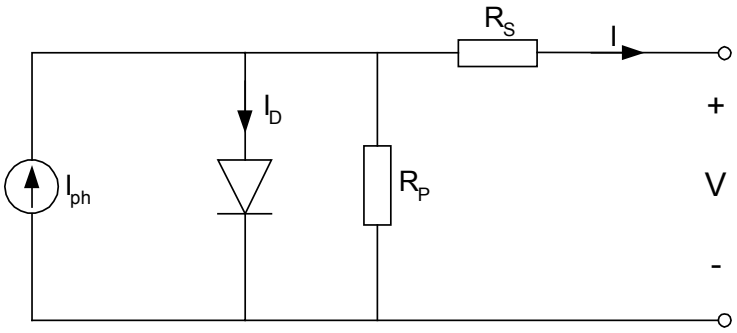

Fig. 3.12 *Single-diode model of a solar cell*

Double-diode models: they simulate the space-charge recombination effect by incorporating a separate current component with its own exponential voltage dependence.

It is a more accurate representation of solar-cell behaviour than single-diode models, particularly at low illuminations, where the recombination that is incurred by the second diode dominates.

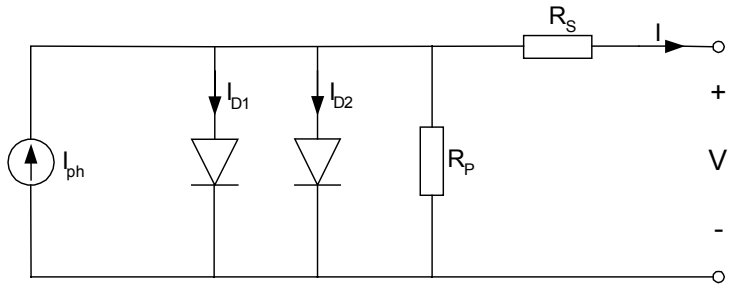

Fig. 3.13 *Double-diode model of a solar cell*

However, these circuit models are based on certain hypothesis that may not always be valid:

- material parameters are supposed to be insensitive to changes in either bias or illumination.
- minority-carrier concentrations at the edges of the space-charge regions are supposed to be dependent on the junction bias and independent of illumination

Considering these two suppositions to be true, the current flowing through the cell can be hypothesised to be a superposition of two currents, one due to junction bias and the other due to illumination.

But this hypothesis may not be accurate. However, the models generally fit experimental I-V characteristics quite accurately and provide a useful tool to characterise the solar-cell performance if their parameters can be determined simply and rapidly, associating them to manufacturing process parameters.

● **Empirical models.** The way to avoid the inaccuracies that can arise when using analytical models based in the hypothesis mentioned above, is to develop an empirical model based in experimental data. If the amount of data is huge enough, the resulting model will be very accurate, but this approximation requires a lot of experimental data.

3.2.3.2. Description of the Simplified Single Diode Model

A solar cell is represented by an electrical equivalent single-diode model as the one shown in
Fig 3.14:

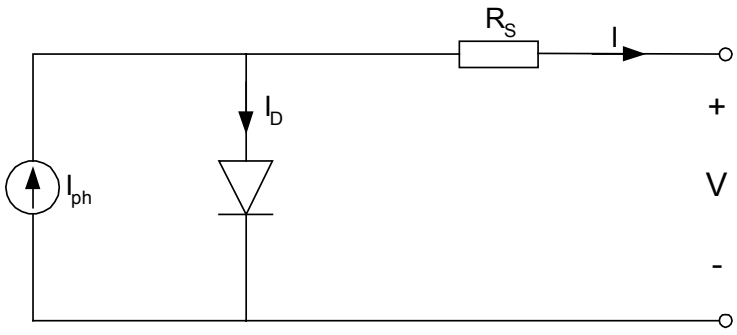

Fig. 3.14 *Simplified Single-diode model of a solar cell.*

The PV module's current I^M under arbitrary operating conditions can be described as:

$$I^M = I_{SC}^M \cdot \left[1 - e^{\frac{V^M - V_{OC}^M + I^M \cdot R_S^M}{V_t^M}} \right] \qquad (3.12)$$

The expression of the PV module's current I^M is an implicit function, being dependent on:

Parameter	Unit	Description
I^M	[A]	Module current.
V^M	[V]	Module voltage.
R_{SM}	[-]	Module series resistance.
I_{SC}^M	[A]	Short circuit current of the module.
V_{OC}^M	[V]	Open circuit voltage of the module.
V_t^M	[V]	Thermal voltage in the module.

Table 3.2 *Simplified Single Diode Model Parameters*

It has been reported that fitting the single-diode model to cell characteristics collected at low illuminations can result in negative series resistance values, while even at higher illuminations up to one sun, the use of the single-diode model can result in significantly different series resistance values. To solve this problem, when calculating the series resistance, it has been adopted the decision of taking the absolute value of it.
The model consists of the following I/O:

Inputs	Output
Ambient Temperature	Array Current
Solar Irradiance	
Array Voltage	

Ambient temperature and Solar Irradiance can be measured by a termometer and a pyranometer respectively. In case that theoric simulations are to be performed, some mean values have been provided in the attatched PV Parameter Database for some european cities.

Voltage will be an input from the MPPT control scheme embedded in the inverter.

3.2.3.3. Hypothesis

The model is based on the following hypothesis:

- All the cells of the module are identical and they work with the same irradiance and temperature.
- Voltage drops in the conductors that interconnect the cells are negligible.
- Short circuit current is affected only by the irradiance and temperature of the solar cells.
- Open circuit voltage of the cells depends exclusively on the temperature of the solar cells.
- Temperature of the solar cells depends exclusively on the irradiance and ambient temperature.
- Series resistance and diode quality factor of the cells are considered constant for all operating temperature and irradiance range.

3.2.3.4. Model Parameters

Parameter	Unit	Description
$I^{M}_{max,0}$	[A]	Module current at standard conditions.
$V^{M}_{max,0}$	[V]	Module voltage at standard conditions.
$P^{M}_{max,0}$	[W]	Module maximum power at standard conditions.
$I^{M}_{SC,0}$	[A]	Module short circuit current at standard conditions.
$V^{M}_{OC,0}$	[V]	Module open circuit voltage at standard conditions.
N_{SM}	[-]	Module number of cells in series.
N_{PM}	[-]	Module number of cells in parallel.
$NOCT$	[ºC]	Module normal operating cell temperature.
$\mu_{I_{SC}}$	[A/ºC]	Module short circuit current variation coefficient with temperature.
$\mu_{V_{OC}}$	[V/ºC]	Module open circuit voltage variation coefficient with temperature.
m	[-]	Module diode quality factor. If not known, use the following value: -In case of crystalline or multi-crystalline silicon solar cells, use 1.3 -In case of amorphous solar cells, use 2.

Table 2.3 *PV Module parameters for Microgrids Parameters Database*

All the parameters of the above table, except the diode quality factor, can be usually obtained from PV module manufacturer's datasheets.

3.2.3.5. Implementation Algorithm

The whole algorithm for the computation of the current of the PV module, under certain operating points (V^M, T_a, G_a) is shown below. The steps in the algorithm are as follows:

1) The required parameters are extracted from the Microgrids Parameters Database.

2) Once the PV module's data for standard conditions are available, the next step is to compute the cell's data for standard conditions:

$$V_{t,0}^C = m \cdot \frac{k \cdot T_{C,0}}{e} \quad , \quad V_{OC,0}^C = \frac{V_{OC,0}^M}{N_{SM}} \quad , \quad I_{SC,0}^C = \frac{I_{SC,0}^M}{N_{PM}} \tag{3.13}$$

3) Determination of module's series resistance:

$$R_S^M = R_S^C \cdot \frac{N_{SM}}{N_{PM}}$$

$$\begin{cases} P_{\max,0}^C = \dfrac{P_{\max,0}^M}{N_{SM} \cdot N_{PM}} \quad , \quad V_{\max,0}^C = \dfrac{V_{\max,0}^M}{N_{SM}} \quad , \quad I_{\max,0}^C = \dfrac{I_{\max,0}^M}{N_{PM}} \quad , \quad v_{OC,0} = \dfrac{V_{OC,0}^C}{V_{t,0}^C} \\ FF_0 = \dfrac{P_{\max,0}^C}{V_{OC,0}^C \cdot I_{SC,0}^C} \quad , \quad FF = \dfrac{v_{OC,0} - \ln\left(v_{OC,0} + 0{,}72\right)}{v_{OC,0} + 1} \\ r_s = 1 - \dfrac{FF}{FF_0} \quad , \quad R_S^C = \left|r_s\right| \cdot \dfrac{V_{OC,0}^C}{I_{SC,0}^C} \end{cases} \tag{3.14}$$

4) The next step is to determine the characteristic parameters of the module under the operating conditions (V^M, T_a, G_a).

   The working temperature of the cells T^C depends exclusively on the irradiance G_a and on the ambient temperature T_a, according to the empirical linear relation:

$$T_C = T_a + G_a \cdot \frac{NOCT - 20}{800} \tag{3.15}$$

   Thus, the short circuit current of the module I_{SC}^M is computed based on its dependency on the irradiance G_a and cell temperature:

$$I_{SC}^M = \frac{G_a}{G_{a0}} \cdot \left[I_{SC,0}^M + \mu_{I_{SC}} \cdot \left(T_C - T_{C,0}\right)\right] \tag{3.16}$$

   The open circuit voltage of the module depends exclusively on the temperature of the solar cells:

$$V_{OC}^M = V_{OC,0}^M + \mu_{V_{OC}} \cdot \left(T_C - T_{C,0}\right) \tag{3.17}$$

   The thermal voltage of the module is:

$$V_t^M = N_{SM} \cdot m \cdot \frac{k \cdot T_C}{e} \tag{3.18}$$

5) Once the steps (3) and (4) are completed, the final step is to determine the module's current for operating conditions:

$$I^M = I_{SC}^M \cdot \left[1 - e^{\frac{V^M - V_{OC}^M + I^M \cdot R_S^M}{V_t^M}} \right] \tag{3.19}$$

6) Once the module's current and voltage for operating conditions have been determined, the current and voltage of the PV Array are calculated:

$$I^A = N_{PA} \cdot I^M$$
$$V^A = N_{SA} \cdot V^M \tag{3.20}$$

3.2.4. Overview of Grid-Connected PV Plants

A grid-connected PV Plant consists of the following components as shown in figure 3.15:

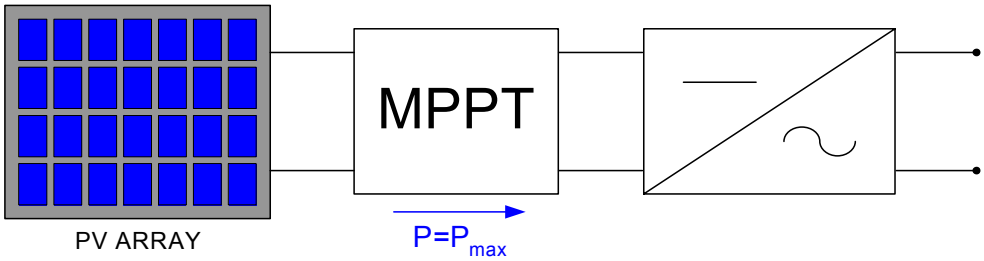

Fig. 3.15 *Grid-Connected PV Plant*

● **PV Array:** A PV Array is a grouping of PV modules in series and/or in parallel, being a PV module a grouping of solar cells in series and/or in parallel.

● **MPPT: Maximum Power Point Tracker.** For a given irradiance and temperature value, a PV Array has an I-V characteristic curve as shown in figure 3.16. So, it can generate power in any of the points of the curve, between the open circuit and short circuit points. The MPPT is used to assure that the PV Array generates the maximum power for all irradiance and temperature values.

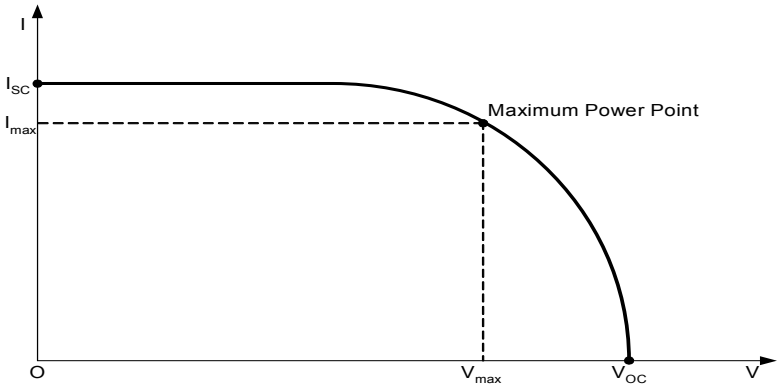

Fig. 3.16 *A typical I-V curve for a PV Array*

● **Inverter:** It converts the generated DC power to AC power.

3.2.5. PV Array with Integrated MPPT model

3.2.5.1. Description

This is a very simple model that considers that the PV Array is working always in its maximum power point for given temperature and irradiance conditions.

The model consists of the following I/O:

Inputs	Output
Ambient Temperature	Array Maximum Power
Solar Irradiance	

3.2.5.2. Hypothesis

The model is based on the following hypothesis:

- All the cells of the PV Array are identical and they work with the same irradiance and temperature.
- No losses in the PV Array with MPPT system
- The PV Array is always working on its maximum power point for given irradiance and ambient temperature conditions.
- If irradiance and ambient temperature conditions change, the model instantaneously changes its maximum power point.
- Temperature of the solar cells depends exclusively on the irradiance and ambient temperature.

3.2.5.3. Model Parameters

Parameter	Unit	Description
$P^{M}_{max,0}$	[W]	Module maximum power at standard conditions.
$NOCT$	[ºC]	Module normal operating cell temperature.
$\mu_{P_{Max}}$	[W/ºC]	Module power variation coefficient with temperature.
N	[-]	Number of modules of the PV Array

Table 3.3 *PV Module parameters for Microgrids Parameters Database*

All the parameters of the above table can be usually obtained from PV module manufacturer's datasheets.

3.2.5.4. Implementation Algorithm

The whole algorithm for the computation of the current of the PV module, under certain ambient conditions (T_a, G_a) is shown below. The steps in the algorithm are as follows:

1) The required parameters are extracted from the Microgrids Parameters Database.

2) A PV module's power is computed based on its dependency on the irradiance Ga and cell temperature as shown in equation 3.21 below:

$$P_{Max}^{M} = \frac{G_a}{G_{a,0}} \cdot \left[P_{Max,0}^{M} + \mu_{P_{Max}} \cdot \left(T_M - T_{M,0} \right) \right] \quad (3.21)$$

Parameter	Units	Description
P_{Max}^{M}	[W]	PV Module Maximum Power
$P_{Max,0}^{M}$	[W]	PV Module Maximum Power at standard conditions
$G_{a,0}$	[W/m^2]	Irradiance at standard conditions (1000 W/m^2)
$\mu_{P_{Max}}$	[W/ºC]	Maximum Power variation with module temperature
T_M	[ºC]	Module Temperature
$T_{M,0}$	[ºC]	Module Temperature at standard conditions

3) The working temperature of a PV module T_M depends exclusively on the irradiance G_a and on the ambient temperature T_a, as shown in equation 3.22 below:

$$T_M = T_a + G_a \cdot \frac{NOCT - 20}{800} \quad (3.22)$$

Parameter	Units	Description
T_M	[ºC]	Module Temperature
T_a	[ºC]	Ambient Temperature
G_a	[W/m^2]	Irradiance
$NOCT$	[ºC]	Normal Cell Operating Temperature

4) Substituting equation 3.22 in equation 3.21 and multiplying by, the number of modules of the plant, we obtain the power output of the PV plant in equation 3.23 below:

$$P_{Max} = N \frac{G_a}{1000} \left[P_{Max,0}^{M} + \mu_{P_{Max}} \cdot \left(T_a + G_a \cdot \frac{NOCT - 20}{800} - 25 \right) \right] \quad (3.23)$$

3.3. Fuel Cells

3.3.1. Fuel Cell Modelling

3.3.1.1. Introduction

The fuel cell technology is one of the most promising new electric's power technologies currently undergoing development. Fuel cell power systems have attracted attention

because of their potential for high efficiency, low emissions, flexible use of fuels, and quietness.

Fuel cells have currently three main applications:

- transportation where they are expected to replace on the long term combustion engines
- power applications where their main competitor in their privileged power range are gas turbines
- portable applications as a dramatically different option than micro-batteries based on Ni or Li.

The state-of-the-art has evolved to the point that fuel cell manufacturers hope to begin marketing fuel cells in just a few years. Full-scale demonstration plants are currently being designed all around the world. In addition, stationary applications of fuel cells are being targeted for every sector of the world energy market, from small residential co-generators to large central power generating stations. The application range includes:

- On-site systems from some Watts to MW´s.
- Distributed and substation systems ranging from kW´s to MW´s.
- Central stations of several hundred MW´s.

As a last point, long life reliable fuel cells constitute the basis of a hydrogen economy that is hoped to be the energetic revolution for this century. The production of hydrogen on a renewable basis and the utilization of this hydrogen in fuel cells promises a clean power source that could be implemented in many places, either as grid connected source or for stand alone applications or small grids.

The best way to generate H_2 and O_2 for these cases is known as the electrolytic water decomposition so-called “electrolysis”. In industrial plants, the alkaline medium is preferred to acid water, because corrosion is more easily controlled and cheaper construction materials can be used compared to acidic electrolysis technology. Other methods of hydrogen production, such as proton exchange membrane electrolysis, steam electrolysis have been developed in recent years. Hydrogen can also be generated as a by-product during the chore-alkali production.

It should be born in mind that Fuel Cells systems and Electrolyser systems are direct current machines and are relatively complex processes, depending on pumps, blowers, electro valves heat exchangers, pressure regulators and so on. Therefore, although these machines are often compared to simple “battery” systems, the response time of such machinery is typically in the ‘couple of seconds’ range and not in the micro- or millisecond range.

3.3.1.2. Fuel Cell Classification

Fuel Cells are well known devices to transform chemical energy into chemical energy by an electrochemical cycle rather than a thermal cycle and, are not subjected to the Carnot cycle limitations of thermal machines, thus offering the potential for very high conversion efficiencies. In the tables hereunder, the nowadays existing fuel cells are presented:

Temperature	Stack Type	Description
Low temperature FC	AFC	**Alkaline Fuel Cell** AFCs were the first fuel cells to be widely used for space applications. Their electrolyte consits of potassium hydroxide at different concentration and different temperature. Their fuel is pure hydrogen
	PEMFC	**Proton Exchange Membrane Fuel Cell** PEMFCs contain an electrolyte that is a layer of solid polymer (usually Nafion®). The polymer electrolyte allows protons to be transported from one half cell to the other. PEMFCs require a limited operating temperature and an accurate control of fuel humidity. PEMFCs are mainly supprted by the transportation sector
	DMFC	**Direct Methanol Fuel Cell** DMFCs are PEMFCs for which the fuel is methanol instead of hydrogen. Methanol delivers directly hydrogen ions on the anode and these protons transfer through the PEM electrolyte towards the cathode.
	PAFC	**Phosphoric Acid Fuel Cell** The PAFC is the most mature fuel cell technology. It uses a 100 % concentrated phosphoric acid (H_3PO_4) electrolyte retained on a silicon carbide matrix. PAFCs can be used for co-generation due to their higher operating temperature (200 °C typically)
High temperature FC	MCFC	**Molten Carbonates Fuel Cell** MCFCs operate at high temperature where the alkali carbonates from a highly conductive molten salt with carbonate ions (CO_3^{2-}) provide ionic conduction through the electrolyte matrix. MCFCs exhibit higher efficiency and greater fuel flexibility that make them a good candidate for combined heat and power generation.
	SOFC	**Solid Oxide Fuel Cell** Operates at high temperature (800 to 1000°C) with a ceramic electrolyte (e.g. zircon oxide). It can be fuelled with a variety of gases.

Table3.4 *Overview and brief description of existing Fuel Cell types*

	AFC	PEMFC	DMFC	PAFC	MCFC	SOFC
Electrolyte	KOH (liquid)	Proton exchange membrane (solid)	Proton exchange membrane (solid)	H_3PO_4 (liquid)	Molten carbonates (liquid)	Ceramic (Solid)
Temperature	60-90	0-80	60 -130	130-220	650	750-1050
Operating Pressure	1 – 1,1	1 – 5 bar		1 – 8 bar	1 – 3 bar	1 - 15 bar
Fuel	Purest H_2	Pure H_2	CH_3OH + H_2O	H_2, littleCO CH_3OH	H_2, CO CH_4	H2, CO CH_4
Poisons	CO_2, H_2S, CO	CO, H_2S	X-OH	CO, H_2S	S, H_2S, HCl, HI, HBr	H_2S
Construction Materials		Graphitic Carbon		Graphitic Carbon	Ni & Stainless Steel	Ceramics and Metals
Charge carrier	OH^-	H^+	H^+	H^+	CO_3^{2-}	O^{2-}

External reformer for CH_4		Yes	Yes	Yes	No Not necessarely	No Not necessarely
Prime cell components		Carbon-based	Carbon-based	Graphite-bessel	Stainless steel	Ceramic
Catalyst	Ag	Pt	Pt	Pt	Nickel	Perovkites
Product water	Mixed with electrolyte	Evaporative	Evaporative	Evaporative	Gazeous	Gaseous
Power Density pounds/kW		DOE Goals 8-10		~25	~60	~40
Heat Rejection (kWt/kW)		~0.48 @ 0.8 V		~0.55 @ 0.74 V	~0.25 @ 0.8 V	~0.52 @ 0.6 V
Product heat		cooling medium	cooling medium	Process gas + cooling medium	Internal reforming + process gas	Internal reforming + process gas
Efficiency	55-60 %	40% (CH_4) 60 % (H_2)	32-40%	36-45%	50-60%	50-55%
Power range (kw)	1-250	1-250	1-100	100-11k	2.2k	50k-100k
Applications	Space Portable Transport	Space Portable Transport Stationnary	Portable Transport	Transport Stationnary	Transport Stationnary	Transport Stationnary
Fuel Requirements	Sensitive to CO, Needs pure O,	Sensitive to CO				
CO		Poison		Poison at > 3%	Fuel	Fuel
CH_4		Diluent		Diluent	Fuel	Fuel
NH_3		Poison		Poison	Diluent	Fuel
Cl_2		Poison		Poison	Poison	Poison ?
S_2		Poison		Poison	Poison	Poison
Maturity	1970	2010	Undefined	1990	Undefined	2015
Special Problems		Moisture control in the membrane		High-voltage Operation	High fuel utilization	High fuel or oxidant utilization

3.3.1.3. Hydrogen Production and Electrolyser Classification

Fuel Cell need hydrogen to function. Hydrogen can be produced either by reforming Hydrocarbons (more than 80 % of the world production) or by electrolysis (less than 20 % of the world production). Hydrocarbon reforming is the preferred way of hydrogen production due to the energy efficiency and cost.
However, electrolysis is a very elegant way to produce hydrogen by means of renewable energies (PV, Windfarms, Hydro electricity) because excess electricity can be transformed into hydrogen (and oxygen) with very high efficiencies by means of electrolysis.

Different methods for reforming coexist:

- Cracking of hydrocarbons such as natural gas, naphta, diesel or alcohols. The process is quite inefficient in terms of hydrogen production (since the syngas consists of hydrogen, CO, CO_2 and methane, typically with 10 to 15% CO). This reaction can be considered as the first step of a steam reformation.

- Oxidation of natural gas on carbon. The method is cheap and very exothermic, what could allow a co-generation, but the efficiency of this technology is also low.

- Steam reforming or water gas shift. $CH_4 + 2\ H_2O \Rightarrow 4\ H_2 + CO_2$ This reaction can take place on the syngas after cracking and uses different catalysts for the different temperatures because it takes place in sub-steps.

Following the reforming, a purification of the obtained gas must take place in order to have a "fuel cell grade" hydrogen i.e. in order to get a low CO content of the hydrogen

- Catalytic processing via methanisation or preferential oxidation for up to 10 kW applications
- Flow through a PSA (pressure swing adsorption) that is very expensive is only justified for hydrogen production of over 50 Nm^3/h
- Use of Pd membranes for applications between 10 and 50 kWe

3.3.2. Modelling of the SOFC system

This section describes the main electrochemical reactions that occur in the SOFC. In Ref. [31] it is assumed that the anode is supplied with H_2 only and the cathode with O_2 only, so that the only reaction that occurs in the fuel cell is:

$$H_2 + \frac{1}{2}O_2 \rightarrow H_2O \tag{3.24}$$

The potential difference between the anode and the cathode is calculated using the Nernst's equation and Ohms law:

$$V_{fc}^{r} = N_0 \cdot \left[E_0 + \frac{R \cdot T}{2 \cdot F} \left(\ln \frac{p_{H_2} \cdot p_{O_2}^{1/2}}{p_{H_2O}} \right) \right] - r \cdot I_{fc}^{r} \tag{3.25}$$

where: E_0 is the voltage associated with reaction free energy (V)

$p_{H_2}; p_{O_2}; p_{H_2O}$ are the partial pressures of the component (N/m^2)

N_0 is the number of cells

r is the electrical resistance of the fuel cell (Ω)

I_{fc}^{r} is the reaction current or the output current (A)

R is the universal gas constant (J/mol K)

T is the channel temperature (assumed constant) (K)

F is the Faraday's constant (Coulombs/mol)

The partial pressure of the components is related to its molar flow. This relationship is given by the ideal gas law:

$$p_i \cdot V_{ch} = n_i \cdot R \cdot T \tag{3.26}$$

where: V_{ch} is the volume of the channel (m^3)

n_i is the number of moles of the species *i* present (moles)

Therefore

$$\frac{dp_i}{dt} = \frac{R \cdot T}{V_{ch}} \cdot \frac{dn_i}{dt} \tag{3.27}$$

and

$$\frac{dn_i}{dt} = q_i^{ch} = \left(q_i^{in} - q_i^{r}\right) \tag{3.28}$$

Where, q_i^{in} is the element *i* flow of input

q_i^{r} is the element *I* flow that reacts

For the H_2 the value of q_i^{r} is:

$$q_{H_2}^{r} = \frac{N_0 \cdot I_{fc}^{r}}{2 \cdot F} = 2 \cdot K_r \cdot I_{fc}^{r} \tag{3.29}$$

The values of q^{r} for the other elements are obtained by the equation (3.24). So:

$$q_{O_2}^{r} = \frac{1}{2} q_{H_2}^{r} = K_r \cdot I_{fc}^{r} \tag{3.30}$$

$$q_{H_2O}^{r} = q_{H_2}^{r} = 2 \cdot K_r \cdot I_{fc}^{r} \tag{3.31}$$

Defining the U_f (fuel utilisation), as the ratio between the fuel flow that reacts and the input fuel flow, and assuming a typical use, between 80 and 90% as described in [31], the demand current of the fuel cell system can be restricted in the range given by:

$$\frac{0.8 \cdot q_{H_2}^{in}}{2 \cdot K_r} \le I_{fc}^{in} \le \frac{0.9 \cdot q_{H_2}^{in}}{2 \cdot K_r} \tag{3.32}$$

The optimal utilisation factor (U_{opt}) is assumed to be 85%, allowing the control of the input flow by the measure of the output current, so that:

$$q_{H_2}^{in} = \frac{2 \cdot K_r \cdot I_{fc}^{r}}{0.85} \tag{3.33}$$

The stoichiometric ratio of hydrogen to oxygen is 2 to 1. Oxygen excess is always taken in, to let hydrogen react with oxygen more completely. According to Ref. [31], under normal operation the value of r_{H_O} should be 1.145, in order to keep the fuel cell pressure difference below 4 kPa. So the input oxygen flow, $q_{O_2}^{in}$, is controlled to keep r_{H_O} at 1.145 by controlling the speed of the air compressor.

$$q_{O_2}^{in} = r_{H\_O} \cdot q_{H_2}^{in} \tag{3.34}$$

All the reactions that occur in the fuel cell had some time delay associated. The chemical response in the fuel processor is usually slow, as it is associated with the time to change the chemical reaction parameters after a change in the flow of reactants. This dynamic response function is modelled as a first-order transfer function with a 5s time delay constant (T_f). The electrical response time delay in the fuel cells is generally short and mainly associated with the speed at which the chemical reaction is capable of restoring the charge that has been drained by the load. This dynamic response function is also modelled as a first-order transfer function, but with a 0.8s time delay constant (T_e). The dynamic response function of the flow is also modelled as a first-order transfer function with the time delay constant of the respective element, τ_{H_2}, for the response time of Hydrogen flow, τ_{O_2} for Oxygen and τ_{H_2O} for water flow.

The peak power capacity is the ratio of maximum theoretical power delivery to the rated power in the fuel cell system. It is only determined with the available active fuel

cell area. For the highest possible total efficiency and the dynamic load-following behaviour, p_i should be as large as possible. As this value is directly proportional to the effective fuel cell area for a constant output, cost considerations restrict the upper value to values preferably between 130 and 180% [31]. In practice, this upper value is also restricted by the safety of system operation. In order to prevent damage to the electrolyte, the fuel cell pressure difference between the hydrogen and oxygen passing through the anode and cathode gas compartments should be below 4 kPa under normal operation and 8 kPa under transient conditions [31]. Because different fuel cell systems have different peak power capacity, by simulation it is shown that p_i in this fuel cell system should be below 170%, which means the maximum power that can be delivered by this fuel cell system is below 1.7 times of the rated power.

Through the power conditioner, the fuel cell system can output not only real power but also reactive power. Usually, the power factor can be in the range of 0.8-1.0. Because the response time of the power conditioner is generally less than 10 ms, it is not necessary to include its detailed model in our dynamic fuel cell system.

Figure 3.17 presents the corresponding block diagram of the dynamic model described. The power conditioner of this figure is represented by a simple power source.

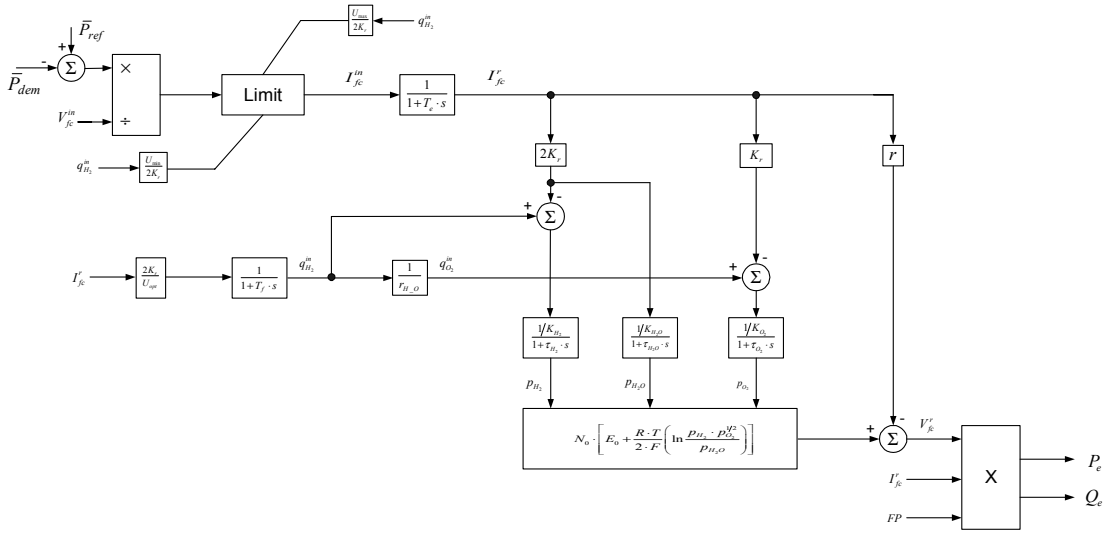

Fig. 3.17 *SOFC system dynamic model, from [31]*

3.3.2.1. Fuel cell Parameters

The parameters that correspond to a SOFC with a nominal power of 100 kW are described in the following table. These model parameters were updated from the Ref. [31].

Parameter	Representation	Value
P_{rate}	Rated power	100 kW
P_{ref}	Real power reference	100 kW
T	Absolute temperature	1273 K
F	Faraday's constant	96 487 C/mol
R	Universal gas constant	8314 J/(kmol K)

E_0	Ideal standard potential	1.18 V
N_0	Number of cells in series in the stack	384
K_r	Constant, $K_r = N_0/4F$	$0.996 \cdot 10^{-6}$ kmol/(s A)
$U_{\max}$	Maximum fuel utilization	0.90
$U_{\min}$	Minimum fuel utilization	0.80
U_{opt}	Optimal fuel utilization	0.85
K_{H_2}	Valve molar constant for hydrogen	$8.43 \cdot 10^{-4}$ kmol/(s atm)
K_{H_2O}	Valve molar constant for water	$2.81 \cdot 10^{-4}$ kmol/(s atm)
K_{O_2}	Valve molar constant for oxygen	$2.52 \cdot 10^{-3}$ kmol/(s atm)
τ_{H_2}	Response time for hydrogen flow	26.1 s
τ_{H_2O}	Response time for water flow	78.3 s
τ_{O_2}	Response time for oxygen flow	2.91 s
r or res	Ohmic loss	0.126 V
T_e	Electrical response time	0.8 s
T_f	Fuel processor response time	5.0 s
r_{H_O}	Ratio of hydrogen to oxygen	1.145
PF	Power factor	1.00

Table 3.5 *Fuel Cell Parameters*

3.4. Micro Turbines

3.4.1. State of the Art

Microturbines are small and simple-cycle gas turbines with outputs ranging typically from around 25 to 300 kW. They are part of a general evolution in gas turbine technology. Techniques incorporated into the larger machines, to improve performance, can be typically found in microturbines as well. These include recuperation, low NO_X emission technologies, and the use of advanced materials, such as ceramics, for the hot section parts [36]. There are essentially two types of microturbines. One is a high-speed single-shaft unit with a compressor and turbine mounted on the same shaft as the electrical synchronous machine. In this case turbine speeds mainly range from 50 000 to 120 000 rpm. The other type of microturbines is a split-shaft designed one that uses a power turbine rotating at 3000 rpm and a conventional generator connected via a gearbox.

3.4.2. Modelling the micro turbine system

In typical microturbine designs, this micro-generation system is composed of the following main parts:

- Turbine: The primary machine is a small gas turbine. There are two kinds of turbines, high-speed single-shaft turbines and split-shaft turbines.
- Electrical generator: In the single-shaft design, an alternator is directly coupled to the single shaft turbine. The rotor is either a two- or four-pole permanent magnet design, and the stator is a conventional copper wound design. In the split-shaft design, a conventional induction or synchronous machine is mounted on the power turbine via a gearbox.
- Power electronics: In the single-shaft design, the alternator generates a very high frequency three phase voltage ranging from 1500 to 4000 Hz. To allow grid interconnection, the high frequency voltage needs to be first rectified and then inverted to a normal 50 Hz voltage. In the split-shaft turbine design, power inverters are not needed.
- Recuperator: The recuperator is a heat exchanger, which transfers heat from the exhaust gas to the discharge air before it enters the combustor. This reduces the amount of fuel required to raise the discharge air temperature to that required by the turbine.
- Control and communication systems: Control and communication systems include full control of the turbine, power inverter and start-up electronics as well as instrumentation, signal conditioning, data logging, diagnostics, and user control communication.

Since in this research we are mainly interested in the dynamic performance of the network and not the fast transients that may happen, the microturbine model adopted is based on the following assumptions:
The recuperator is not included in the model as it is only a heat exchanger to raise engine efficiency. Also, due to the recuperator's very slow response time, it has little influence on the timescale of our dynamic simulations.
The gas turbine's temperature control and acceleration control are of no significance under normal system conditions. Therefore they can be omitted in the turbine model.
Next figure shows a simplified block diagram of a split-shaft design [31].

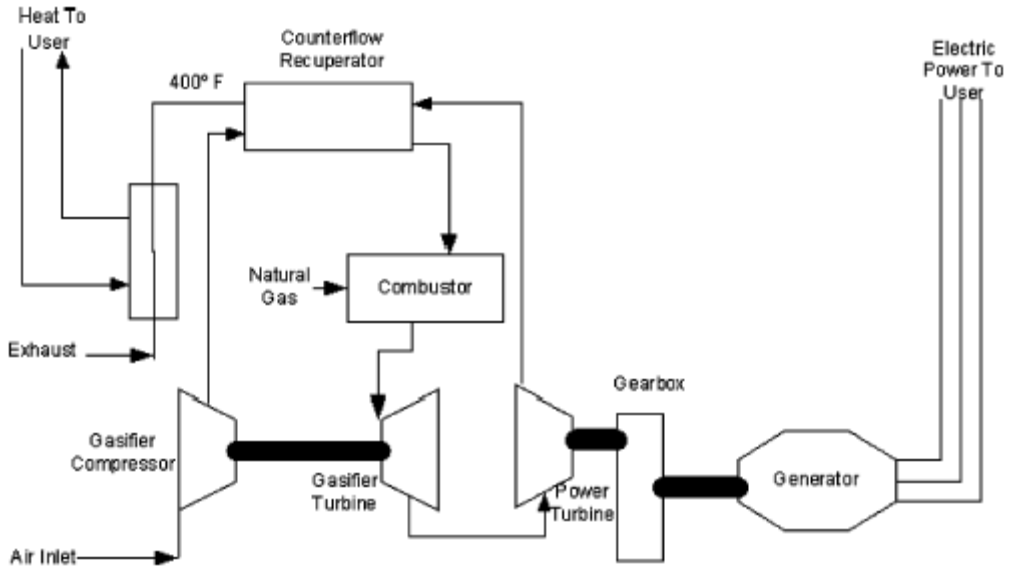

Fig.3.18 *PowerWorks microturbine diagram[31]*

A simplified block diagram for the microturbine for load following dynamic behaviour analysis purposes is shown in figure 3.19. The details of these control blocks with all parameters are given next.

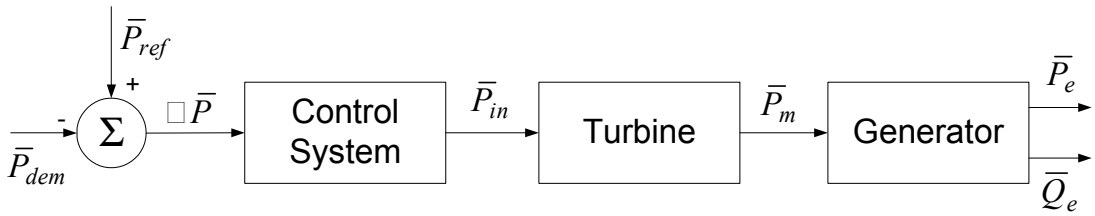

Fig. 3.19 *Main blocks in microturbine model*

3.4.2.1. Control systems

If load following control in the activated control function, the real power control can be described as a real power proportional-integral (PI) control function as in figure 3.20. The controlled real power Pin is then applied to the turbine.

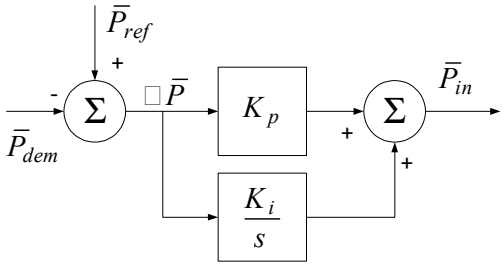

Fig. 3.20 *Load following control system model*

where: P_{dem} is the demanded power;
P_{ref} is the reference power;
P_{in} is the
K_p is the proportional gain in the PI;
K_i is the integral gain in the PI.

3.4.2.2. Turbine

In the split-shaft design, although there are two turbines, one is a gasifier turbine driving a compressor and another is a free power turbine driving a generator at rotating speed of 3000 rpm, there is only one combustor and one gasifier compressor. This is largely different from the twin-shaft combustion-turbine, which has two combustors and two compressors [31]. So it is more suitable to model this split-shaft turbine as a simple-cycle, single-shaft gas turbine. The GAST turbine-governor model is one of the most commonly used dynamic model of gas turbine units [37]. The model is simple and follows typical modelling guidelines [31]. For simplicity and wider acceptability, the turbine part in this microturbine design is modelled as GAST model.

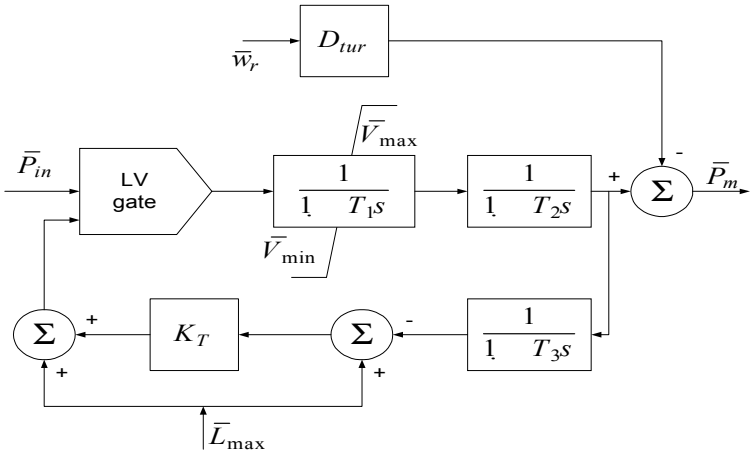

Fig. 3.21 *Turbine model*

Where P_m is the mechanical power;
D_{tur} is the damping of turbine;
T_1 is the fuel system lag time constant 1;
T_2 is the fuel system lag time constant 2;
T_3 is the load limit time constant
L_{max} is the load limit;
V_{max} is the maximum value position;
V_{min} is the minimum value position;
K_T is the temperature control loop gain.

3.4.2.3. Micro Turbine Parameters

The parameters that correspond to this model are described in the following table and numerical values for a 250 kW machine have been added for illustrative purposes.

Parameter	Representation	Value
P_{dem}	Demanded power	250 kW
V_{rate}	Rated voltage	660 V
P_{ref}	Real power reference (pu)	1.00
K_p	Proportional gain in PI	1.00
K_i	Integral gain in PI	1.08
D_{tur}	Damping of turbine	0.03
T_1	Fuel system lag time constant 1	10.0s
T_2	Fuel system lag time constant 2	0.10s
T_3	Load limit time constant	3.00s
L_{max}	Load limit	1.20
V_{max}	Maximum value position	1.20
V_{min}	Minimum value position	-0.10
K_T	Temperature control loop gain	1.00
H	Turbine inertia	8.22s
D_{gen}	Damping of generator	0.10
p	Number of poles	4.00

Table 3.7 *Microturbine Parameters*

4. Modelling the Storage Devices

It is a fact : very often the supply of Renewable Energy doesn't correspond with the demand and an Energy Storage System is required.

Several devices have been studied and developed in order to store energy :

- mechanical systems : flywheels
- pneumatically systems : compressed air
- thermal systems : hot water or oil in insulated reservoirs
- electrical systems : capacitors , "Supercapacitors"
- electrochemical systems : batteries, fuel cell

The energy storage system is a compromise between many options. It should have a low self-discharge for mid- and long-term storage. It should have an high overall efficiency, a high lifetime in unpredictable cycling conditions, able to slowly or fast deliver the energy. It should operate in a wide range of temperature, it should be safe with low maintenance, considered as non polluting and of course its cost should be as low as possible.

Today the most common technique for energy storage and especially in intermittent Renewable Energy applications is the electrochemical technology which is dominated by the familiar lead acid battery from its commencement in 1859.

4.1. Batteries

4.1.1. Overview of the LEAD-ACID Batteries

4.1.1.1. Definition and Components

A battery is a device that converts the chemical energy contained in its active materials directly into electric energy by means of an electrochemical oxidation-reduction (redox) reaction. This type of reaction involves the transfer of electrons from one material to another through an electric circuit. Although the term "battery" is often used, the basic electrochemical unit is the "cell". A battery consists of one or more of these cells, connected in series or parallel, or both, depending on the desired output voltage and capacity.

The cells consist of **three major components**, as shown schematically in Figure 4.1:

- **The anode** or negative electrode which gives up electrons to the external circuit and is oxidised during the electrochemical reaction.
- **The cathode** or positive electrode, which accepts electrons from the external circuit and is reduced during the electrochemical reaction.
- **The electrolyte** which provides the medium for transfer of electrons, as ions, inside the cell between the anode and cathode.

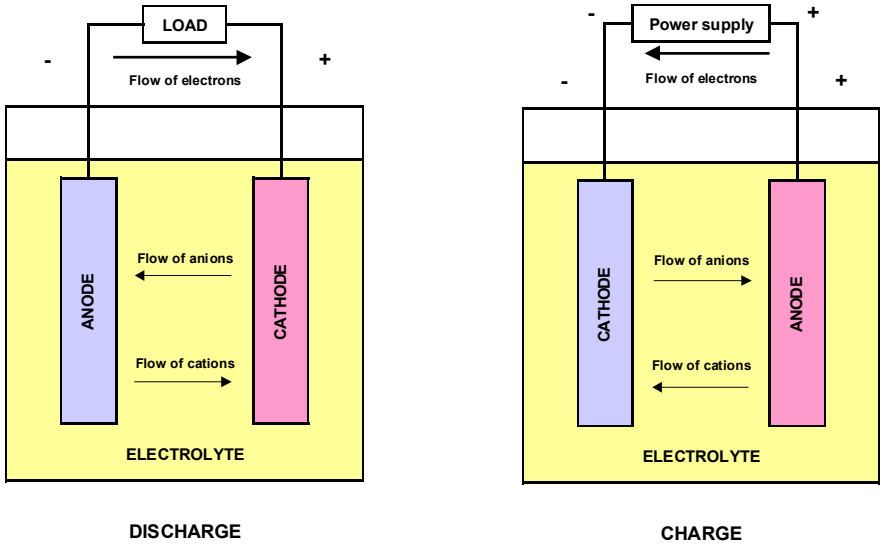

Fig. 4.1 *Electrochemical operation of a cell: a) discharge b) charge*

Physically the anode and cathode electrodes are electronically isolated in the cell to prevent internal short-circuiting, but are surrounded by the electrolyte. In practical cell designs a separator material is used to separate the anode and cathode electrodes mechanically. The separator, however, is permeable to the electrolyte in order to maintain the desired ionic conductivity.
The cell itself can be built in many shapes and configurations -cylindrical, button, flat and prismatic- and the cell components are designed to accommodate the particular cell shape.

4.1.1.2. Operation conditions

The operation of a cell during discharge is illsutrated in Figure 4.1(a). When the cell is connected to an external load, electrons flow from the anode, which is oxidised, through the external load to the cathode, where the electrons are accepted and the cathode material is reduced. The electric circuit is completed in the electrolyte by the flow of anions (negative ions) and cations (positive ions) to the anode and cathode, respectively.
During the recharge of a rechargeable or secondary battery, the current flow is reversed and oxidation takes place at the positive electrode and reduction at the negative electrode, as shown in Figure 4.1(b).

4.1.1.3. Chemistry of the lead-acid battery

The basic electrode reactions are both based on lead but on different states of oxidation.
The complete reactions at both electrodes involve the participation of the sulphuric acid used as electrolyte, which is converted into lead sulphate on both electrodes. For this reason, the chemistry of the lead-acid battery is known as the “double sulphate” reaction. The two electrode reactions results in the global cell reaction:

$$PbO2 + Pb + 2\,H2SO4 \underset{\text{charge}}{\overset{\text{discharge}}{\leftarrow\rightarrow}} 2\,PbSO4 + 2\,H2O \qquad (4.1)$$

When the lead-acid battery is discharged, lead (Pb) and lead dioxide (PbO2) are converted into lead sulphate (PbSO4) or, in other words, during discharge the sulphate of the sulphuric acid is absorbed into the electrodes. When the battery is charged, these reactions are reversed (see fig 4.2).

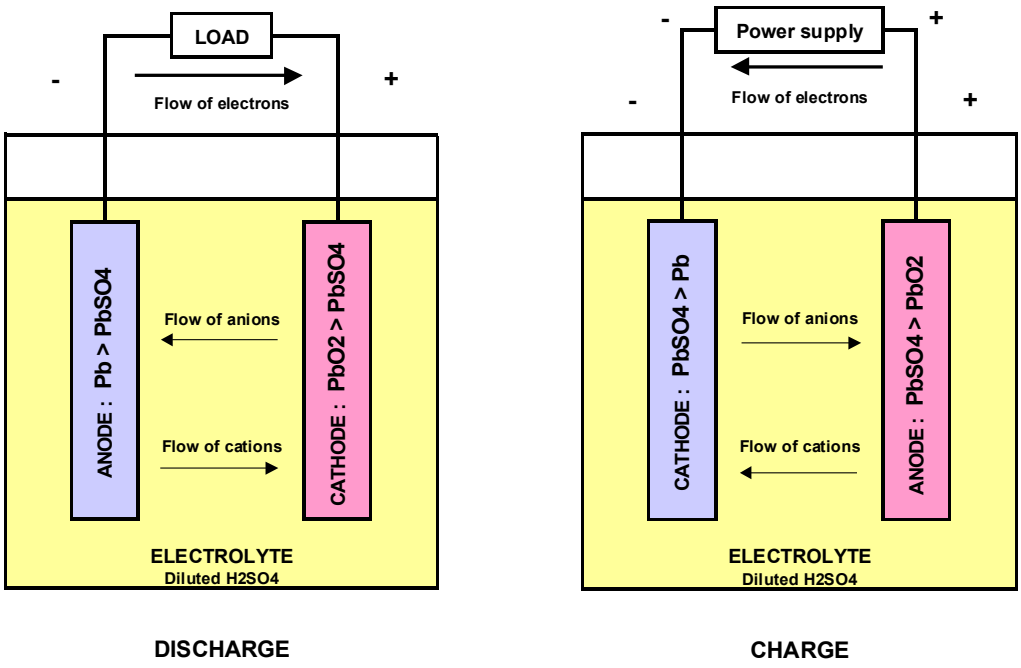

Fig. 4.2 *electrochemical reactions occuring during charge and discharge*

4.1.1.4. Batteries Classification

The lead acid batteries could be classified mainly in two technologies following the state of the electolyte :

- Flooded lead-acid batteries
- Valve-regulated lead-acid batteries (VRLA batteries)

Sub classification are also used such :

- shape of the positive electrode (flat / tubular / spiral plates)
- methods of fixing the electrolyte for VRLA batteries : AGM / Gel electrolyte

Since 1859 Researchers made of course a lot of improvements in the lead system and they have specialised designs with the demand.

4.1.1.5. Data and performance characteristics

System Voltage

The rated voltage of a lead-acid cell is 2 volts.
The nominal voltage of battery is then **Nx2V** where N is the number of cells connected in series.
The open circuit voltage gives a rough estimation of the state of charge of the battery. It is mainly a function of the specific gravity of the electrolyte and the temperature. The output voltage and particularly the final discharge voltage shall be limited according to the discharge rate, in order to avoid battery deterioration and hazards. The input voltage during charge can be summarised for stationary applications in the following curves:

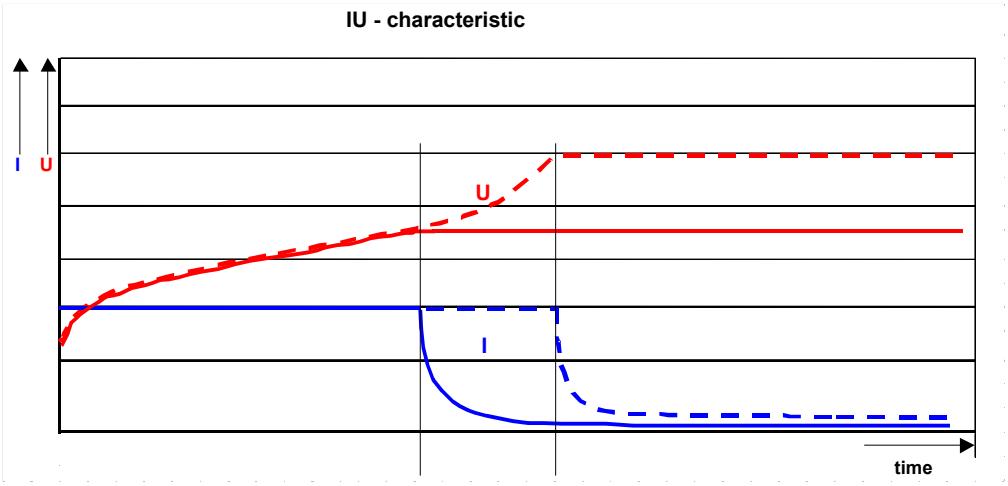

Fig. 4.3 *I-U vs time during recharge*

Range of capacities

Usually the capacity of a battery is defined by the quantity of Ah that the battery is able to release after a charge. It depends of the current applied to the battery during the discharge as well as the final voltage according to values given by the manufacturer.
The influence of the temperature on the battery capacity is usually expressed as following:

$$C_{25^oC} = \frac{C_{t^oC}}{1 + 0.0008\left(t^oC - 25\right)} \quad (4.2)$$

Energy and power density

Based on a nominal voltage of 2 volts the theoretical energy density of the lead system is 167 Wh / kg. Nevertheless, the comparison should include electrolyte, current collectors, containers, lids, terminals, weight or volume of all external devices that are needed to enable power supply such as reservoirs, filters pumps converters to get an electricity to electricity system. Therefore energy density of the lead storage system depends on the battery design and technology. Usually the energy density of the tubular technology concerning photovoltaic applications is about 35 Wh / kg.

The power density is an open notion and it can be heard a lot of things.
Based on a discharge of 10 sec. at room temperature and a final voltage of 3/4 U° lead acid systems are able to supply 400 W/kg.

Cycling service and lifetime

Battery type	Lifetime	
	Number of cycles (deep DOD)	Number of years
Lead-acid, pasted	300-750	3-7
Lead-acid, tubulaire	1200-1800	5-15
Lead-acid, Planté or lead-calcium	1000-1500	12-25

Table 4.1 *Lifetime of different battery types*

The lifetime of the batteries depends of the DOD of the cycles the battery sees during its life. The deepper the cycles are, the shorter the battery life is.
The service life depends also of the temperature : the warmer room temperature is, the shorter the battery life is.

Faradic and energy efficiency

The faradic efficiency is the ratio between the Ah discharged and the Ah recharged.

Ah-efficiency = Discharged Ah / Recharged Ah

The common faradic efficiency varies from 95 % to 83 %.

The energy efficiency depends on the current efficiency of the electrode processes and the overpotentials involved in both discharge and charge reactions as well as the battery resistance. It will depend on the rate of charge and discharge.

SOC (%)	Energy efficiency (Wh/Wh) (%)
50	78
75	75

Table 4.2 *Influence of the rate of discharge and the depth of the previous discharge on the energy efficiency*

Self-discharge

Self-discharge for lead-acid batteries is around 2 % per month @ 25°. It depends on temperature and battery technology.

Temperature

Lead acid systems are very tolerant with the temperature.
High temperatures increase the performances without charge problems but decrease its life. Low temperature reduce performances.
The usual operating temperature range for lead-acid batteries is –20°C to 45°C. In some cases the battery can be designed for –30°C or lower.

4.1.1.6. Technology developers and manufacturers

Here are some examples of companies producing lead-acid batteries:
- EnerSys Inc (Hawker / VB Baterrien / Oldham)
- Exide Technologies (Tudor / Fulmen / Sonnenschein / Chlorie Motive Power / Fulmen / CEAC)
- C&D Technologies
- Johnson Control : Hoppecke / Varta
- Fiamm
- Yuasa

4.1.1.7. Main conventional applications

The main field of applications are:
- automotive (Starting Lightening Ignition)
- traction
- stationary batteries

The electric vehicle might be the next possible market for lead batteries.

Example of stationary applications:

Company/localisation	Power/Energy	Type de fonction/Batterie	Starting year
Southern California Edison Chino, CA USA	10 MW / 40 MWh	Load leveling / **Lead-Acid (Open/vented)**	1988
Elektrizitätswerk Hammermuhle Selters, Germany	400 kW / 400 kWh	Load leveling / **Lead-Acid (Open/vented)**	1980
Puerto Rico El. Power Authority San Juan, Puerto Rico	20 MW / 14 MWh	Frequency regulation / **Lead-Acid (Open stirred e*lectrolyte)***	1993
GNB Industrial Power Metlakatla, AK USA	1 MW / 1.4 MWh	Load supply/ **Lead-Acid (Sealed, Valve Regulated)**	1997

4.1.1.8. Cost of the storage technology

Usually the cost of the lead-acid battery varies from 50 to 150 € / kwh, depending of the battery type.
As for a of a stand-alone energy system, storage may represent up to 50% of the total cost, mainly due to the maintenance and replacement of the battery during the system life.
Battery investment cost represent around 20% of the energy system investment cost.

4.1.1.9. Current knowledge on environmental issues of the storage technology

The dangerous materials inputs are lead and sulphuric acid. During manufacturing lead is dangerous in the first stage of the fabrication, acid emission is dangerous in the final stage: plates formation.
During operation, sulphuric acid is the main dangerous material, owing to its corrosive nature. In case when the battery room is not well ventilated, gases given off by vented lead-acid batteries on charge are explosive

4.1.2. Batteries Modelling

4.1.2.1. Description of the model

The lead-acid battery is a complex, non-linear electrochemical device. In order to develop a mathematical model that describes it, a lot of parameters should be taken into account. These parameters are needed to describe phenomena as water loss, ageing of the battery, gassing, self-discharge, heat evolution, electrolyte stratification, sulfation of the battery plates.

The model used here is based on the results obtained in [45]. It calculates the voltage and the remaining charge of the battery given the charge/discharge current and the battery temperature. Relations for obtaining the so-called “extracted charge”, the gassing and the self-discharge currents are needed. These equations are stated at the following section.

“Extracted Charge” - AhD

Instead of State of Charge (SOC) usually used in such models, another measure of the energy stored within the battery is adopted in this report, the “extracted charge”. That is the charge (i.e. number of Ah) that would have to be discharged from a fully charged battery to bring it to its current state of charge.

$$AhD = -\int (I - \max(I_{gas}, I_{SD}))dt + AhD_0 \quad (4.3)$$

Gassing Current - Igas

Gassing occurs in a lead-acid battery during charging when the battery is nearly fully charged. Gassing reaction consumes a potion of the charge current. The gassing current is calculated by

$$I_{gas} = \begin{cases} CK\tau_1 e^{\frac{V_{diff}}{\tau_3}} & V_{diff} \geq V_{tafel} \\ \frac{V_{diff}\left(CK\tau_1 e^{\frac{Vtafel}{\tau_3}}\right)}{V_{tafel}}\left(1-\frac{V_{diff}}{V_{tafel}}\right) + CK\tau_1 e^{\frac{V_{diff}}{\tau_3}}\left(\frac{V_{diff}}{V_{tafel}}\right) & 0 \leq V_{diff} \leq V_{tafel} \end{cases} \quad (4.4)$$

Where:

$$V_{diff} = \max(0, V - (\tau_2(1- CaTg(T-25))) \quad (4.5)$$

Self-Discharge Current I_{SD}

Due to internal mechanisms a battery undergoes a reduction in state of charge. Self-Discharge Current I_{SD} is used to describe this phenomenon. I_{SD} is calculated by

$$I_{SD} = (C - AhD)\left(\frac{-\ln(1-\beta_{SD}10^{m_{SD}T}}{720}\right) \quad (4.6)$$

Voltage of the battery

The cell voltage during discharging (*I* negative) can be described from the following equation:

$$V = DV_{oc} + \frac{\partial V_{oc}}{\partial T}(T-25) - DV_{slope}(1-AhR) + \frac{I}{DK_T}\left(\frac{DP_1}{1+(-I)^{DP_2}} + \frac{DP_3}{AhR0.0001^{DP_4}}\right)(1-DaTr(T-25)) \quad (4.7)$$

Where:

$$AhR = 1 - \frac{AhD}{CK} \quad (4.8)$$

and $DT_K = \text{DK}(1+\text{DaTc}(\text{T-25}))$ (4.9)

The partial derivative of the open circuit voltage with respect to temperature can be calculated based on a curve fit to data from reference [45].

Likewise, the cell voltage during charging (*I* positive) can be described from the following equation:

$$V = \min(V_{\max}, CV_{oc} + \frac{\partial V_{oc}}{\partial T}(T-25) + CV_{slope}AhC + \frac{I}{CK_T}\left(\frac{CP_1}{1+I^{CP_2}} + \frac{CP_3}{(1-AhC)^{CP_4}}\right)(1-CaTr(T-25)) \quad (4.10)$$

Where

$$V_{\max} = \tau_3 \ln\left(\frac{I}{CK\tau_1}\right) + \tau_2(1-CaTg(T-25)) \quad (4.11)$$

and $$AhC = 1 - \frac{AhD}{CK} \qquad (4.12)$$

Description of the parameters

I	current (negative for discharge and positive for charge), A
I_{gas}	gassing current, A
I_{SD}	self discharge current, A
t	time, hr
AhD	number of Ah
AhD_0	AhD at t = 0
AhR	useable amount of charge remaining during discharging, Ah
AhC	useable amount of charge remaining during charging, Ah
T	battery temperature, °C
DT_K	discharge capacity at temperature T
V_{max}	the maximum attainable voltage i.e. the voltage that would occur with all charge current being used in the gassing reaction, V
V_{diff},	the difference between the battery voltage and the voltage at the onset of gassing, V

The remaining parameters are fit parameters

4.1.2.2. Thevenin Battery Model

The Thevenin Battery Model is the best option for the task in hand. It provides a high degree of accuracy while maintaining simplicity. It is believed that this model could describe the electrical response of a battery rather accurately for a period of few minutes.

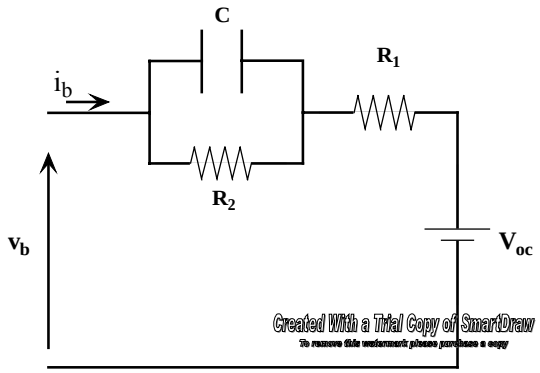

v_b = Battery voltage
i_b = Terminal current
R_1 = Internal resistance
V_{oc} = Open-circuit voltage

Over-voltage is represented by the parallel combination of R_2 and C

Fig. 4.4 *Thevenin Battery Model*

A major shortcoming of this model is that all circuit parameters are modelled as constants whereas they are functions of various battery conditions.

Short-term Discharge Model (from [48])

This model is based on the Thevenin model and is an improvement over it as circuit parameters have been modified to ensure higher accuracy with a parameter identification method.

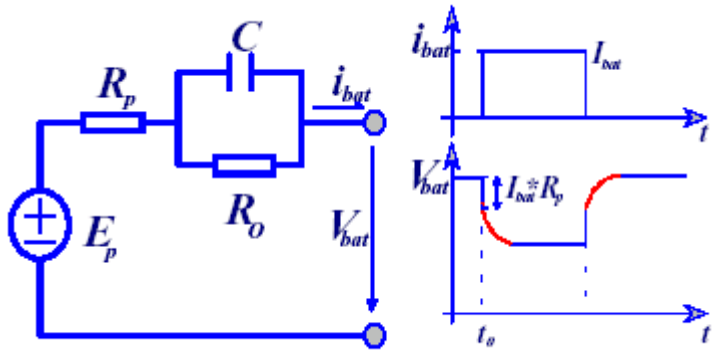

Fig. 4.5 *Equivalent circuit of the Short-term Thevenin-discharge Battery Model*

The parameters are

1. Resistance R_p representing ohmic polarisation (voltage drop due to the internal resistance)
2. Discharge over-voltage resistance R_o representing the charge transfer losses
3. Over-voltage capacitance C representing the double-layer effect dynamics
4. Open circuit electrochemical potential E_p representing the equilibrium *e.m.f.* of the battery under no load conditions

These strongly non-linear elements are dependent on the discharge rate, state of charge and temperature.

Assumptions

1. State Of Charge (SOC) is about 100%. [Battery is re-charged in the stand-by condition]
2. Temperature is constant during the period of discharge

Thus the discharge current is the main governing factor of the parameters [Please refer to Figures 4.4 (a), (b) and (c)]. The parameter values of a battery could be obtained from the measured battery output voltage during a series of step-load tests on it.

A typical lead-acid battery dynamic response to a step load can be described by

$$V_{bat} = E_p - I_{bat} \times (R_p + R_o) + I_{bat} \times R_o \times \exp\left(-t / R_o \times C\right) \quad (4.13)$$

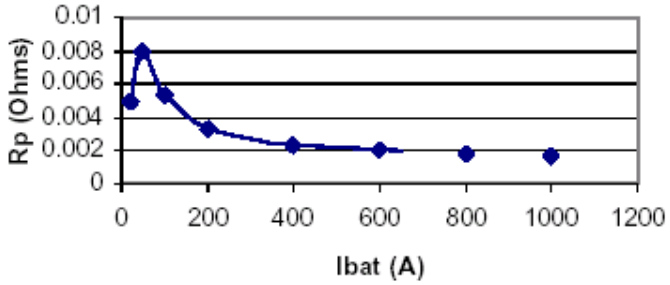

Fig 4.4(a) *Ohmic polarization* R_p *corresponding to discharge current* I_{bat}

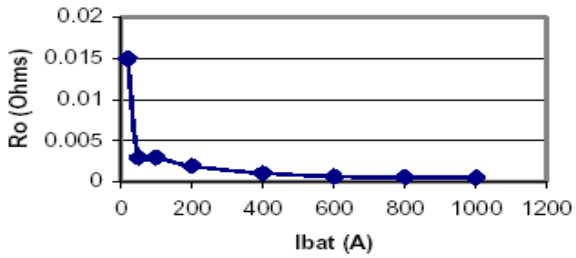

Fig 4.4(b) *Discharge overvoltage resistance* R_o *corresponding to discharge current* I_{bat}

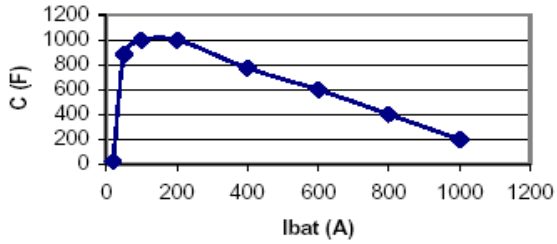

Fig4.4(c) *Overvoltage capacitance C corresponding to discharge current* I_{bat}

4.1.2.3. Long-term integrated electrical model

This is a reduced order model of Giglioli's 4th order model [49]. The diffusion time constant and active-polarisation time constant of the 4th order model had been combined into an integrated electrical time coefficient in this simplified model.

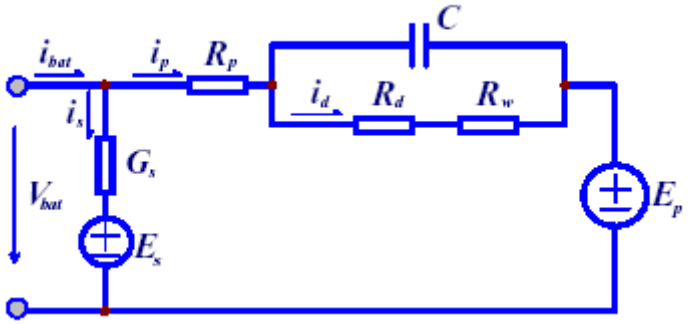

Fig. 4.5 *Equivalent circuit of the long-term integrated battery model*

Parameters new to this model are

R_d = Charge-transfer resistance representing the activation polarization of the active materials

R_w = Diffusion resistance representing the concentration polarization due to electrolyte diffusion

G_s = Self discharge conductance representing the self-discharge and gassing losses

E_s = Gassing voltage representing gassing giving rise to self discharge when the battery voltage reaches this value

Differential equations

$$\frac{dI_d}{dt} = \frac{1}{\tau} \times \left(i_p - i_d\right)$$
$$\frac{d\Delta\theta}{dt} = \frac{1}{\tau_\theta} \times \left(P_{loss} \times R_\theta - \Delta\theta\right) \qquad (4.14)$$
$$\frac{dQ}{dt} = -i_p$$

Battery resistances

$$R_p = R_{p0}\left(1 - \beta \times \theta\right) - R_{cp} \ln\left(SOC\right)$$
$$R_d = R_{d0}\left[\frac{\frac{A_{d1}}{1-SOC} + \exp\left[A_{d2}\left(1-SOC\right)\right]}{1 + \exp\left[A_{d3} \times I_d / I^*\right]}\right]$$
$$R_w = -R_c \ln\left\{\frac{1-\left(1-SOC\right)}{SOC\left(K_c - 1\right) \times \left|I_w / I^*\right|^\delta}\right\} \qquad (4.15)$$
$$G_s = G_{s0} \times \exp\left[A_{sv} \times V_{bat} + A_{s\theta} \times \left(\theta - \theta_f\right)\right]$$

Electrochemical potential (EMF)

$$E_p = E_{p0} + k_e\left(273 + \theta\right)\ln\left(SOC\right) \qquad (4.16)$$

Electrical time coefficient

$$\tau = \left(R_d + R_w\right) \times C \qquad (4.17)$$

4.2. Super-capacitors

Super-capacitors, like batteries, can also be used for power quality issues in the Micro-grids systems. Whether or not to use a super-capacitor rather than a battery will depend mainly on the application.

A simplified electrical equivalent model of the super-capacitor in relation to the actual structural elements is given below. This is an approximate model. However since we are concerned with short-term discharge, modelling more complex behaviour is probably inappropriate. Also the super-capacitors would be connected to the system through a power electronic interface whose dynamics are of more concern in our interest.

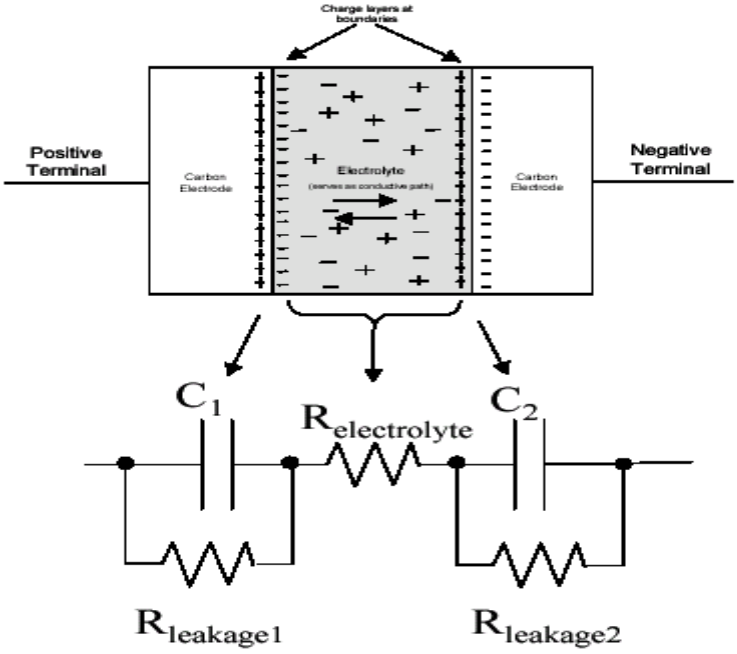

Fig. 4.6 *DC Electrical Model of Electrochemical Capacitor (Super-capacitor)*

The model of Figure 4.6 shows that the super-capacitor structure really is equivalent to two capacitors in series connected by the resistance of the electrolyte. This resistance is much lower than the internal resistance of a typical battery. Therefore super-capacitors can achieve much higher power density than batteries (by a factor of 10 or more). But their energy density at low discharge rates is still less than batteries.

Applications of a super-capacitor can be broadly divided in to 'long duration energy storage' and 'short duration energy storage' applications. Examples for long duration applications are charging a capacitor at night (off peak) and then dispatching it in the daytime for 3-4 hours during peak utility system loading or storing enough energy from a PV system to power loads at night. Power Quality related applications that need seconds or minutes of energy are examples of short duration applications.

Due to its lower energy density (compared to batteries) and higher capital cost, super-capacitor is not as well suited for long duration applications as it is for short duration

applications at present. Our current interest in super-capacitors for Micro-grids is for power quality applications that need high power for short durations of time only.

The super-capacitor is ideal for this (especially for applications less than a few minutes) because it has a much higher power density than batteries and can be very quickly recharged. In fact, at a rapid discharge rate, the super-capacitor can actually deliver more joules of energy per dollar of capital cost than a battery. Also on a lifecycle basis, the cost of the super-capacitor for use in most short duration applications should be less than batteries.

5. Distribution Grid Model

5.1. Lines

Lumped parameter models are adapted for simulations involved in Microgrids project. They are based on the traditional line representation used in short-circuit and power flow program. They are used primarily for steady-state solutions, but can also be used for some transient simulations.

5.1.1.Line modelling

Assuming that a typical distribution line can be represented by a serial resistance R_f and reactance X_f then the terminal line voltages in terms of the flowing current expressed in the arbitrary reference are:

$$\left.\begin{aligned} V_{bd} \equiv V_b = V_{id} - R_f I_d + \omega_b X_f I_q + \frac{X_f}{\omega_o}\frac{dI_d}{dt} \\ V_{bq} \equiv 0 = V_{iq} - R_f I_q - \omega_b X_f I_d + \frac{X_f}{\omega_o}\frac{dI_q}{dt} \end{aligned}\right\} \Leftrightarrow \left\{\begin{aligned} \frac{dI_d}{dt} = \omega_o(-R_f I_d + \omega_b X_f I_q + V_{id} - V_b) / X_f \\ \frac{dI_q}{dt} = \omega_o(-R_f I_q - \omega_b X_f I_d + V_{iq})/X_f \end{aligned}\right. \quad (5.1)$$

$$\mathbf{Y} = \begin{bmatrix} I_d \\ I_q \end{bmatrix} = \begin{bmatrix} 1 & 0 \\ 0 & 1 \end{bmatrix}\mathbf{X} \quad (5.2)$$

This way of modeling the line has the advantage that includes the derivatives of the currents that are not taken into account in case of using the admittance matrix of the grid.

5.1.2. Three- and four-phase line modelling

PI model :

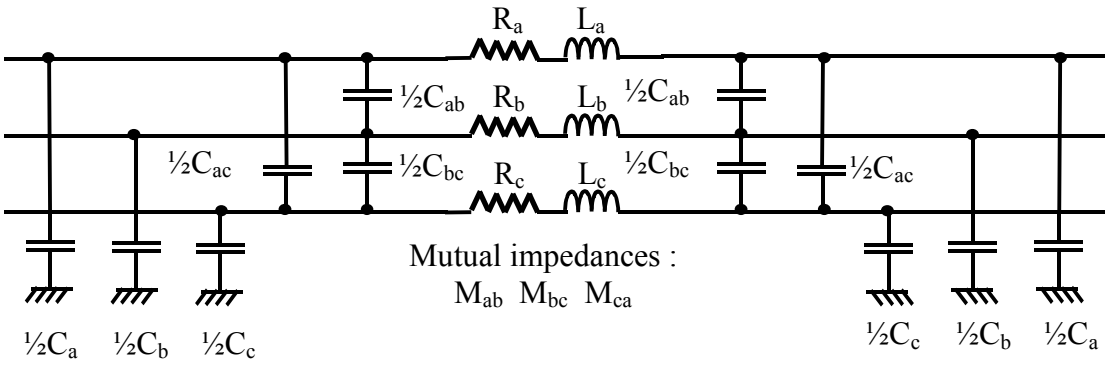

Fig. 5.1 *Three-phase PI model*

PI model with neutral conductor as a fourth phase:

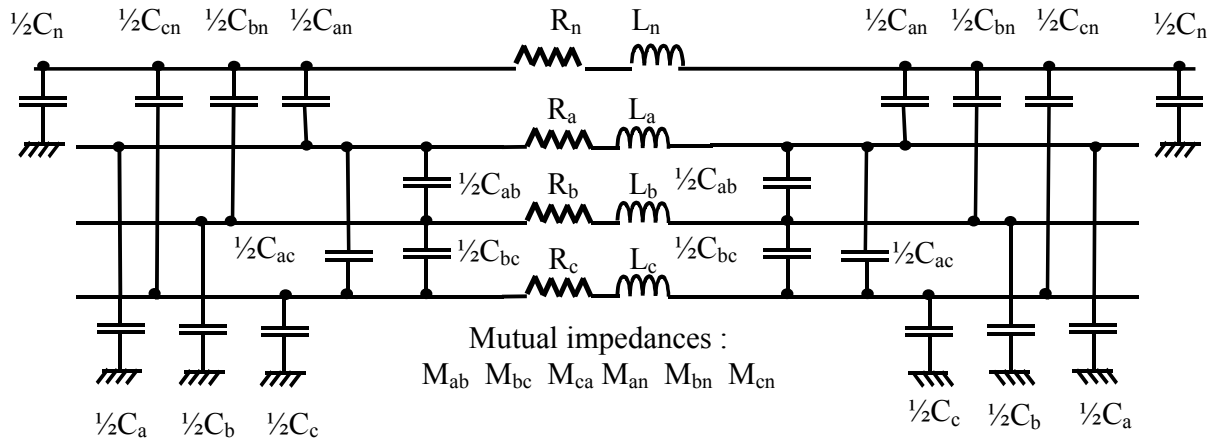

Fig. 5.2 *Four-phase PI model*

5.1.2.1. Equations

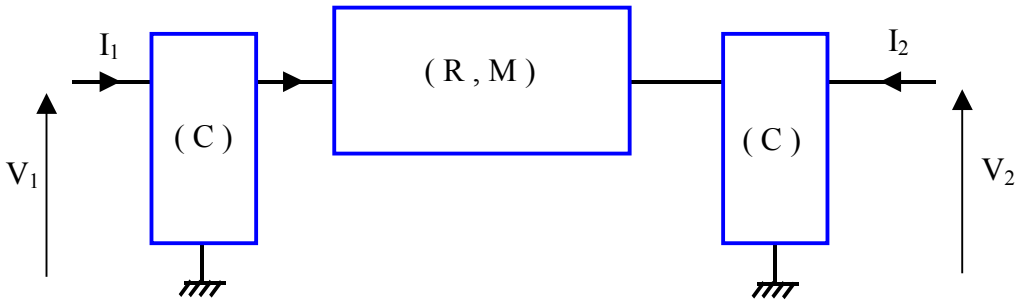

Fig. 5.3 *Matrix form PI model*

$$I_1 = \begin{pmatrix} I_{1,a} \\ I_{1,b} \\ I_{1,c} \\ I_{1,n} \end{pmatrix} \quad I_2 = \begin{pmatrix} I_{2,a} \\ I_{2,b} \\ I_{2,c} \\ I_{2,n} \end{pmatrix} \quad I = \begin{pmatrix} I_a \\ I_b \\ I_c \\ I_n \end{pmatrix} \quad V_1 = \begin{pmatrix} V_{1,a} \\ V_{1,b} \\ V_{1,c} \\ V_{1,n} \end{pmatrix} \quad V_2 = \begin{pmatrix} V_{2,a} \\ V_{2,b} \\ V_{2,c} \\ V_{2,n} \end{pmatrix}$$

$$\text{(5.3)} \quad \begin{cases} V_1 - V_2 = R.I + M.\dfrac{dI}{dt} \\ I_1 = I + C.\dfrac{dV_1}{dt} \\ I_2 = -I + C.\dfrac{dV_2}{dt} \end{cases}$$

In case of symmetrical line or cable :

$$\begin{aligned} R_a = R_b = R_c = R_n &= R_p \\ L_a = L_b = L_c = L_n &= M_p \\ M_{ab} = M_{bc} = M_{ca} = M_{an} = M_{bn} = M_{cn} &= M_m \\ C_a = C_b = C_c = C_n &= 2.C \\ C_{ab} = C_{bc} = C_{ca} = C_{an} = C_{bn} = C_{cn} &= 2.C' \end{aligned}$$

$$R = \begin{bmatrix} R_p & 0 & 0 & 0 \\ 0 & R_p & 0 & 0 \\ 0 & 0 & R_p & 0 \\ 0 & 0 & 0 & R_p \end{bmatrix} \qquad M = \begin{bmatrix} M_p & M_m & M_m & M_m \\ M_m & M_p & M_m & M_m \\ M_m & M_m & M_p & M_m \\ M_m & M_m & M_m & M_p \end{bmatrix} \quad \text{(5.4)}$$

$$C = \begin{bmatrix} C_p & C_m & C_m & C_m \\ C_m & C_p & C_m & C_m \\ C_m & C_m & C_p & C_m \\ C_m & C_m & C_m & C_p \end{bmatrix} \qquad \text{with : } \begin{cases} C_p = C + 3.C' \\ C_m = -C' \end{cases}$$

5.1.2.2. Simulation in Park system

- **Park transformation matrix**

The transformation matrix from the *abcn* phase variables to the *dqon* variables used is

$$M_\theta = \sqrt{\frac{2}{3}}.\begin{bmatrix} \cos(\theta) & \cos(\theta - \frac{2.\pi}{3}) & \cos(\theta + \frac{2.\pi}{3}) & 0 \\ -\sin(\theta) & -\sin(\theta - \frac{2.\pi}{3}) & -\sin(\theta + \frac{2.\pi}{3}) & 0 \\ \frac{1}{\sqrt{2}} & \frac{1}{\sqrt{2}} & \frac{1}{\sqrt{2}} & 0 \\ 0 & 0 & 0 & \sqrt{\frac{3}{2}} \end{bmatrix} \quad \text{(5.5)}$$

The inverse matrix is given by :

$M_\theta^{-1} = M_\theta^T$ where $M^T{}_\theta$ is the transposed matrix of M_θ .

- **Transformation of a differential equation**

Let's consider S_1 and S_2 two four-phase vectors in the natural reference frame *abcn* that verify :

$S_1 = M.\frac{dS_2}{dt}$, *M* is a 4x4 matrix.

Let's transform this equation in Park reference frame :

$$
\begin{aligned}
M_\theta.S_1 &= M_\theta.M.\frac{dS_2}{dt} \\
S_{1,pk} &= M_\theta.M.\frac{d}{dt}(M_\theta^{-1}.S_{2,pk}) \\
S_{1,pk} &= M_\theta.M.\frac{d}{dt}(M_\theta^{-1}).S_{2,pk} + M_\theta.M.M_\theta^{-1}.\frac{d}{dt}S_{2,pk} \quad (5.6) \\
S_{1,pk} &= M_{pk}.M_\theta.\frac{d}{dt}(M_\theta^{-1}).S_{2,pk} + M_{pk}.\frac{d}{dt}S_{2,pk} \\
S_{1,pk} &= M_{pk}.D_4.S_{2,pk} + M_{pk}.\frac{d}{dt}S_{2,pk}
\end{aligned}
$$

where : (5.7) $\begin{cases} D_4 = M_\theta.\frac{d}{dt}(M_\theta^{-1}) \\ M_{pk} = M_\theta.M.M_\theta^{-1} \end{cases}$

- **Application case : synchronous reference frame ($\theta = \omega t$)**

In that case, D_4 is quite simple :

$$D_4 = \begin{bmatrix} 0 & -\omega & 0 & 0 \\ \omega & 0 & 0 & 0 \\ 0 & 0 & 0 & 0 \\ 0 & 0 & 0 & 0 \end{bmatrix}$$

- **Transformation of line/cable equation**

Let's apply the Park transformation in the synchronous reference frame to the line/cable equations.

(5.3) can then be written in the following form :

$$(5.8)\quad \begin{cases} V_{1,pk} - V_{2,pk} = R_{pk}.I_{pk} + M_{pk}.\dfrac{dI_{pk}}{dt} + M_{pk}.D_4.I_{pk} \\ I_{1,pk} = I_{pk} + C_{pk}.\dfrac{dV_{1,pk}}{dt} + C_{pk}.D_4.V_{1,pk} \\ I_{2,pk} = -I_{pk} + C_{pk}.\dfrac{dV_{2,pk}}{dt} + C_{pk}.D_4.V_{2,pk} \end{cases}$$

Where :

$$I_{1,pk} = \begin{pmatrix} I_{1,d} \\ I_{1,q} \\ I_{1,o} \\ I_{1,n} \end{pmatrix} \quad I_{2,pk} = \begin{pmatrix} I_{2,d} \\ I_{2,q} \\ I_{2,o} \\ I_{2,n} \end{pmatrix} \quad I_{pk} = \begin{pmatrix} I_d \\ I_q \\ I_o \\ I_n \end{pmatrix} \quad V_{1,pk} = \begin{pmatrix} V_{1,d} \\ V_{1,q} \\ V_{1,o} \\ V_{1,n} \end{pmatrix} \quad V_{2,pk} = \begin{pmatrix} V_{2,d} \\ V_{2,q} \\ V_{2,o} \\ V_{2,n} \end{pmatrix}$$

$$M_{pk} = M_\theta.M.M_\theta^{-1} = \begin{bmatrix} M_p - M_m & 0 & 0 & 0 \\ 0 & M_p - M_m & 0 & 0 \\ 0 & 0 & M_p + 2.M_m & \sqrt{3}.M_m \\ 0 & 0 & \sqrt{3}.M_m & M_p \end{bmatrix}$$

$$C_{pk} = \begin{bmatrix} C_p - C_m & 0 & 0 & 0 \\ 0 & C_p - C_m & 0 & 0 \\ 0 & 0 & C_p + 2.C_m & \sqrt{3}.C_m \\ 0 & 0 & \sqrt{3}.C_m & C_p \end{bmatrix}$$

and $R_{pk} = diag(R_p, R_p, R_p, R_p)$

(5.8) could be also written :

$$(5.9)\quad \begin{cases} \dfrac{dV_{1,pk}}{dt} = -D_4.V_{1,pk} - C_{pk}^{-1}.I_{pk} + C_{pk}^{-1}.I_{1,pk} \\ \dfrac{dV_{2,pk}}{dt} = -D_4.V_{2,pk} + C_{pk}^{-1}.I_{pk} + C_{pk}^{-1}.I_{2,pk} \\ \dfrac{dI_{pk}}{dt} = M_{pk}^{-1}.V_{1,pk} - M_{pk}^{-1}.V_{2,pk} - (M_{pk}^{-1}.R_{pk} + D_4).I_{pk} \end{cases}$$

This system is computerised by the matlab function called *four_ph_line.m* and an ODE solver.

$I_{1,pk}$ and $I_{2,pk}$ are the inputs. $V_{1,pk}$, $V_{1,pk}$ and $I_{1,pk}$ are the outputs.

5.2. Transformers

5.2.1. Single and Three Phase Models for transformers

5.2.1.1. Single-phase transformer

The usual model for single-phase transformer is following :

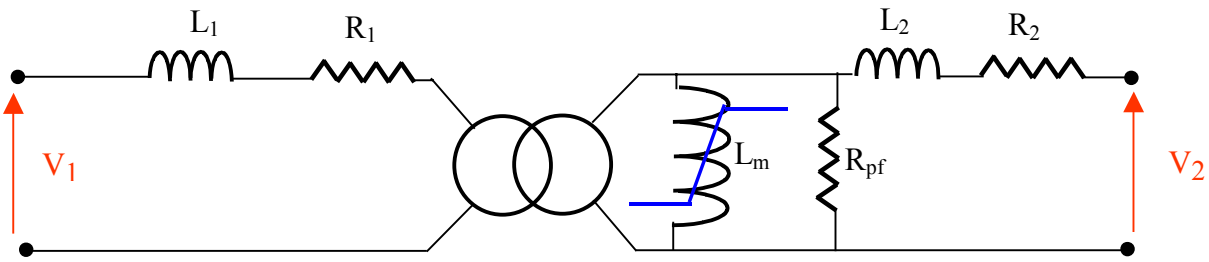

Fig. 5.4 *Model of single-phase transformer*

- R_1 : primary winding resistance
- R_2 : secondary winding resistance
- L_1 : primary leakage inductance
- L_2 : secondary leakage inductance
- L_m : magnetizing inductance (saturable)
- R_{pf} : iron-core losses resistance

5.2.1.2. Three-phase transformer

- A three-phase transformer could be modelled as three single-phase transformers connected each other. In that case, each of them is separate from the others, there's no magnetic coupling.

But almost all transformers have one common core with three, four or five legs. It means that there is magnetic coupling. This one can't be well represented by this model during homopolar generating events, like phase-to-earth fault.

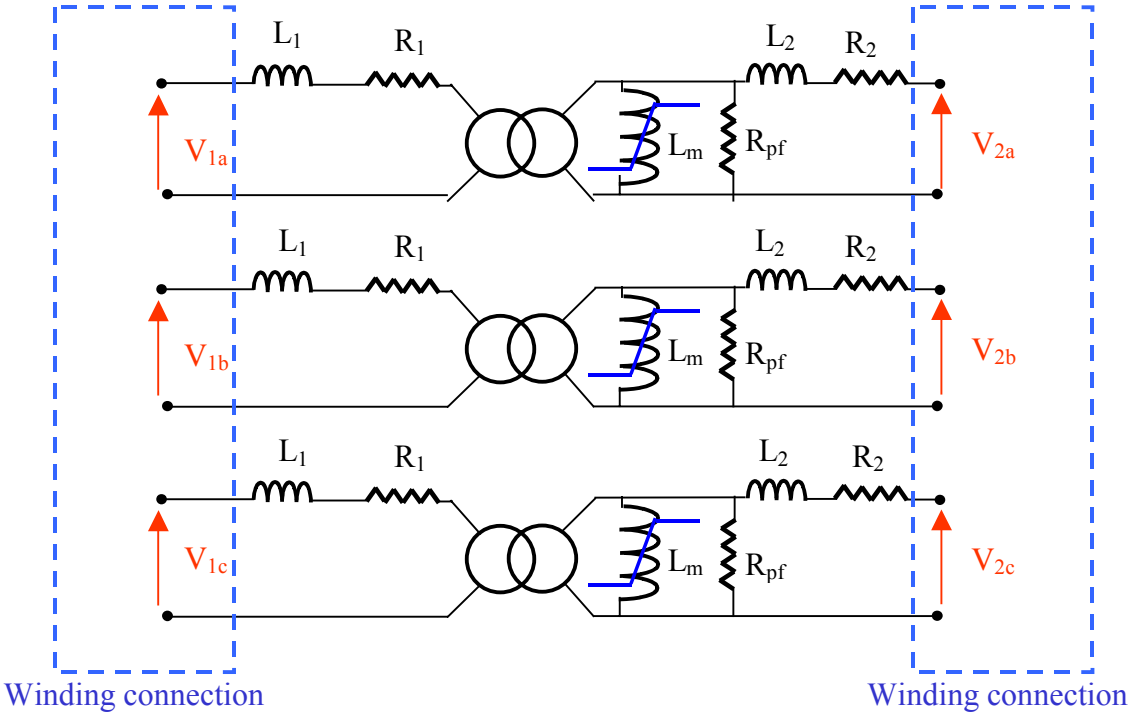

Fig. 5.5 *Model with 3 single-phase transformers*

- Another possibility to model three-phase transformer is to represent magnetic coupling, magnetic leakage and resistances by two 6x6 matrices as shown on figure 2-3. If necessary, non linear impedances could be modelled by non linear inductances located out of the main element. Winding connections are also represented.

We can write :

$$V = R.I + M.\frac{dI}{dt} \qquad \text{with :}$$

$$V = \begin{pmatrix} V_{1,a} \\ V_{1,b} \\ V_{1,c} \\ V_{2,a} \\ V_{2,b} \\ V_{2,c} \end{pmatrix} \qquad I = \begin{pmatrix} I_{1,a} \\ I_{1,b} \\ I_{1,c} \\ I_{2,a} \\ I_{2,b} \\ I_{2,c} \end{pmatrix}$$

$$R = \begin{bmatrix} R_{1a} & 0 & 0 & 0 & 0 & 0 \\ 0 & R_{1b} & 0 & 0 & 0 & 0 \\ 0 & 0 & R_{1c} & 0 & 0 & 0 \\ 0 & 0 & 0 & R_{2a} & 0 & 0 \\ 0 & 0 & 0 & 0 & R_{2b} & 0 \\ 0 & 0 & 0 & 0 & 0 & R_{2c} \end{bmatrix} = \begin{bmatrix} R_{1,abc} & 0 \\ 0 & R_{2,abc} \end{bmatrix}$$

and :

$$M = \begin{bmatrix} L_{1a} & M_{1a1b} & M_{1a1c} & M_{1a2a} & M_{1a2b} & M_{1a2c} \\ M_{1b1a} & L_{1b} & M_{1b1c} & M_{1b2a} & M_{1b2b} & M_{1b2c} \\ M_{1c1a} & M_{1c1b} & L_{1c} & M_{1c2a} & M_{1c2b} & M_{1c2c} \\ M_{2a1a} & M_{2a1b} & M_{2a1c} & L_{2a} & M_{2a2b} & M_{2a2c} \\ M_{2b1a} & M_{2b1b} & M_{2b1c} & M_{2b2a} & L_{2b} & M_{2b2c} \\ M_{2c1a} & M_{2c1b} & M_{2c1c} & M_{2c2a} & M_{2c2b} & L_{2c} \end{bmatrix} = \begin{bmatrix} M_{1,abc} & M_{12,abc} \\ M_{21,abc} & M_{2,abc} \end{bmatrix}$$

$R_{1,abc}$, $R_{2,abc}$, $M_{1,abc}$, $M_{2,abc}$, $M_{12,abc}$ and $M_{21,abc}$ are 3x3 matrices.

$$\begin{pmatrix} V_{1a} \\ V_{1b} \\ V_{1c} \\ V_{2a} \\ V_{2b} \\ V_{2c} \end{pmatrix} = \begin{pmatrix} R_{1a} & 0 & 0 & 0 & 0 & 0 \\ 0 & R_{1b} & 0 & 0 & 0 & 0 \\ 0 & 0 & R_{1c} & 0 & 0 & 0 \\ 0 & 0 & 0 & R_{2a} & 0 & 0 \\ 0 & 0 & 0 & 0 & R_{2b} & 0 \\ 0 & 0 & 0 & 0 & 0 & R_{2c} \end{pmatrix} \cdot \begin{pmatrix} I_{1a} \\ I_{1b} \\ I_{1c} \\ I_{2a} \\ I_{2b} \\ I_{2c} \end{pmatrix} + \begin{pmatrix} L_{1a} & M_{1a1b} & M_{1a1c} & M_{1a2a} & M_{1a2b} & M_{1a2c} \\ M_{1b1a} & L_{1b} & \dots & \dots & \dots & \dots \\ \dots & \dots & L_{1c} & \dots & \dots & \dots \\ \dots & \dots & \dots & L_{2a} & \dots & \dots \\ \dots & \dots & \dots & \dots & L_{2b} & M_{2b2c} \\ M_{2c1a} & \dots & \dots & \dots & M_{2c2b} & L_{2c} \end{pmatrix} \cdot \frac{d}{dt} \begin{pmatrix} I_{1a} \\ I_{1b} \\ I_{1c} \\ I_{2a} \\ I_{2b} \\ I_{2c} \end{pmatrix}$$

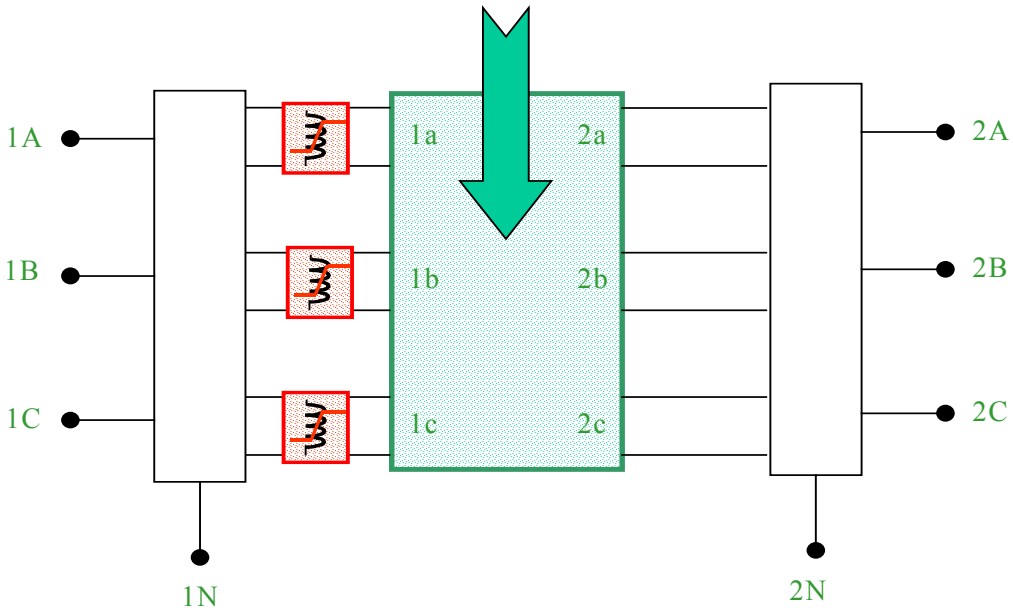

Fig. 5.6 *Model with magnetic coupling*

The inductance matrix is considered as symmetrical so : $M_{12,abc} = M_{21,abc} = M_{abc}$.
The equations of the main part of the model are :

$$(5.10) \quad \begin{cases} V_{1,abc} = R_{1,abc}.I_{1,abc} + M_{1,abc}.\frac{d}{dt} I_{1,abc} + M_{abc}.\frac{d}{dt} I_{2,abc} \\ V_{2,abc} = R_{2,abc}.I_{2,abc} + M_{2,abc}.\frac{d}{dt} I_{2,abc} + M_{abc}.\frac{d}{dt} I_{1,abc} \end{cases}$$

5.2.2. Equations in Park reference frame

5.2.2.1. Three-phase transformer

In the synchronous reference frame (5.10) becomes :

$$(5.11) \begin{cases} V_{1,dqo} = R_{1,dqo}.I_{1,dqo} + M_{1,dqo}.\frac{d}{dt} I_{1,dqo} + M_{1,dqo}.D_3.I_{1,dqo} + M_{dqo}.\frac{d}{dt} I_{2,dqo} + M_{dqo}.D_3.I_{2,dqo} \\ V_{2,dqo} = R_{2,dqo}.I_{2,dqo} + M_{2,dqo}.\frac{d}{dt} I_{2,dqo} + M_{2,dqo}.D_3.I_{2,dqo} + M_{dqo}.\frac{d}{dt} I_{1,dqo} + M_{dqo}.D_3.I_{1,dqo} \end{cases}$$

Where :

$$I_{1,dqo} = \begin{pmatrix} I_{1,d} \\ I_{1,q} \\ I_{1,o} \end{pmatrix} \quad I_{2,dqo} = \begin{pmatrix} I_{2,d} \\ I_{2,q} \\ I_{2,o} \end{pmatrix} \quad V_{1,dqo} = \begin{pmatrix} V_{1,d} \\ V_{1,q} \\ V_{1,o} \end{pmatrix} \quad V_{2,dqo} = \begin{pmatrix} V_{2,d} \\ V_{2,q} \\ V_{2,o} \end{pmatrix} \quad D_3 = \begin{bmatrix} 0 & -\omega & 0 \\ \omega & 0 & 0 \\ 0 & 0 & 0 \end{bmatrix}$$

And :

$$M_{1,dqo} = M_\theta . M_{1,abc} . M_\theta^{-1}$$

$$M_{2,dqo} = M_\theta . M_{2,abc} . M_\theta^{-1}$$

$$M_{dqo} = M_\theta . M_{abc} . M_\theta^{-1}$$

$$R_{1,dqo} = M_\theta . R_{1,abc} . M_\theta^{-1}$$

$$R_{2,dqo} = M_\theta . R_{2,abc} . M_\theta^{-1}$$

$$M_\theta = \sqrt{\frac{2}{3}} . \begin{bmatrix} \cos(\theta) & \cos(\theta - \frac{2.\pi}{3}) & \cos(\theta + \frac{2.\pi}{3}) \\ -\sin(\theta) & -\sin(\theta - \frac{2.\pi}{3}) & -\sin(\theta + \frac{2.\pi}{3}) \\ \frac{1}{\sqrt{2}} & \frac{1}{\sqrt{2}} & \frac{1}{\sqrt{2}} \end{bmatrix}$$

5.2.2.2. Wye winding connection

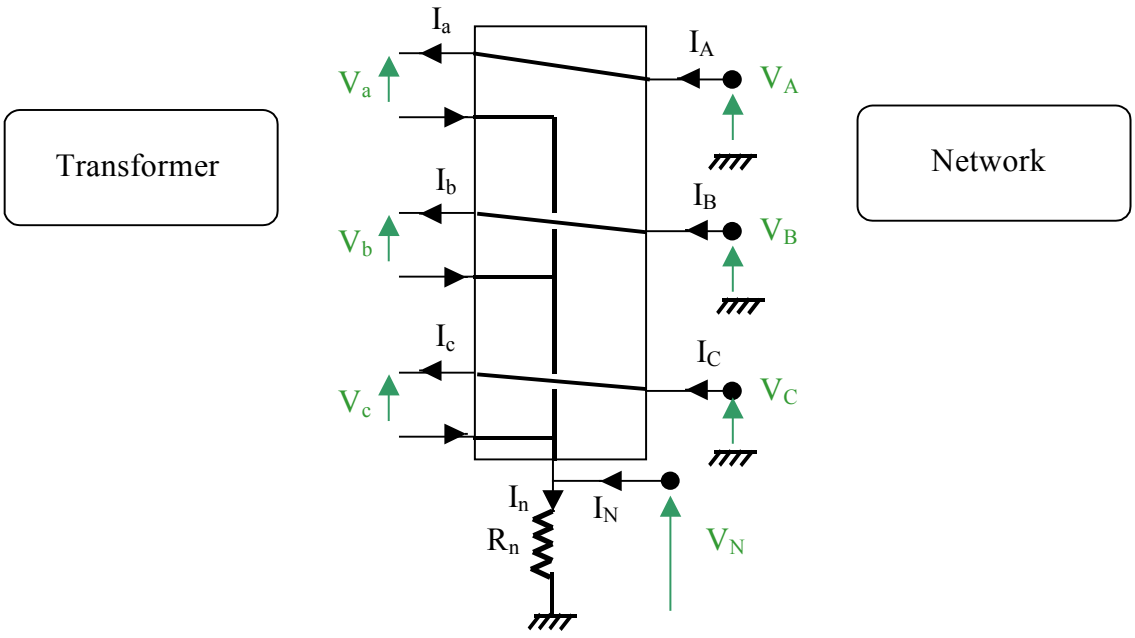

Fig. 5.7 *Y-winding connection*

$V_A = V_a + R_n . I_n$
$V_B = V_b + R_n . I_n$
$V_C = V_c + R_n . I_n$
$V_N = V_n + R_n . I_n \qquad (V_n = 0)$

So : $V_{ABCN} = V_{abcn} + R_n . I_n [1]_{4x1}$ (5.12)

About currents, we have :

$I_A = I_a$, $I_B = I_b$, $I_C = I_c$ and $I_N = I_n - (I_a + I_b + I_c)$

Therefore :

$I_{ABC} = I_{abc}$ and $I_{DQO} = M_\theta . I_{ABC} = M_\theta . I_{abc} = I_{dqo}$.

$$I_n = \sqrt{3}.I_O + I_N$$

(5.12) can be written in the following form :

$$V_{DQON} = V_{dqon} + \begin{bmatrix} 0 \\ 0 \\ \sqrt{3}.R_n.I_n \\ R_n.I_n \end{bmatrix} = V_{dqon} + R_n.(\sqrt{3}.I_O + I_N).\begin{bmatrix} 0 \\ 0 \\ \sqrt{3} \\ 1 \end{bmatrix}$$

To resume, the relations between the two sides of the Y-connections in Park system are :

(5.13)
$$\begin{cases} I_{dqo} = I_{DQO} \\ I_n = \sqrt{3}.I_O + I_N \\ V_{DQON} = V_{dqon} + R_n.(\sqrt{3}.I_O + I_N).\begin{bmatrix} 0 \\ 0 \\ \sqrt{3} \\ 1 \end{bmatrix} \\ V_n = 0 \end{cases}$$

5.2.2.3. Delta winding connection

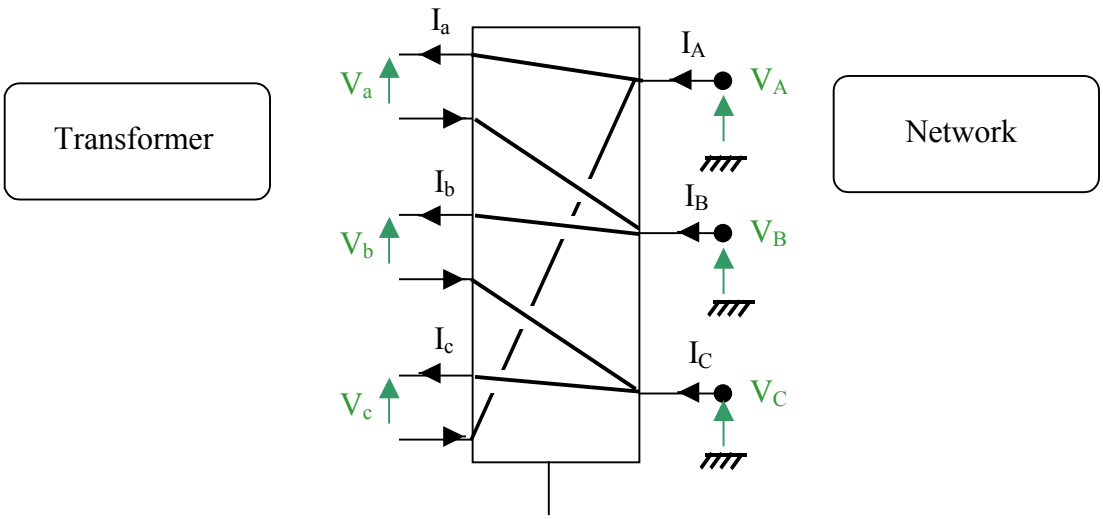

Fig. 5.8 *Δ-winding connection*

Equations of this winding connection are :

$$\begin{cases} V_a = V_A - V_B \\ V_b = V_B - V_C \\ V_c = V_C - V_A \end{cases} \qquad \begin{cases} I_A = I_a - I_c \\ I_B = I_b - I_a \\ I_C = I_c - I_b \end{cases}$$

$\Rightarrow$ $V_o = 0$ and $I_O = 0$. (5.14)

Zero sequence voltage on network side can't be calculated from transformer voltage, and zero sequence current on transformer side can't be calculated from network current.

Let's transform current equation in Park reference frame :

$$I_{DQO} = M_\theta I_{ABC} = M_\theta . I_{abc} - M_\theta . I_{cab}$$

$$I_{DQO} = I_{dqo} - M_{\theta - 2.\pi/3} . I_{abc} = I_{dqo} - M_{\theta - 2.\pi/3} . M_\theta^{-1} . I_{dqo}$$

$$I_{DQO} = I_{dqo} - \begin{bmatrix} -\frac{1}{2} & -\sqrt{\frac{3}{4}} & 0 \\ \sqrt{\frac{3}{4}} & -\frac{1}{2} & 0 \\ 0 & 0 & 1 \end{bmatrix} . I_{dqo}$$

$\Rightarrow$ $$I_{dq} = \frac{1}{2} \begin{bmatrix} 1 & -\frac{1}{\sqrt{3}} \\ \frac{1}{\sqrt{3}} & 1 \end{bmatrix} . I_{DQ} \qquad (5.15)$$

By the same way, we can prove that :

$$V_{DQ} = \frac{1}{2} \begin{bmatrix} 1 & \frac{1}{\sqrt{3}} \\ -\frac{1}{\sqrt{3}} & 1 \end{bmatrix} . V_{dq} \qquad (5.16)$$

5.2.2.4. Resolution of equations

We assume that inputs are currents $I_{1,ABCN}$ and $I_{2,ABCN}$ that became in Park synchronous reference frame : $I_{1,DQON}$ and $I_{2,DQON}$ .The outputs are voltages V_1 and V_2 .We are going to study and develop methods for the different connecting possibilities : i.e. YY, Δ Δ and Δ Y.

5.2.2.5. Wye-Wye connection

We have :

$I_{1,dqo} = I_{1,DQO}$ and $I_{2,dqo} = I_{2,DQO}$

Resolution of (5.11) leads to voltages on the two transformer sides, then it's possible to come back to network sides by using (5.13) :

$$\begin{cases} V_{1,DQON} = V_{1,dqon} + R_{1,n}.(\sqrt{3}.I_{1,O} + I_{1,N}).\begin{bmatrix} 0 \\ 0 \\ \sqrt{3} \\ 1 \end{bmatrix} \\ V_{2,DQON} = V_{2,dqon} + R_{2,n}.(\sqrt{3}.I_{2,O} + I_{2,N}).\begin{bmatrix} 0 \\ 0 \\ \sqrt{3} \\ 1 \end{bmatrix} \end{cases}$$

5.2.2.6. Delta-delta connection

Because of delta connection there is no zero sequence currents on network sides and those on transformer sides are unknown. Zero sequence voltages can't be calculated on network sides.

$I_{1,dq}$ and $I_{2,dq}$ are calculated from (5.15) :

$$I_{1,dq} = \frac{1}{2}\begin{bmatrix} 1 & -\frac{1}{\sqrt{3}} \\ \frac{1}{\sqrt{3}} & 1 \end{bmatrix}.I_{1,DQ}$$

$$I_{2,dq} = \frac{1}{2}\begin{bmatrix} 1 & -\frac{1}{\sqrt{3}} \\ \frac{1}{\sqrt{3}} & 1 \end{bmatrix}.I_{2,DQ}$$

We assume that the transformer is symmetrical so $M_{1,abc}$, $M_{2,abc}$ and M_{abc} are symmetrical, therefore $M_{1,dqo}$, $M_{2,dqo}$ and M_{dqo} are diagonal matrices.
In that case, it is possible to resolve (5.11) on dq-axis (no coupling with zero sequence) and obtain $V_{1,dq}$ and $V_{2,dq}$.

Then by using (5.16) :

$$V_{1,DQ} = \frac{1}{2}\begin{bmatrix} 1 & \frac{1}{\sqrt{3}} \\ -\frac{1}{\sqrt{3}} & 1 \end{bmatrix}.V_{1,dq}$$

$$V_{2,DQ} = \frac{1}{2}\begin{bmatrix} 1 & \frac{1}{\sqrt{3}} \\ -\frac{1}{\sqrt{3}} & 1 \end{bmatrix}.V_{2,dq}$$

$V_{1,O}$ and $V_{2,O}$ can't be calculated from the knowledge of currents feeding the transformer.

5.2.2.7. Delta-wye connection

We have :

$I_{2,dqo} = I_{2,DQO}$ $V_{1,o} = 0$

And :

$$I_{1,dq} = \frac{1}{2}\begin{bmatrix} 1 & -\frac{1}{\sqrt{3}} \\ \frac{1}{\sqrt{3}} & 1 \end{bmatrix} . I_{1,DQ}$$

We assume that the transformer is symmetrical so $M_{1,abc}$, $M_{2,abc}$ and M_{abc} are symmetrical, therefore $M_{1,dqo}$, $M_{2,dqo}$ and M_{dqo} are diagonal matrices.
The homopolar part of (5.11) can be written as :

$$V_{1,o} = 0 = R_{1,o}.I_{1,o} + M_{1,o}.\frac{d}{dt} I_{1,o} + M_{o}.\frac{d}{dt} I_{2,o}$$

By resolving this differential equation we obtain $I_{1,o}$.

Then it became possible to resolve the entire system (5.11) :

$$\begin{cases} V_{1,dqo} = R_{1,dqo}.I_{1,dqo} + M_{1,dqo}.\frac{d}{dt} I_{1,dqo} + M_{1,dqo}.D_3.I_{1,dqo} + M_{dqo}.\frac{d}{dt} I_{2,dqo} + M_{dqo}.D_3.I_{2,dqo} \\ V_{2,dqo} = R_{2,dqo}.I_{2,dqo} + M_{2,dqo}.\frac{d}{dt} I_{2,dqo} + M_{2,dqo}.D_3.I_{2,dqo} + M_{dqo}.\frac{d}{dt} I_{1,dqo} + M_{dqo}.D_3.I_{1,dqo} \end{cases}$$

The next step leads to network sides voltages :

$$\begin{cases} V_{1,DQ} = \frac{1}{2}\begin{bmatrix} 1 & \frac{1}{\sqrt{3}} \\ -\frac{1}{\sqrt{3}} & 1 \end{bmatrix} . V_{1,dq} \\ V_{2,DQON} = V_{2,dqon} + R_{2,n}.(\sqrt{3}.I_{2,O} + I_{2,N}).\begin{bmatrix} 0 \\ 0 \\ \sqrt{3} \\ 1 \end{bmatrix} \end{cases}$$

$V_{1,O}$ remains unknown, its value depends on the network.

5.3. Electrical loads

Electrical loads are assumed as constant active and reactive power loads. There are also two more options for the loads, i.e. they can be considered as constant admittance or constant current loads. The assumption of constant active and reactive power absorption is modeled by the following dq axis current components obtained from the absorbed active and reactive powers:

$$I_d = \frac{V_d}{V_d^2 + V_q^2} P + \frac{V_q}{V_d^2 + V_q^2} Q, I_q = \frac{V_q}{V_d^2 + V_q^2} P - \frac{V_d}{V_d^2 + V_q^2} Q \quad (5.17)$$

Generally power loads satisfy a relation of the following form

$$I_{dq} = f(V_{dq}, a_l) \quad (5.18)$$

Where α_l a vector of load characteristics.

The models of loads in different cases are aggregated in table 5.1.

$I_d = ct, I_q = ct$	$I_d = Y_d V_d - Y_q V_q, I_q = Y_d V_q + Y_q V_d$
Constant Current loads	*Constant admittance loads*
$I_d = \frac{V_d}{V_d^2 + V_q^2} P + \frac{V_q}{V_d^2 + V_q^2} Q, I_q = \frac{V_q}{V_d^2 + V_q^2} P - \frac{V_d}{V_d^2 + V_q^2} Q$	
Constant Power loads	

Table 5.1

6. References

[1] P. Kundur, "Power System Stability and Control", New York: McGraw-Hill, 1994

[2] Chapman, S. J. "Electric Machinery Fundamentals", 2nd edition, New York: McGraw-Hill, 1991

[3] Krause, P.C, "*Analysis of Electric Machinery*", IEEE Press, 1994

[4] Krause, P.C, "Simulation of Unsymmetrical 2-Phase Induction Machines", *IEEE Trans. Power Apparatus and Systems*, Vol. 84, November 1965.

[5] Arulampalam, A., "Power Quality Improvement with Battery supported Voltage Source Converters", PhD Thesis, UMIST, November 2002.

[6] Kaura, V., Blasko, V., "Operation of a Voltage Source Converter at Increased Utility Voltage", *IEEE Trans. Power Electronics*, Vol. 12, January 1997.

[7] Blasko, V., Kaura, V., "A New Mathematical Model and Control of a Three-phase AC-DC Voltage Source Converter", *IEEE Trans. Power Electronics*, Vol. 12, January 1997.

[8] Wu, R., Dewan, S.B., Slemon, G.R., "Analysis of an ac-to-dc Voltage Source Converter using PWM with Phase and Amplitude Control.

[9] Andersen, B.R., Xu, L., Horton, P.J., Cartwright, P., "Topologies for VSC transmission", Power Engineering Journal, June 2002.

[10] Xu, L., Andersen, B.R., Cartwright, P., "Control of VSC Transmission Systems under Unbalanced Network Conditions"

[11] Itoh, R., Ishizaka, K., "Series Connected PWM GTO Current/ Source Converter with Symmetrical Phase Angle Control", IEE Proceedings on Electric Power Applications, Vol. 137, No. 4, July 1990

[12] Shen, C., Yang, Z., Crow, M.L., Atcitty, S., "Control of STATCOM with Energy Storage Device", IEEE Power Engineering Society Winter Meeting, Conference Proceedings, 2000

[13] Ye, Y., Kazerani, M., "Decoupled State Feedback Control of CSI-based STATCOM", 32nd Annual North America Power Symposium, Oct. 23-24, 2000, Waterloo, Ontario, Canada
[14] Ye, Y., Kazerani, M., Quintana, V.H., "A Novel Modelling and Control Method for Three-Phase PWM Converters", PESC 2001, 32nd Power Electronics Specialists Conference, Canada, June 2001.
[15] Schauder, C., Mehta, H., "Vector Analysis and Control of Advanced Static VAR Compensators", *IEEE PROCEEDINGS-C,* Vol. 140, No.4, July 1993
[16] Cartwright, P., "Voltage Source converters for HVDC Transmission Schemes", MPhil/PhD 1st Year Transfer Report, UMIST, February 2002.
[17] Mohan, N., Underland, T.M., Robbins, W.P., "Power Electronics – Converters, Applications and Design", Second Edition, John Wiley and Sons, INC. 1995
[18] Akagi, H., Kanazawa, Y., Akira, N., "Instantaneous Reactive Power Compensators Comprising Switching Devices without Energy Storage Components", IEEE Transactions on Industry Applications, Vol. 1A-20, No. 3. May/June 1984.
[19] Barbosa P. G., Rolim, L. G. B., Watanabe E. H., Hanitsch, R., "Control Strategy for Grid-Connected DC-AC Conveters with Load Power Factor Correction", IEE Proc.-Gener. Transm. Distrib., Vol. 145, ,No. 5, September 1998.
[20] Barbosa P. G., Rolim, L. G. B., Watanabe E. H., Hanitsch, R., "Control Strategy for Grid-Connected DC-AC Conveters with Load Power Factor Correction", IEE Proc.-Gener. Transm. Distrib., Vol. 145, ,No. 5, September 1998.
[21] J.C.H. Phang, D. S. H. Chan, J. R. Phillips, "Accurate Analytical Method for the Extraction of Solar Cell Model Parameters", Electronics Letters, 10th May 1984 Vol. 20 No. 10, pp. 406-408.
[22] E. Lorenzo, "Solar electricity: engineering of photovoltaic systems". 1999.
[23] *D. L. King, "Photovoltaic Module and Array Performance Characterization Methods for All System Operating Conditions," NREL/SNL Program Review, AIP Press, 1996, pp.347-368.*
[24] S. Busquet, D. Mayer, R. Metkemeijer, "Development of a clean stand-alone power system integrating PV, fuel cell and electrolyser" Proceedings of the Photovoltaic Hybrid Power Systems conference, Aix en Provence, 7-9 September, Session I, Oral n°5, 2000.
[25] JC. Amphlett, RM. Baumert, RF. Mann, BA. Peppley, PR. Roberge, TJ. Harris, "Performance modeling of the Ballard Mark IV solid polymer electrolyte fuel cell I. Mechanistic model development", J. Electrochem. Soc. Vol 142, No 1, 1995.
[26] JC. Amphlett, RM. Baumert, RF. Mann, BA. Peppley, PR. Roberge, TJ. Harris, "Performance modeling of the Ballard Mark IV solid polymer electrolyte fuel cell II. Empirical model development", J. Electrochem. Soc. Vol 142, No 1, 1995.
[27] RF. Mann, JC. Amphlett, MAI. Hooper, HM. Jensen, BA. Peppley, PR. Roberge, "Development and application of a generalised steady-state electrochemical model for a PEM fuel cell", J. of. P. Sources, 86 (2000), 173-180.
[28] MW. Fowler, RF. Mann, JC. Amphlett, BA. Peppley, PR. Roberge, "Incorporation of voltage degradation into a generalised steady state electrochemical model for a PEM fuel cell", J. of. P. Sources, 106 (2002), 274-283.
[29] J. Kim & al. & C.E. Chamberlin, "Modeling of proton exchange fuel cell membrane with an empirical equation", J. Electrochem. Soc. Vol. 142, No 8, pp. 2670-2674, 1995.
[30] S. Busquet, R. Metkemeijer, P. Leroux, D. Mayer, "Stand-alone power system coupling a PV field and a fuel cell : Experimental results of the FC system", Proceedings of the France-Deutschland Fuel Cell Conference 2002, October 7th to 10th 2002, Forbach-Saarbrücken, pp. 85-92, 2002.

[31] Y. Zhu, K. Tomsovic, Development if models for analysing load-following performance of microturbines and fuel cells, Electric Power Systems Research 62 (2002) 1-11.
[32] Stefano Campanari, Thermodynamic model and parametric analysis of tubular SOFC module
[33] J. Padulles, G.W. Ault, J.R. McDonald, An integrated SOFC plant dynamic model for power systems simulation, J. Power Sources 86 (2000) 495-500.
[34] B. Thorstensen, A parametric study of fuel cell system efficiency under full and part load operation, J. Power Sources 92 (2001) 9-16.
[35] W. He, Dynamic model for molten carbonate fuel-cell power generation systems, J. Energy Conv. Manage. 39 (8) (1998) 775-783.
[36] J.H. Watts, Microturbines: a new class of gas turbine engines, Gas Turbine News in Brief 39 (1) (1999) 5-11
[37] M. Nagpal, A. Moshref, G.K. Morison, et al., Experience with testing and modelling of gas turbines, Proceedings of the IEEE/PES 2001 Winter Meeting, Columbus, Ohio, USA, January/February 2001, pp. 652-656.
[38] A. Feijoo, J. Cidras, Analysis of mechanical power fluctuations in asynchronous WEC's, IEEE Trans. Energy Conv. 14 (3) (1999) 284-291.
[39] R.H. Lasseter, Control of distributed resources, Proceedings of the 1998 International Conference on Bulk Power Systems Dynamics and Control IV-Restructuring, Santorini, Greece, August 1998, pp. 323-330.
[40] L.N. Hannett, G. Jee, B. Fardanesh, A governor/turbine model for a twin-shaft combustion turbine, IEEE Trans. Power Syst. 10 (1) (1995) 133-140.
[41] C.D. Parker, "Lead-acid battery energy-storage systems for electricity supply networks," J. Power Sources, 100 (2001) 18.
[42] H.G. Zimmerman and R.G. Peterson, "An electrochemical cell equivalent circuit for storage battery/power systems calculations by digital computer," In Proceedings of the 13th Intersociety Energy Conversion, (1978) 33–38.
[43] E. Hyman, W.C. Spindler and J.F. Fatula, "Phenomenological discharge voltage model for lead-acid batteries," In Proceedings of AIChe Meeting—Mathematical Modeling of Batteries, (1986).
[44] J.B. Copetti, E. Lorenzo and F. Chenlo, "A General Battery Model for PV System Simulation," Progress in Photovoltaics, 1(1993)283.
[45] M.M.D. Ross, "A simple but Comprehensive Lead-acid Battery Model for Hybrid System Simulation," cetc-varennes.nrcan.gc.ca/eng/publication/r2002-049e.html
[46] D.U. Sauer, "Modeling of local conditions in flooded lead/acid batteries in photovoltaic systems," J.Power Sources, 64 (1997) 181
[47] Salameh, Z.M., Casacca, M.A., Lynch, W.A., " A Mathematical model for Lead-Acid batteries", IEEE Transactions on Energy conversion, Vol.7, No.1, March 1992
[48] Zhan, C.J., Wu, X.G., Kromlidis, S., Ramachandramurthi, V.K., Barnes, M., Jenkins, N., Ruddel, A.J., "Two electrical models of the lead-acid battery used in a dynamic voltage restorer", IEEE Proceedings on Generation, Transmission and Distribution, Vol. 150, No.2, March 2003
[49] Giglioli, R.,Buaonarota, A., and Cerolo, P., "Charge and discharge fourth orde dynamic model of lead battery", 10th International Electric Vehicle Symposium, Hong Kong, 1990, pp. 371-382
[50] Kromlidis, S., "Battery Modelling for Energy Storage", M.Sc. Dissertation, September 1999
[51] Barker, P.P, "Ultracapacitors for Use in Power Quality and Distributed Resource Applications", Power Engineering Society Summer Meeting, 2002 IEEE, Volume: 1, 2002, Page(s): 316-320 vol.1

[52] CIGRE Brochure TF 38.01.10 “Modelling New Forms of Generation and Storage”, N. Hatziargyriou et al., April 2001.